Liquid Phase Electroepitaxial Bulk Growth of Binary and Ternary Alloy Semiconductors under External Magnetic Field

by

HAMDI SHEIBANI

Master of Science, Mechanical Engineering, Clarkson University, Potsdam, NY. 1990.

Bachelor of Science, Mechanical Engineering, Clarkson University, Potsdam, NY. 1988.Graduated with Distinction.

Bachelor of Science, Mathematics, ST. Michael's College, Winooski, VT. 1987.

A Dissertation Submitted in Partial Fulfillment of the Requirements
for the Degree of

DOCTOR OF PHILOSOPHY

in the Department of Mechanical Enginerring

We accept this dissertation as conforming
to the required standard

Dr. S. Dost, Supervisor, Dept. of Mechanical. Engineering.

Dr. Y. Stepanenko, Member, Dept. of Mechanical. Engineering.

Dr. Z. Dong, Member, Dept. of Mechanical. Engineering.

Dr. V. Bhargava, Outside Member, Dept. of Elect. & Comp. Eng.

Dr. T. Sukegawa, External Examiner (Aichi University of Technology. Japan)

Supervisor: Dr. S. Dost

ABSTRACT

Semiconducting single crystals are vital to the electronics industry. A number of methods have been developed to produce or "grow" these materials. A widely used group of growth techniques is known as the growth from solution. In these methods layers of single crystals are grown at relatively low temperatures. Liquid Phase Electroepitaxy (LPEE) falls in this category, and is a relatively new, promising technique for producing high quality, thick compound semiconductors and their alloys.

The availability of thick alloy substrates will solve problems arising from lattice mismatch encountered in the integration of different material layers, and will open new horizons in the fabrication technology of opto-electronic devices and integrated circuits . The growth of $GaAs$ and $InGaAs$ crystals is an ideal vehicle for the development of a ternary crystal growth process.

Various features of LPEE as well as a low cost of hardware make this technique quite attractive for the growth of high quality alloy semiconductors in the form of both bulk crystals and buffer layers. However, reproducible growth of such crystals depends on the understanding and control of the key mechanisms governing the LPEE growth process. Among these factors, both the gravity induced natural convection in the solution and Joule heating in the growth cell are of the utmost importance. They have adverse effects on the quality of grown crystals and the stability of the growth interface.

The main objectives are to reduce the adverse effect of natural convection and to determine the optimum growth conditions for reproducible desired crystals for the optoelectronic and electronic device industry. Among the available techniques for suppressing the adverse effect of natural convection, the application of an external magnetic field seems the most feasible one.

The research work in this dissertation consists of two parts. The first part is focused on the design and development of a state of the art LPEE facility with a novel crucible design, that can produce bulk crystals of quality higher than those achieved by the existing LPEE system. A growth procedure was developed to take advantage of this novel crucible design. The research of the growth of $InGaAs$ single crystals presented in this thesis will be a basis for the future LPEE growth of other important material and is an ideal vehicle for the

development of a ternary crystal growth process.

The second part of the research program is the experimental study of the LPEE growth process of high quality bulk single crystals of binary/ternary semiconductors under applied magnetic field. The compositional uniformity of grown crystals was measured by Electron Probe Micro-analysis (EPMA) and X-ray microanalysis .

The state-of-the-art LPEE system developed at University of Victoria, because of its novel design features, has achieved a growth rate of about 4.5 mm/day (with the application of an external fixed magnetic field of 4.5 KGauss and 3 A/cm^2 electric current density), and a growth rate of about 11 mm/day (with 4.5 KGauss magnetic field and 7 A/cm^2 electric current density). This achievement is simply a breakthrough in LPEE, making this growth technique absolutely a bulk growth technique and putting it in competition with other bulk growth techniques. The growth rates achieved can even be higher for higher electric current and magnetic field intensities.

Examiners:

Dr. S. Dost, Supervisor, Dept. of Mechanical. Engineering.

Dr. Y. Stepanenko, Member, Dept. of Mechanical. Engineering.

Dr. Z. Dong, Member, Dept. of Mechanical. Engineering.

Dr. V. Bhargava, Outside Member, Dept. of Elect. & Comp. Eng.

Dr. T. Sukegawa, External Examiner (Aichi University of Technology, Japan)

Table of Contents

List of Figures

List of Tables

Acknowledgement

I am deeply indebted and grateful to my thesis advisor, Dr. Sadik Dost, for his continuous guidance, patience, encouragement and sincere friendship. Professor Sadik Dost introduced me into this area and gave me the opportunity to interact with others in his research group. He not only gave me guidance when I met difficulties but also let me develop my own ideas during this study. His guidance and instructions made this project possible.

I also would especially like to thank Mr. Brian Lent and Mr. Nick.Audet. Through collaborations with them, I learned the experimental sides of this research and realized the potential applications of my study. They have been a valuable resource and true friends.

I also would like to take this chance to thank my Ph.D. committee members

Furthermore, I thank all my friends and colleagues at UVic and the Crystal Growth Laboratory, Mr. Michael Crowle, Mr. Ray Brougham, Dr. Andrew Rowe, and Dr. Mohamed El-Kharashi for their warm friendship and for their constant help. I also would especially like to thank Dr. Susumu Sakai, who has volunteered a lot of his time to help in this project.

I appreciate the technical assistance provided by Mr. Rodney Katz and Mr. George Csanyi-Fritz during the course of this work.

I would like to express my gratitude to my family for their constant support and encouragement. My deepest thanks must go to my parents, Mr. and Mrs. Sheibani, for their unending support and encouragement in achieving this goal, and for their love and prayer during all my studies. I thank GOD for blesses and loves.

With the contribution from all of these individuals, it is with gratitude and pleasure that I have able to complete this thesis. Thank you.

Financial supports were provided through funding by the The Canadian Space Agency (CSA), National Science and Engineering Research Council (NSERC), and Amistar Research and Development, B.C.

Dedication

To My Beloved Parents,
Supportive Wife, lovely childern (Mustafa, Ibrahim, Arwa)
and All My brothers and Sisters
For love and patience

Chapter 1

Introduction

1.1 Motivation and Goals

Indium gallium arsenide ($InGaAs$) is used in the fabrication of electronic, optoelectronic, and microwave semiconductor devices. At present, $InGaAs$ is available only by epitaxial growth on binary substrates, such as gallium arsenide ($GaAs$) and indium phosphide (InP). The practice of epitaxial growth of ternary layers on binary substrates is known as bandgap engineering, and requires that the substrate and the epitaxial layer be closely lattice-matched. When the two layers could not be lattice-matched close enough, the grown epitaxial layer will be of lower quality and will either be highly strained or have a high dislocation density. As a result, the design of the planned device and consequently its performance will ultimately be constrained by the limitations of the capability of bandgap engineering.

An alternate approach to bandgap engineering is to eliminate the binary substrate, and instead, grow ternary substrates of the desired composition. The ability to grow ternary substrates, such as $InGaAs$, of any desired composition, would eliminate the major constraints currently faced by the III-V device designers, and would likely usher in a plethora of new device designs. Presently, there is no technology that supports the routine (reproducible) growth of ternary crystals. The growth $InGaAs$ crystals (substrates) is an ideal vehicle for developing such capability. However, the challenges encountered in growth of $InGaAs$ wafers, such as constitutional supercooling and In concentration gradients along the length of the ingot, have forestalled the widespread usage of $InGaAs$ substrates.

At lower In concentration ranges, $InGaAs$ and $GaAs$ possess electrically similar characteristics, but the defectivity level in $InGaAs$ is much lower than in $GaAs$. Presently, typical liquid encapsulated Czochralski (LEC) grown $GaAs$ wafers range in diameter from

2-6 inches, and often contain dislocation defect densities as high as $10^4 - 10^5\ cm^{-2}$. In comparison, 6 inch Czochralski grown silicon (Si) wafers routinely contain as few as 0 - 100 dislocations/cm^2. Generally, high defect densities are unacceptable because defects can have a negative impact on device performance, resulting in lower wafer yields and higher die costs. As a result, the current level of dislocation densities in $GaAs$ substrates is unacceptable. Researchers have found that if $GaAs$ is appropriately doped with certain impurities, the impurities can lessen the number of defects. In particular, In-doped $GaAs$ wafers, produced under optimized crystal growth conditions, have reportedly reduced dislocation counts to the $10^2\ cm^{-2}$ range. This suggests that devices fabricated on $InGaAs$ substrates may have higher yields and improved device performance.

A number of methods have been developed to produce or grow these materials. Commercially available bulk crystals are produced using high temperature melt growth techniques such as Horizontal Bridgman (HB) [1], and Liquid Encapsulated Czochralski (LEC) [2]. Electronic properties of these crystals and their behaviors during device processing are affected in a critical way by electrically active points defects [3], low compositional uniformity, and dislocation structure [4]. A widely used group of growth techniques is known as the growth from solution. These low temperature growth techniques offer in principle much higher controllability of defects than melt growth. Liquid Phase Electroepitaxy (LPEE) falls in this category, and is a relatively new, promising technique for producing high quality, compound semiconductors and their alloys [5].

Considering all this, the interest of using LPEE to grow $InGaAs/GaAs$ substrates is clear. There is a need for high quality LPEE grown $InGaAs$ substrates that are required for the fabrication of presently designed very high performance electronic and optoelectronic devices. However, there are some formidable challenges in growing bulk crystals by LPEE. First, the maximum growth rate and crystal thickness presently achievable by LPEE are about two orders of magnitude lower than those by LEC and HB. This results in much higher production costs per volume for $InGaAs$ bulk crystals grown by LPEE, compared to LEC and HB. Second, the maximum crystal size of $InGaAs$ single crystals currently achievable by LPEE, in both thickness and diameter, is much smaller than the dimensions achieved by LEC and HB. The combination of these two factors results in much higher production costs per volume of $InGaAs$ bulk crystals grown by LPEE. In addition, some applications require substrates of large diameter without which many integrated circuit

applications would simply not be possible. Hence, the development of a reliable LPEE process for growing bulk binary and ternary, production-quality, crystals is necessary.

In spite of these two main disadvantages, namely the low growth rate and smaller crystal size (in both diameter and thickness), the other aforementioned features of the LPEE growth process as well as the low cost of hardware make this technique quite attractive for the growth of high quality alloy semiconductors in the form of both bulk crystals and buffer layers. However, a reproducible growth of such crystals depends on the understanding and control of the key mechanisms governing the LPEE growth process. One of these mechanisms is the natural convection occurring in the solution. Although the effect of convective flow in LPEE growth is minimum compared with other solution growth techniques, the adverse effect of convection is one of the most important parameters and it must be reduced to a minimum.

One efficient means of reducing the adverse effect of convection is through the application of an external magnetic field. The application of an external magnetic field induces a magnetic body force that acts on the points of the liquid solution. The two competing body forces, namely the magnetic body force due to the application of an external static magnetic field and the buoyancy force due to the gravitational field of Earth, reduce the intensity of convection in the solution. A numerical simulation model for the LPEE growth of a binary system ($GaAs$) was given in [6, 7]. The results showed the feasibility of such a procedure.

One must however examine experimentally the effect of such a strong magnetic field on the LPEE growth process, through carefully designed experiments. These include the effects on the growth mechanisms of electromigration, Peltier heating and cooling, natural convection, growth rates, and quality of grown crystals. These are the objectives of this thesis research. The aim is to determine the optimum growth conditions for reproducible, high quality bulk $InGaAs$ crystals for industrial applications.

To achieve these goals, a state-of-art-LPEE technology, including a novel growth crucible and the utilization of an external magnetic field must be developed. Such a system, under suppressed gravity conditions, will be able to grow better quality and thicker ternary crystals of desired uniform compositions.

The present research is believed to set the stage for the LPEE growth process to achieve these goals, and promote the LPEE growth technique from being an epitaxial growth tech-

nique to the category of bulk growth. We hope in the future the name of LPEE will be modified to a proper name that reflects its capability of growing bulk crystals.

1.2 Approach

A number of experimental investigations have been conducted to reduce the adverse effect of convection by various means such as configuration stabilization [8], reduced gravitational field [9], and applied magnetic field [6, 10]. Among the available techniques for suppressing the adverse effect of natural convection, the application of an external magnetic field seems the most feasible one. As mentioned earlier, the application of an external magnetic field to a liquid solution induces an electromagnetic body force which tends to balance the effect of the buoyancy force. To the best of our knowledge, there is no published work containing LPEE experiments under magnetic field.

Therefore, the design of a new LPEE system for the growth of $GaAs$ and $InGaAs$ crystals was a logical effort to achieve the objectives of the present research. Based on the available knowledge in the open literature, the present state of the LPEE technique was inadequate for obtaining bulk crystals. It is the achievement of this thesis work that a novel and unique LPEE growth system was developed to produce desired bulk (thickest) binary and ternary crystals with remarkably uniform compositions.

There are a number of technological and scientific achievements as a result of this thesis work. It is hoped that the results obtained here will take the current research efforts in LPEE at the University of Victoria to the next level; a commercial-scale crystal growth system with a capability that will allow the growth of other bulk crystals of III-V, II-VI and IV-IV materials such as $CdZnTe$ and $SiGe$.

1.3 Outline of the Thesis

In addition to brief introductory comments on the subject matter, Chapter 2, gives an introduction to crystal imperfections and discusses their impact and behavior in $GaAs$ crystals. A summary of the properties and characteristics important to the performance of semiconductors performances are also presented in this chapter. Special emphasis is given to $GaAs$ and $InGaAs$, along with a discussion as why they are generating so much interest in the

electronic industry. Keeping in mind the single crystal $GaAs$ and $InGaAs$ materials, the different types of defects that are usually present in every non-ideal crystalline material are discussed.

The quality of crystals is usually defined by the level of crystals defects, and low-defect materials are therefore said to be of high quality. Since the amount and severity of these crystal defects are often dependent on the types of methods used to grow them, Chapter 3 is devoted to the discussion of the most common techniques used for growing $GaAs$ and $InGaAs$ bulk crystals. The solution growth technique, namely liquid phase epitaxy (LPE) gets special attention due to its importance to the growth technique of Liquid Phase Electroepitaxy which is introduced in Chapter 4. A few selected devices, in which the use of $GaAs$ and $InGaAs$ has advantages over other types of semiconductors, are also described.

Chapter 5 stresses the importance of crystal quality in the world of electronic and opto-electronic devices, and in particular, the high requirements expected from semiconductor substrates.

The theory of LPEE is introduced in detail in Chapter 6. Taking advantage of the knowledge acquired through the first four chapters to fully appreciate the information presented, a review of the results achieved to date in growing bulk $GaAs$ and $InGaAs$ crystals is given. Crystals grown by various techniques are compared in terms of their various properties such as quality, size, and electrical characteristics.

Chapters 7 and 8 describe the experimental conditions and setup of the LPEE growth system, post-growth treatments, and sample preparation. The methods used to characterize the grown crystals are described in Chapter 9.

Chapter 10 discusses the results of the experiments with and without an external magnetic field. Results are compared. In Chapter 11, we conclude the thesis by summarizing the findings and giving a rationale pointing out the great interest in growing high quality $GaAs$ and $InGaAs$ bulk crystals using LPEE. The major limitations associated with this technique and the possible areas of future research are also discussed.

Chapter 2

Crystallography and Physics of III-V Compounds

A semiconductor is a substance, usually a solid chemical element or compound, that can conduct electricity under some conditions but not others, making it a good medium for the control of electrical current. Its conductance varies depending on the current or voltage applied to a control electrode, or on the intensity of irradiation by infrared (IR), visible light, ultraviolet (UV), X rays.

The specific properties of a semiconductor depend on the impurities, or dopants, added to it. An N-type semiconductor carries current mainly in the form of negatively-charge electrons, in a manner similar to the conduction of current in a wire. A P-type semiconductor carries current predominantly as electron deficiencies called holes. A hole has a positive electric charge, equal and opposite to the charge of an electron. In a semiconductor material, the flow of holes occurs in the direction opposite to the flow of electrons.

Elemental semiconductors, include antimony, arsenic, boron, carbon, germanium, selenium, silicon, sulfur, and tellurium. Common semiconductor compounds include gallium arsenide, indium antimonide, and the oxide of most metals. Of those, gallium arsenide ($GaAs$) is widely used in low-noise, high-gain, weak-signal amplifying devices.

2.1 Compound Semiconductor Materials

Compound semiconductor materials can be realized by the formation of "solid solutions" of two or more starting materials. These solutions occur when atoms of a different element are able to substitute a given constituent of a material without altering its crystal structure. The ability to do so by the new atom is referred to as its miscibility. In order that atoms can

form solid solutions over large ranges of miscibility, they must satisfy the Hume Rothery rules:

- They must belong to the same group of the periodic table.
- They must have comparable atomic diameters allowing substitution without large mechanical distortion.
- Their ionicity must not be very different so as not to affect the tendency to attract / repel electrons from the site by a large amount.
- The crystal structure of each constituent must be the same.

A two component alloy is known as a binary alloy; some common examples include $GaAs$, $AlAs$, GaP, InP and $InAs$ all of which have the Zincblende (diamond) crystal structure. Similarly a ternary alloy is one with three components and a quaternary alloy is one with four.

$In_xGa_{1-x}As$ is a ternary compound where both Ga and In are from group III enabling In to replace Ga on the alpha sites of the diamond compound lattice. As the compound $InAs$ has the same structure as $GaAs$, this makes the formation of solid solutions of In in $GaAs$ easy and preserves the same crystal structure over the full range of In substitution. The beta sites with As atoms are not altered in anyway. Thus effectively, $InGaAs$ is an alloy of $InAs$ and $GaAs$.

Simultaneous replacement of atoms from alpha and beta sites of binary compounds allows quaternary alloys to be formed. $In_xGa_{1-x}As_yP_{1-y}$ is one such example. This gives a more flexible scheme for tailoring material properties. In this case, the binary compounds $GaAs$, InP, $InGa$ and GaP are part of the system and together they determine the limits to the range of properties of the resultant compound.

2.2 Crystal Structure and Lattice Parameters

Most III-V compounds crystalize in the zinc blend structure. This structure may be derived by first superimposing two cubic (fcc) structures and then displacing one of them one-quarter of the distance along the cubic diagonal. If the atoms of the two fcc structures are identical, then the diamond structure (e.g., Si) results. However, if they are different, the Zinc-blend structure results. In the case of III-V compounds, the group III atoms all lie on one of the face substructures while the group V atoms lie on the other.

$GaAs$ crystallizes in the zinc blend structure. The zinc blend structure can be described as two interpenetrating face-centered cubic (fcc) lattices which are offset from one another by (1/4, 1/4, 1/4) **a**, where **a** is the lattice constant. Ga atoms occupy one of the fcc sublattices and As atoms occupy the other. The result is an alternating sequence of (111) Ga and (111) As planes. Typically, the letters **A** and **B** are used as identifiers to distinguish between the (111) Ga and (111) As layers, respectively.

$GaAs$ and $InAs$, which are both known to have the zinc blend structure, are also completely miscible. When $InAs$ and $GaAs$ are mixed to form $InGaAs$, the original $GaAs$ crystal structure distorts to accommodate the In atoms [11]. The two cations, In and Ga, share the same fcc sublattice, while As occupies the other sublattices. However, because In atoms are slightly larger than Ga atoms (crystal radii of 0.94 Å for In^{3+} ions, compared to 0.76 Å for Ga^{3+} ions) [12], adding In increases the lattice parameter. The increase in lattice parameter can be predicted using Vegard's law. Vegard's law predicts the relationship between solid composition and lattice constant for $(In,Ga)As$ alloys. Lattice constant is calculated as a function of the weighted average of the constituents. In the case of $In_xGa_{1-x}As$, the expression for the lattice parameter is given by

$$a_{InGaAs} = 6.0583 - 0.4050(1 - x). \tag{2.1}$$

if 6.0583 Å is used as the lattice constant for $InAs$ and 5.65325 Å is used for $GaAs$ at 298.15 K [13]

2.3 Energy Gap

The band gap is the energy separating the point of highest energy in the valence band to the point of lowest energy in the conduction band. If these two points are at the same momentum, it is referred to as a direct bandgap. $InGaAs/GaAs$ have a direct bandgap, whereas semiconductors such as Si and Ge do not.

In the case of direct bandgaps, the electron needs only to be excited by a photon (quantum of electromagnetic energy) of the appropriate energy level to make the transition from the top of the valence band to the bottom of the conduction band. For indirect bandgaps, the electron needs both the input of a photon and a phonon (quantum of vibrational energy, providing extra momentum to the particle) to accomplish a similar jump. This property is very important when dealing with semiconductor photo-devices.

The band structure of $In_xGa_{1-x}As$ is direct over the entire range of composition. The bandgap E_g variation may be expressed with good accuracy at 300 K by [14]

$$E_g = 0.36 + 0.505(1-x) + 0.555(1-x)^2. \tag{2.2}$$

2.4 Imperfections in Crystals

In a perfect lattice, all atoms would occupy their pre-determined lattice sites and there would be no departures from the periodicity of the lattice structure. In reality, however, perfect lattices rarely, if ever, exist, first because of the presence of lattice defects, and second because of thermal vibrations of lattice atoms around their equilibrium position. All lattices contain imperfections ranging from point defects to line defects (dislocations) to planar defects (stacking faults). The density and distribution of these defects are important because defects have been found to alter the electrical properties of materials by increasing the number of scattering sites in the matrix, introducing leakage paths in devices, and distorting junction shapes.

2.4.1 Point Defects

A point defect is localized about a point in the crystal. Two elementary point defects are vacancy and interstitial. A vacancy is created when an atom moves out of its regular site, and an interstitial is formed when an atom gets located in one of the interstitial voids in the crystal. Certainly the most obvious type of imperfection, and also the one that plays the most vital part in the properties of the semiconductor, is the presence of foreign atoms in the crystal. Even a small impurity content of one PPB still leaves about 10^{14} impurity atoms per cm^3 in a crystal. We must distinguish between two types of impurities: substitutional impurities, which replace atoms of the host crystal on their lattice site, and interstitial impurities, which occupy positions in between the lattice sites. The second type of point defects occurs when an atom of the host crystal is present in between the lattice sites (interstitial atoms), or when a lattice site is left vacant (vacancies).

2.4.2 Dislocations Motion

The movement of dislocations through the lattice by the glide process is termed slip. A slip system is defined by the plane on which the dislocation glides (referred to as the slip plane) and the direction that the dislocation glides (indicated by the Burgers vector). The slip plane is generally the plane with the highest density of atoms and the slip direction is a close-packed direction on the slip plane. For $GaAs/InGaAs$ and other zinc blend crystals, the slip planes are (111) planes and the slip directions are [110] directions.

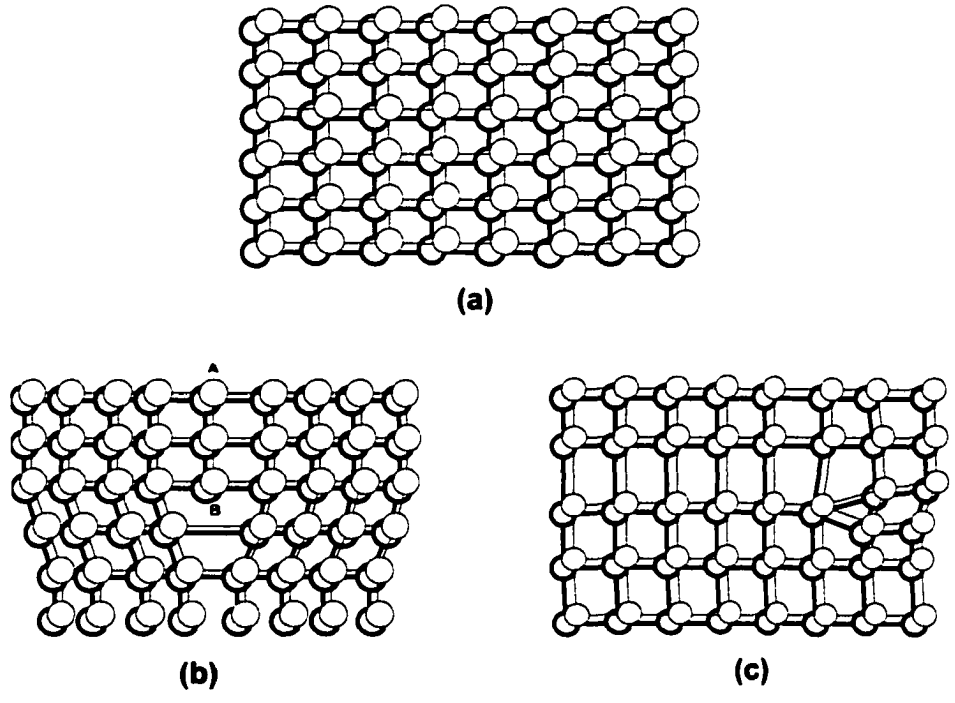

Figure 2.1. *Basic dislocation features in a simple cubic lattice. Impact on the periodicity of (a) a perfect lattice structure by (b) an edge dislocation and (c) a screw dislocation.*

Dislocations are identified as having edge, screw, or a mixture of edge and screw character [14]. These terms describe the arrangement of atoms around the dislocation line. Edge dislocations are formed by the removal or the addition of an extra half plane of atoms, resulting in a row of unsatisfied bonds (figure. 2.1b). The dislocation line follows the edge of the extra plane. For elemental semiconductors, such as Si, only a single half plane is needed to form the edge dislocation. With compound semiconductors, however, the "extra half plane" consists of a pair of AB planes in order to maintain charge neutrality. With

screw dislocations, a continuous plane spirals the dislocation line, similar to a spiral staircase or the path of the threads on a screw (figure. 2.1c). Actually, dislocations of pure edge or pure screw character are rare in GaAs and the majority of dislocations possess both edge and screw character. These mixed dislocations are usually 600 dislocations. Because slip occurs in the {111} planes in $< 110 >$ directions, 600 mixed dislocations readily occur and are the most common dislocation type in $GaAs$.

As edge dislocations move through the crystal, the atoms shift in a direction parallel to the movement of the dislocation. For an edge dislocation, the Burgers vector is perpendicular to the dislocation line. As screw dislocations move through the crystal, the atoms shift perpendicularly to the direction of motion. For screw dislocations, the Burgers vector is parallel to the dislocation line. Therefore, any plane which contains the dislocation line is also a slip plane. By contrast, edge and mixed dislocations have fixed slip planes. In order to move out of their slip planes, they require interaction with vacancies. If vacancies diffuse towards the dislocation line, the dislocation climbs up and out of the slip plane. If vacancies diffuse away from the dislocation line, then the dislocations will climb below the slip plane. Climb is considered non-conservative because it requires either the creation or destruction of point defects.

$GaAs$ and $InGaAs$ possess a complicated dislocation structure because the AB double layer arrangement of zinc blend introduces alternate configurations for each dislocation type. First of all, the half-planes of dislocations can end at either Ga-In sites or at As sites.

There is nothing in the literature which suggests that the character of the dislocations changes when In is added to the $GaAs$ matrix. What does change, however, is the behavior of the dislocations. Some of the differences between the material properties of $GaAs$ and $InGaAs$ include differing Poisson's coefficients, shear moduli, and critical resolved shear stress (CRSS) values. Because these differences result in increased stress fields around the dislocations and lower dislocation mobilities, the ultimate result can be a dramatic decrease in the number of dislocations in $InGaAs$ ingots.

The desire to reduce dislocation counts in $GaAs$ stems from the recognition that dislocated substrates can impair the performance of devices fabricated on them. The typical fabrication sequence for lasers and light emitting diodes (LED) involves growing a series of epitaxial layers on the substrate. The quality of these epitaxial layers is largely impacted by substrate quality and the amount of lattice mismatch. If the materials are properly lattice

matched, quality of the' substrate is generally the gating factor which determines the quality of the epitaxial layer. Wehyer and Van de Ven [15] report that if the epitaxial layers are grown under optimal conditions, then the correspondence between dislocations in GaAs substrates and those in homoepitaxial metal organic chemical vapor deposition (MOCVD) layers will be 1:1, at best. Otherwise, numerous new defects will be introduced at the interface.

2.4.3 Volume Defects

Volume defects include volumes which differ from the rest of the crystal in one or more of the following characteristics: crystal orientation, structure, or composition. A volume differing from the crystal matrix in orientation is called a grain. If a crystal is made of a series of grains in different orientations, it is said to be polycrystalline. All crystals grown for device applications need to be single crystals. Failure to respect this condition lowers tremendously the yield of the material. In case of a volume of different structure, it is said to be a grain of second phase material. This problem is quite common for II-VI compounds, but is not of major importance in the case of $GaAs/InGaAs$

2.4.4 Twinning

Twinning is a gross defect that occurs when one part of the crystal forms the mirror image of the other, with the two parts remaining in intimate contact over the bounding surface. A twinned material has a very high dislocation content.

2.5 Epitaxy

Epitaxy refers to the ordered growth of one crystal upon another crystal [16]. Because of the large range of possible semiconductor compounds and their alloys, it is rare in device fabrication to grow bulk crystals of all these materials. Instead, it is more attractive to realize the wider range of materials by epitaxial growth. This is partly due to the difficulties involved in developing easy bulk crystal growth techniques for each new material and also because of historical reasons. Two materials for which thorough research and bulk crystal growth and polishing methods have already been developed are $GaAs$ and InP.

There are three main modes of epitaxial growth: (a) monolayer, (b) nucleated and (c) nucleation followed by monolayer. Monolayer growth occurs when the deposited atoms are more strongly bound to the substrate than they are to each other. The atoms aggregate to form monolayer islands of deposit which enlarge and eventually a complete monolayer coverage has taken place. The process is repeated for subsequent layer growth. In case of nucleated growth, the initial deposit atoms aggregate as small three-dimensional (3D) islands which increase in size as further deposition continues until they touch and intergrow to form a continuous film. This mode is favored where the forces of attraction between the deposited atoms is greater than that between them and the substrate. In the final mode, growth starts with the formation of a single or few monolayers on the substrate followed by subsequent nucleation of 3D islands on top of these monolayers.

2.6 Epitaxial Lattice Matching

Epitaxy, although a highly successful approach for growing a wide range of materials, nonetheless suffers from an important deficiency. Epitaxial growth requires that the atomic spacing, the lattice constant, of the layer material and of the substrate not differ by more than a few percent and that they have the same crystal structure. While most materials of interest have diamond structure, satisfying the latter requirement, the lattice matching imposes a serious constraint on the range of compositions that can be grown on a given bulk substrate. Although, traditionally, these were provided by $GaAs$ and InP, increasing use is being made of $InSb$ and $GaSb$ as the substrate.

This problem is best appreciated by a graph of the energy gap versus lattice constant for major compounds, as shown in figure 2.2 This is also known as a phase diagram. For a possible range of ternary alloy systems, a solid line is generated between the starting binary materials. In the case of a quaternary compound, the boundary is laid out by four intersecting lines.

Ternary, III-V bulk single crystals are of interest as lattice-matched substrates for a variety of homo- and heteroepitaxial applications. Close lattice matching of the substrate to epilayers avoids the need for compositional grading of layers necessary for minimizing strain and misfit dislocations.

The ability to tailor the bandgap of III-V alloys to a desired wavelength makes them

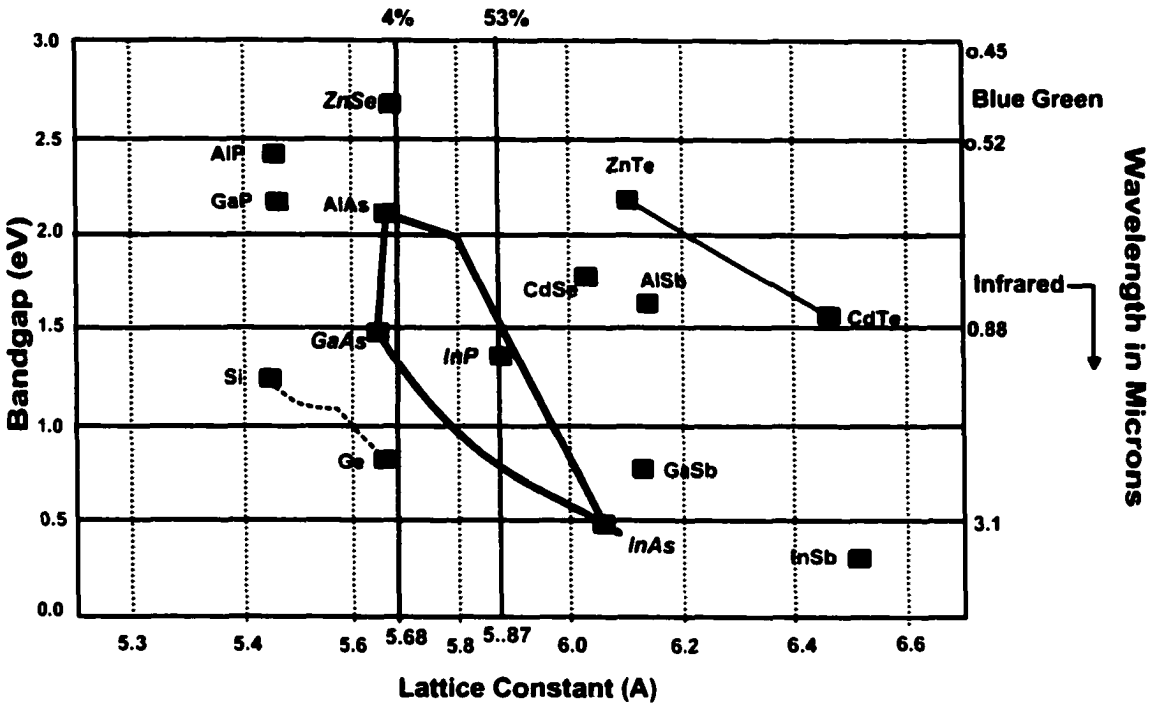

Figure 2.2. *A plot of energy bandgap and lattice constant for major semiconductor compounds with their application.*

particularly attractive for optoelectronic applications. The dark currents are significantly reduced in compound detectors from their Ge and Si predecessors. In addition, heterojunction structures can be easily used to enhance their high speed operations. One such system that is of great interest is the $InP/InGaAs$ superstructures which is sensitive to 1.55 μm wavelength. In this case the composition of $In_{0.53}Ga_{0.47}As$ ternary compound, with the desired bandgap of 0.75 Ev, is dictated by the lattice matching constraint to the InP substrate.

$Ga_{1-x}In_xAs$ substrates with x=0.04 are of particular interest since they are closely lattice-matched to $ZnSe$ for the fabrication of blue-emitting lasers diodes. Major applications of immediate interest for blue laser diodes include optical data storage, very high density compact disc players, and high resolution laser color printers for which efficient blue generation is required to complement the red and green currently available.

Lattice mismatch, on the other hand, manifests itself in the form of dislocation-induced junction leakage and low quantum efficiency in optoelectronic devices.

The availability of bulk crystals with desired characteristics will eliminate the above mentioned problems and improve device performance.

these methods are much more stoichiometric and possess less dislocations and electrically and/or optically active point defects. In spite of these advantages, the above noted epitaxial techniques permit the growth of thin (less than 10 μm) layers or films rather than bulk crystals with sufficient thickness to slice wafers. Exception to this is the development of an innovative temperature modulation technique, [17, 18], which combines both dissolution and growth phases in a cyclic manner. This technique however relies on the beneficial use of solutal convection and although it has been successfully used to grow thick Si substrates from indium solutions, it is not suitable for growth of thick $InGaAs$ substrates due to insufficient solutal convection. [19, 20] have also grown thick $Ga_{1-x}In_xAs_ySb_{1-y}$ crystals by a modified Bridgman technique. Yet, their quality is presently in part limited by the substrate's quality. Certainly, the growth of higher quality bulk crystals would generate many opportunities in the world of semiconductor devices.

In 1987, the growth of a bulk $GaAs$ crystal achieved by liquid phase epitaxy (LPEE), was reported for the first time [5]. Even though the size of the crystal was impressive (4 mm thick, 20 mm in diameter) compared to what was previously grown by LPEE, it was not at all in the same range as the bulk GaAs crystals commercially grown with a melt method such as liquid encapsulated Czochralski or Horizontal Bridgman (crystals of 75 mm in diameter or more, with lengths over 1 m possible). So why the interest in LPEE for the growth of bulk crystals, when other techniques seem to have an incredible advantage in performing similar functions? It is this question that we will try to answer in this thesis.

Crystals may be grown from solution, from melt, and from vapor. While methods differ widely, the conditions necessary for growth are similar in each case.

Over the years, an amazing number of growth techniques have been developed. Because of the nature of crystal growth, which is still considered as a form of Black Art for some, practically not a single "crystal grower" uses the exact same technique or apparatus. This makes it very difficult to discuss each of theses techniques within this thesis. To overcome this problem, various growth techniques were regrouped into four categories, according to the classification given by Pamplin [21] which takes the nature of the phase change involved in growth as the basis for characterization. From there, subtechniques are derived, and only the most frequently used ones were discussed further.

The crystals grown by various techniques are compared according to quality, size, electrical characteristics, and so on at the end of each subsection. These comparisons include

semi-insulating substrates and conductive (n- or p-doped) substrates.

3.2 Solid Growth Techniques

Solid state growth is usually achieved by atomic diffusion, thus involving very low growth rates. The various solid state techniques are, in the most cases, avoided when other, more rapid, techniques can be used. For this reason, they will not be covered in this chapter.

3.3 Melt Growth Techniques

Melt growth is presently the most popular method for growing large single crystals, especially in the field of semiconductors. These techniques involve gradually freezing a part of the melt to form an ingot, freezing which occurs at a temperature of 1238^{o} C for $GaAs/InGaAs$.

The three techniques that will be reviewed here are crystal pulling, zone melting, and normal freezing. Together, they account for the high majority of bulk semiconductor crystals grown from the melt.

3.3.1 Crystal Pulling (Czochralski's Method, CZ)

All crystal pulling processes are based on a method developed in 1918 [22]. This technique and its many derivatives have become the dominant processes used in industry today for the production of bulk crystal semiconductors.

The basic process is as follows. The material to be grown is held in a crucible which is heated until the charge is melted. The temperature of the charge is then adjusted so that the center of the free surface of the liquid is at its freezing point. A seed crystal is then placed in contact with the melt, and the crystal growth is performed by slowly withdrawing the seed from the melt. When the desired crystal length has been reached, the crystal is quickly removed from the melt, or the liquid temperature is raised to gradually reduce the diameter of the crystal. The temperature is then lowered to room temperature, and the crystal removed from the apparatus.

The apparatus (shown in figure 3.1) includes a crucible, usually made out of fused silica. The power is provided by a furnace, the most common being resistance heating and

induction heating. The seed is kept in a rotational motion relative to the melt to provide a temperature distribution as uniform as possible.

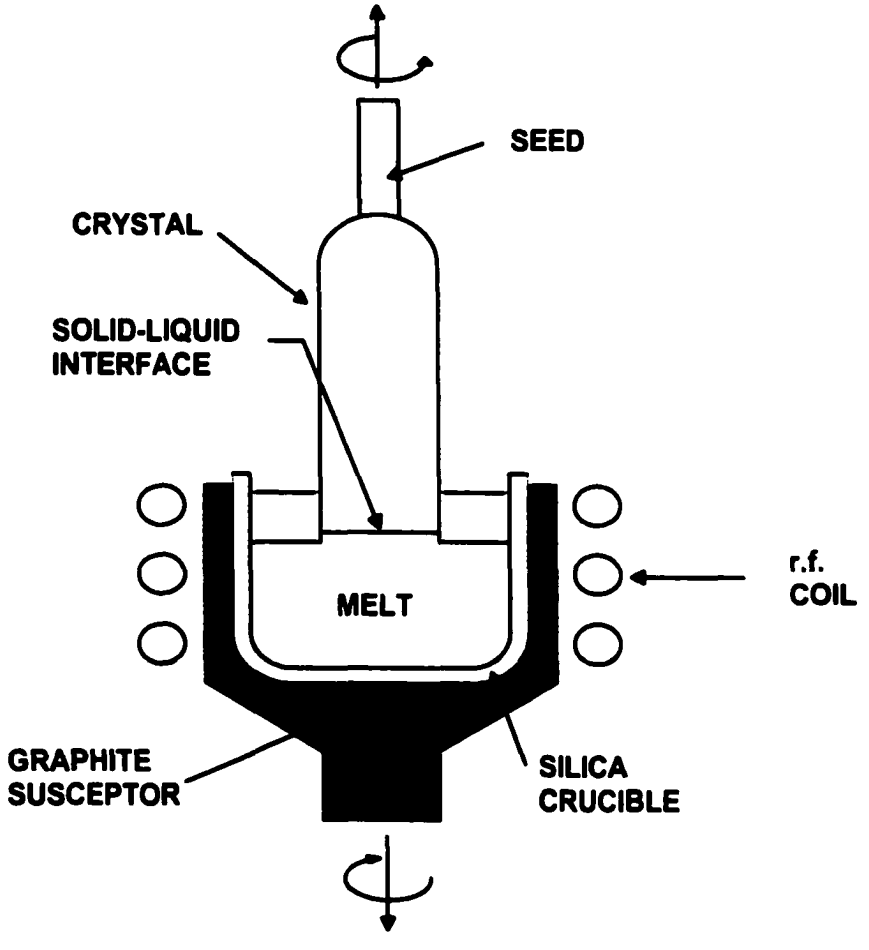

Figure 3.1. *Schematic of LEC apparatus*

The success of crystal growth using crystal pulling depends on many factors: pulling rate, rotation rate, thermal geometry, quality of atmosphere surrounding the growth area and crucible. All these, coupled with the initial impurity concentration and the various diffusion and segregation coefficients of the components in the melt, will determine the level and type of impurities in the resulting crystal. The segregation coefficients depend on both dopant and host material. Most segregation coefficients in the case of $GaAs/InGaAs$ are under 1, indicating that the concentration of impurities in the solidified layers is lower than in the liquid phase [2]. Thus, the doping in the most recently solidified layers increases. This effect can be minimized by proper choice of the speeds of rotation and rotation.

The growth is usually controlled by providing a stable temperature within the furnace, and detection and compensating for changes in the crystal's diameter due to temperature fluctuations. The diameter of the crystal can be evaluated either by a direct optical system, or a weighing system. One problem associated with the pulling method is growth striations, which come from the temperature variations. Growth rates change, often fluctuating up to a factor of ten with respect to the average growth rate, manifest themselves as striations in the crystal, and are due to local differences in chemical composition.

Special techniques developed to improve the performance of the original Czochralski method include necking, and liquid encapsulation. Necking is used to eliminate crystal imperfections by reducing the diameter of the crystal before enlarging it again to the final diameter, thus allowing the dislocations to grow out of the crystal toward the surface instead of growing into the bulk. Liquid Encapsulation Czochralski (LEC) is used when one of the components in the melt has a vapor pressure above atmosphere pressure, as is often the case with arsenic and phosphorus. The idea is to cover the surface of the melt with a liquid coating, usually B_2O_3, and to apply inert gas pressure exceeding the decomposition pressure to prevent the outgassing of the volatile component. B_2O_3 is chosen because of its transparency, chemical stability, low melting point, and density lower than that of the melt.

Presently, the most popular technique used for the growth of semi-insulating $GaAs$ and $InGaAs$ is the liquid encapsulated Czochralski technique (LEC). LEC allows for crystals of large diameters (over 75 mm), and of great thicknesses (50 cm and more) to be grown. Growth orientation is typically $< 100 >$ or $< 111 >$. The usual cross-section shape of the crystal is circular, even [23] have shown the possibility of growing various configurations by obtaining polycrystalline "plates" using a slightly modified version of LEC (liquid encapsulated Stepanov with die). Growth rates vary between 7 to 20 mm per hour.

Another problem associated to LEC is the occurrence of polycrystallization during growth. The origin of polycrystallization, or twinning, seems to be related to the shape of the solid/liquid interface during growth. Shibata et al. [24] have recently proposed a method for controlling this shape, and thus insuring good stability. However, it is yet too early to confirm the applicability of their approach.

Problems associated with the growth of conductive material with LEC are:

- Radial segregation, resulting in up to a factor of 10 variation in the doping level across the diameter of the substrate.

- Axial segregation, causing high fluctuations of characteristics, often varying by a factor of 40 or more from start to end of growth [23].
- Possibility of striations along the growth axis, up to 20 μm in thickness, again resulting in inhomogeneous doping levels [25].
- Possibility of precipitates and As-rich microdefects ($10^7 - 10^{11} cm^{-3}$), 0.1-0.5 μm in diameter [23, 25].

3.3.2 Zone Melting (ZM)

Zone melting refers to all growing techniques where a liquid zone is created by melting a small amount of material in a relatively large solid charge, with the melt zone then made to traverse through a part or the whole of the charge. These techniques allow one to manipulate the distribution of soluble impurities through the solid (uniform doping, controlled discontinuities in impurity distribution, or impurity removal).

The main components of a zoning apparatus are the following: a heater/cooler, to provide a means of producing a liquid zone; a traverse mechanism for the transport of the molten zone; and a means of mounting or holding the charge. The heating of the melt zone can be achieved by electrical arc (d.c., or a.c.), electron beam, or induction. If the apparatus does not include a container for the charge, it is referred to as the Float-Zone method (FZ). This last method, always vertical in its design, has the advantage to be contamination-free from the crucible, but is limited by the surface tension of the melt (a break in the surface of the liquid, under its own weight, will cause the melt to leak, thus stopping the growth process).

The most important operational parameters in zone melting are the zone length of the melt, the zone traverse velocity, the temperature gradient at the solid-liquid interface, the degree of mixing in the liquid and the matter transport in zone melting. In some cases, the process may be repeated many times, thus improving the impurity distribution at each occasion.

Like in the case of the LEC, it is possible to use a liquid, again usually B_2O_3, to cover the melt in cases of highly volatile components present in the melt. Also, to improve the heat transfer and minimize the localized density difference arising from concentration differences, it is often done to stir the melt, either by forced convection, mechanical means, induced current, or magnetic and electromagnetic effects.

Liquid encapsulated vertical zone melting (LE-VZM), favored zone melting growth technique for semi-insulating $GaAs/InGaAs$ substrate, has quite a few advantages over LEC. First, whereas the impurity content of the crystal in LEC is primarily controlled by the quality of the starting material in LEC, most of these impurities can be removed (or more evenly distributed in case of a dopant such as Cr using a series of re-melts) with LE- VZM. Second, there is much more flexibility in controlling the shape of the growth interface, which is a function of the length of the molten zone [26]. And third, the LE-VZM process uses smaller temperature gradients since, as opposite to LEC which uses high temperature gradients to control the crystal's diameter, the diameter of the crystal is in this case controlled by the crucible. This allows for dislocation densities in the 1 to $5x10^3 cm^{-2}$ range [26].

The crystals grown by LE- VZM can reach 50 to 75 mm in diameter, with heights usually under 10 cm. Even though the crystal is typically grown at around 5 mm per hour, the effective growth rate is much smaller considering that many re-melts are often required.

Zone melting has still not been established for the production of conductive wafers over 50 mm in diameter, this because of a difficulty of growing single crystals while decreasing the dislocation density, a difficulty of growing a long crystal (over 10 cm), and the complicated structure of the ZM apparatus with a short length melting zone [27]. Still, it is recognized that ZM has interesting merits, as were described in earlier sections. Some substantial improvements are expected in the future, with the use of horizontal apparatus (HZM) , which is at its early stages of development. HZM should allow for increase in the crystal's dimensions, and lower the average dislocation density [27].

3.3.3 Normal Freezing (Bridgman-Stockbarger)

Normal freezing, or the Bridgman-Stockbarger process, is very close to the zone melting process. The main difference is that in this case, the whole of the charge is melted initially, and then solidified unidirectionally. This solidification can be achieved in one of the following three ways: by moving the melt slowly relative to a stationary temperature gradient, by moving the furnace relative to the melt, or by static freeze, meaning that a linear temperature gradient is lowered progressively, causing the freezing isotherm to run up the ingot.

In this approach, a seed is usually placed in contact with the melt to initiate the growth.

This prevents problems of over-saturation and spontaneous nucleation. Also, in case of a volatile component present in the melt, this pressure can be controlled either by liquid encapsulation or by having a connection to a source at a fixed temperature.

In this later approach, the vapor pressure within the growth cell is determined and fixed at an appropriate level via diffusion. Both a horizontal and a vertical version of this technique are used, with the horizontal version (Horizontal Bridgman, HB) preferred when the material expands on freezing (the expansion would crack the container in the case of vertical apparatus).

Some time ago, Horizontal-Bridgman (HB) was the most popular technique used to grow semi-insulating $GaAs/InGaAs$ crystals. This situation has changed, with LEC taking more and more the leading role in this field. Even though the same electrical characteristics are obtainable with these two processes, HB has certain drawbacks that will now be discussed.

The most important problem of HB grown $GaAs/InGaAs$ is Si contamination. This comes from the high quantity of $GaAs/InGaAs$ melt in contact with the crucible during the early stages of the growth, where the whole volume of material is kept above its melting point. Thus, only small quantities of semi-insulating material can be produced this way without substantial deep level doping.

Crystals of similar dimension to those achieved by LEC are possible using HB. Some advantages of HB over LEC are its lower dislocation density, usually in the $10^3 - 10^4 cm^{-2}$ range, and an easier stoichiometric control of the growth.

Another type of normal freezing is being studied at the moment, the liquid encapsulated vertical Bridgman (LE-VB). Undoped semi-insulating crystals, of the same dimension and of the same characteristics as those produced by LEC, have been grown [28] using this approach. By complete liquid-encapsulation of B_2O_3, the contamination of Si has been prevented, with this time the apparition of EL2 traps at the concentration of $1.3\text{x}l0^{16}$ per cm^3 [29].

As was the case for semi-insulating substrates, the preferred normal freezing method to grow conductive wafers is the horizontal Bridgman. Because of the natural Si contamination occurring during growth in HB, it is the most favored way of growing bulk Si n-type $GaAs/InGaAs$ crystals. P-type crystals using Zn as dopant is also quite common. Again, low dislocation density (under $10^4 cm^{-2}$) is perhaps the main advantage of this method

which tends to lose more and more of its importance.

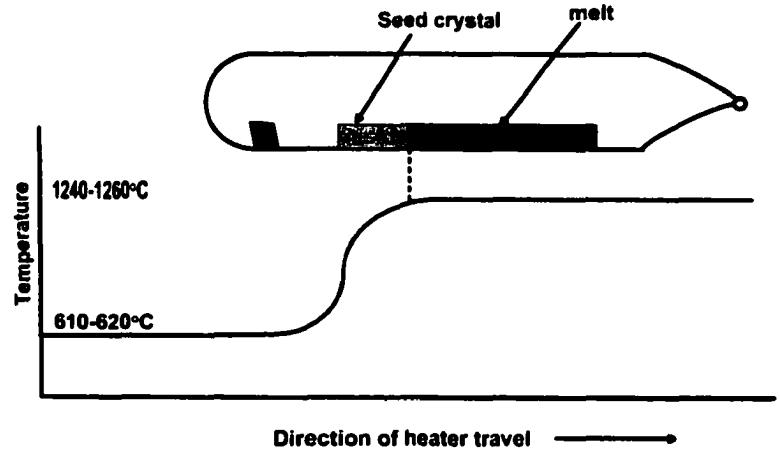

Figure 3.2. *Schematic of horizontal Bridgman apparatus*

3.3.4 Disadvantages of Melt Growth Techniques and Phase Diagrams

The major difficulty which is common to all melt growth techniques is related to materials and their phase diagrams. For a melt growth to achieve the best result, the material should have a congruent melting point, or in other words, the stoichiometric composition of the solid be in equilibrium with the same composition for the melt at the melting temperature. If this is not the case a stoichiometric crystal cannot be grown from a stoichiometric charge. To grow a crystal of uniform composition, a solid with a composition corresponding to that of the congruent melting point will have to be used. In the case of $GaAs/InGaAs$, the congruent melting point is somewhat As-rich.

The biggest disadvantage in melt growth techniques is the difficulty of growing ingots which are of constant composition and are single crystalline. $InGaAs$ ingots suffer from compositional grading along the growth axis or only have short single crystal regions with the majority of the ingot being polycrystalline. Worse yet, many are affected by both.

The pseudobinary $InGa$-$GaAs$ phase diagram (figure. 3.3) reveals that although solid solutions exist over a full composition range, there is a large separation between the solidus and liquidus lines. This large separation implies that a solid in equilibrium with the liquid solution will have a higher In content. The points labeled A and B in figure 3.3, illustrate the large concentration differences between a liquid and solid in equilibrium. The figure

shows that at 1160°C, a liquid (point A) with approximately 40 mol % In is in equilibrium with a solid (point B) which contains only about 6 mol % of the impurity in the melt and in the solid generally differ at a given temperature. The ratio of these solubilities is expressed by the equilibrium segregation coefficient:

$$K_o = \frac{C_s}{C_L} < 1. \tag{3.1}$$

where C_L is the impurity concentration in the liquid and Cs is the concentration in the solid. With $InGaAs$, on the $GaAs$ side of the phase diagram, In can be considered as the impurity. The literature reports that for In in $GaAs$, K_o varies between 0.13 and 0.22. When the segregation coefficient is less than one, only a fraction of the impurity concentration in the melt is actually incorporated in the growing crystal. The rejected fraction effectively increases the concentration in the melt, which forces the concentration in the solid to increase also (for a given value of K_o). The normal freezing relation describes the distribution of impurities along the length of a Cz grown crystal, as:

$$C_s = K_o C_o (1 - X)^{k_0 - 1}. \tag{3.2}$$

The model assumes that the impurity is uniformly distributed throughout the melt and that it arrives at the solid-liquid interface in the same concentration that exists in the melt. However, as solidification occurs, the impurity segregation creates a boundary layer at the solid-liquid interface. This boundary layer will contain either an enhanced or depleted concentration of solute, depending on whether K_o is greater or less than one. In either case, the assumption of a uniform melt distribution is invalid and so an effective distribution coefficient, K_{eff}, should be used:

$$K_{eff} = \frac{K_o}{[K_o + (1 - K_o)e^{(\frac{-vd}{DL})}]}. \tag{3.3}$$

where k_o is the equilibrium distribution coefficient, v is the growth rate, d is the width of the boundary layer, and DL is the diffusion coefficient of the solute in the melt.

The continual increase in In concentration in the melt during crystal growth, also causes an additional problem for crystal growers, known as constitutional supercooling.

The rejection of solute by the growing crystal causes a reduction in the freezing point in the melt adjacent to the interface, causing a temperature gradient in the melt. The gradient can cause the bulk of the melt to become supercooled and unstable. Constitutional supercooling is a major problem because the temperature instability will initially cause cellular growth and ultimately lead to polycrystallization.

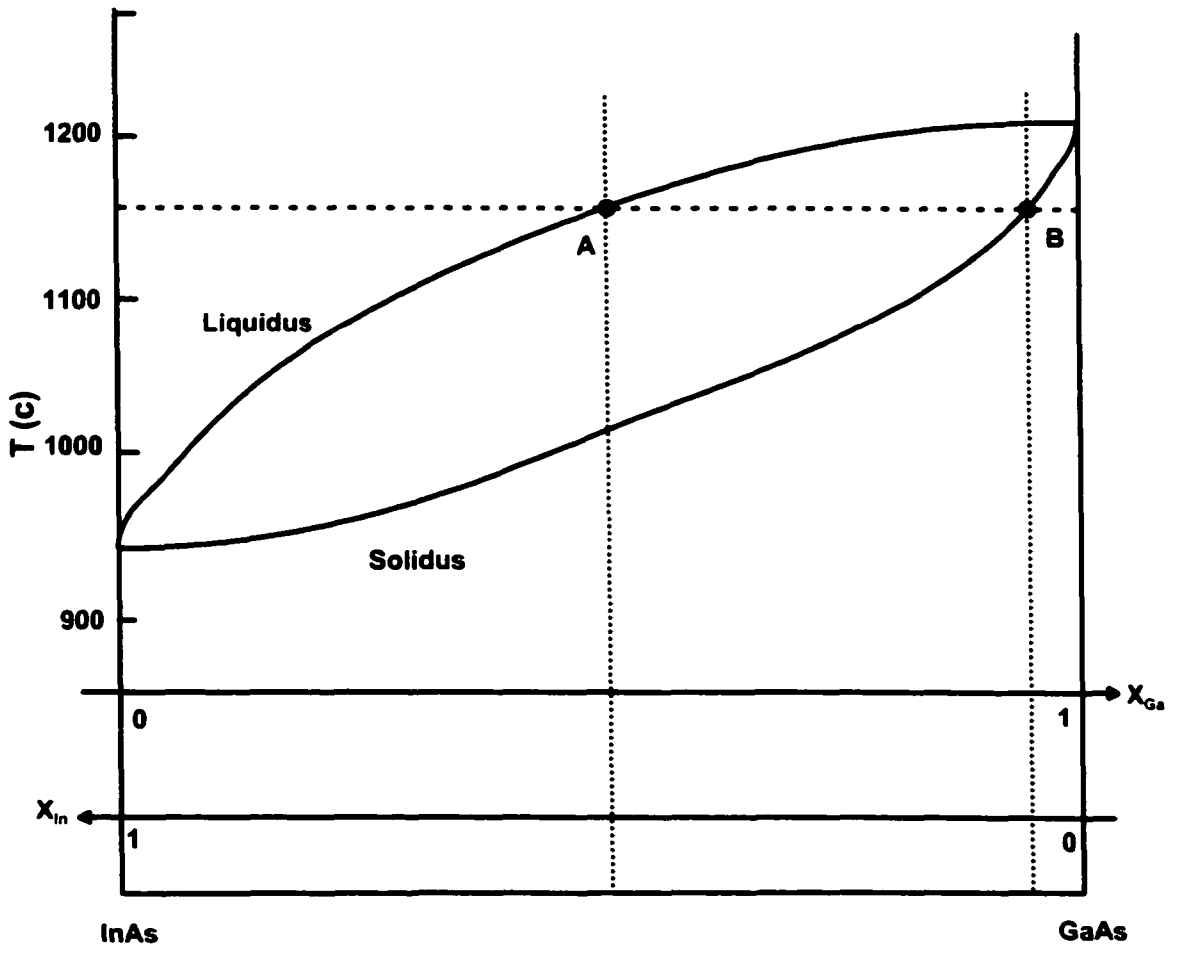

Figure 3.3. *InGaAs phase diagram.*

Another disadvantage of *InGaAs* ingots is the fact that it is common for the ingots to have stress fractures which encourage breakage at sawing operations. This makes it difficult to obtain whole wafers, which are required for wafer processing. Moreover, handling the wafers can also be problematic because the wafers break so easily due to their fragile nature. Post-growth whole boule annealing is reported to eliminate the stress fractures.

3.4 Solution Growth Techniques

In solution growth, the stoichiometry of the crystal is not respected in the liquid phase. One of the components is used as the solvent, and the other (or others) is present as the solute. The main advantage of these methods over the melt growth methods is that the solute usually crystallizes well below its melting point ($650^oC - 950^oC$ in the case of $GaAs/InGaAs$) and, thus lowering the requirements for the heaters.

Solution growth is normally not considered as being a bulk growth technique due to its low growth rate (under 4 μm per minute). Still, with liquid phase electroepitaxy (LPEE), high quality crystals of over 4 mm in height have been grown recently [1], large enough to be considered as bulk crystals. Taking this accomplishment as preliminary justification, we will first discuss Travelling Solvent Techniques (TSM), and then Liquid Phase Epitaxy (LPE), and finally LPEE. Since the present study involves LPEE growth, LPE is not a bulk growth method, but its study will be of help since LPEE is a special version of LPE.

3.4.1 Travelling Solvent Techniques

The Travelling Solvent Techniques can be divided into two main groups, the Travelling Solvent Method (TSM) and the Travelling Heater Method (THM). The first one was introduced by Pfann[30], who called it Temperature Gradient Zone Melting (TGZM). However, in Pfann's original meaning a melt, and not a solution, was used for TGZM. THM for III-V compounds was first introduced by Broder and Wolff [31]. They grew GaP from a Ga solution at a growth temperature of about 1000^oC. In TSM no moving parts are necessary, whereas in THM either a moving ampoule or a travelling heater can be used.

In III-V semiconductor growth and technology, TSM has sometimes been used in the preparation of small-area well-defined crystals and large-area abrupt rectifying p-n junctions. On the other hand, THM is better suited to the growth of large single crystals of well-defined form. For this reason, the THM method only will be covered in this section.

3.4.1.1 The Travelling Heater Method (THM)

Figure 3.5 shows the principle THM arrangement. The solvent zone, which is placed between a solid seed and the feed material, is heated by a special heater (electrical resistance heater[30]), direct RF[32] coupling, laser heating or mirror furnace facility. By moving the

charge with respect to the fixed heater (3.5), crystallization at the advancing seed/solvent interface can be achieved. Simultaneously, feed material is dissolved at the feed/solvent phase boundary. The solute transport in the liquid zone may be established by diffusion and/or convection.

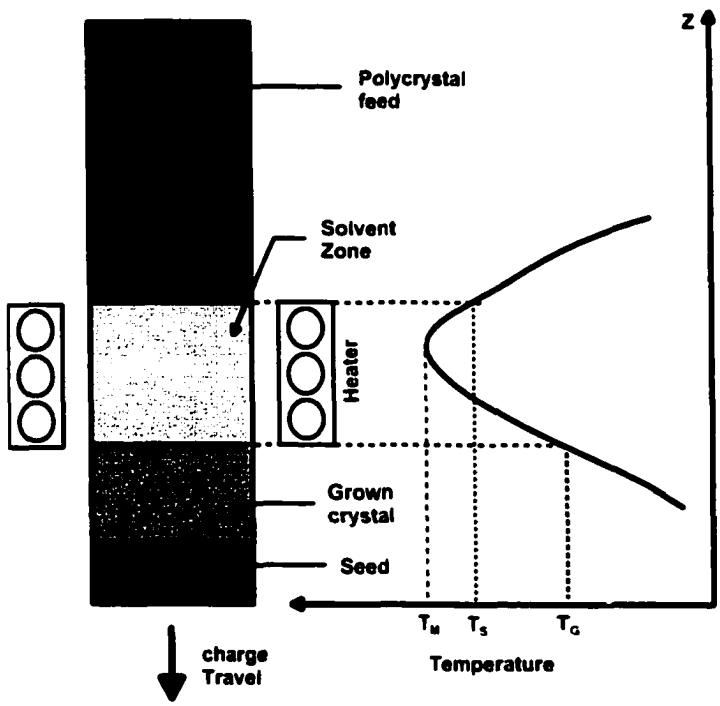

Figure 3.4. *Schematic of THM arrangement.*

THM growth has been applied to various III-V compounds, e. g., $GaAs$ [30], GaP [31] $GaSb$[32] $InSb$ and InP [31], as well as ternary compounds [30].

Before a growth experiment is conducted, the knowledge of the axial and radial temperature distribution during crystal growth might be very helpful. This is because the shape of the seed/solution interface influences the quality of the growing crystal. For longer solution zones the seed/solution interface becomes concave, where for shorter zones it becomes convex. In order to prevent undesirable seeding during crystal growth, the interface should be convex curved, especially in the immediate vicinity of ampoule wall. Therefore, a short solution zone with a long heater is desirable. A large temperature gradient at the interface implies a short heater (in order to prevent constitutional supercooling and to achieve fast growth rate). The best configuration must be determined for each different crystal-solution system.

A limitation of THM is the low growth rate, typically over an order of magnitude less than those associated with melt growth techniques. The growth rate for $GaAs$ and $GaAlAs$ are less than 5 mm/day [32]. THM-grown material exhibited a greater compositional uniformity than melting techniques.

3.4.2 Liquid Phase Epitaxy (LPE)

LPE refers to the growth of semiconductor crystals from a liquid solution at temperatures well below their melting point 1200°C. This is made possible by the fact that a mixture of a semiconductor and a second element has a lower melting point than the pure semiconductor alone. Thus, for example, the melting point of a mixture of $GaAs$ and Ga is considerably lowered from 1238°C, the melting point of pure $GaAs$. The actual melting point of the mixture is determined by the proportion of the constituent Ga and $GaAs$.

For example, in the growth of $GaAs$, LPE is commenced by placing a $GaAs$ seed crystal in contact with a solution of liquid Ga and $GaAs$ which is molten at a temperature below the melting point of the seed. As the solution is cooled gradually, a single crystal $GaAs$ begins to grow on the seed leaving a Ga rich liquid mixture with an even lower melting point; further cooling causes more $GaAs$ to crystalize on the seed.

By this technique single crystals can be grown at seifficiently low temperatures to avoid the problems associated with impurity introduction at temperatures near the melting point of the crystal. It is particularly useful for growing III-V compounds based on Ga and In as these metals form solutions at conveniently low temperatures. LPE remains a successful production technique for structures that do not require thin, uniform and high quality epitaxial layers needed for microwave devices. The rate of the process itself is largely limited by the diffusion of the solid forming species in the solution. The epitaxial layers are often very pure because the dilute solution and favorable segregation coefficients keep the unwanted impurities out of the freezing process.

LPE is practiced in three major ways: tipping, dipping, and sliding. The first growth systems explored were the tipping device [32] in 1963 and the dipping device [16] in 1967

In liquid phase epitaxy, a dilute solution is put in contact with a seed or substrate, which can be of different composition than the grown epitaxial layers. The temperature of the system is then cooled, forcing solute and solvent to slowly crystallize on the seed.

As for the apparatus, the crucible confining the solution and the substrate is certainly

the heart of the system. The crucible needs to be designed to provide means of holding the substrate and moving it into and out of the solution. Also needed are a well-controlled furnace, a reactor tube, usually made out of quartz, and a gas-handling system, since high purity hydrogen is the standard gas to prevent oxidation during growth.

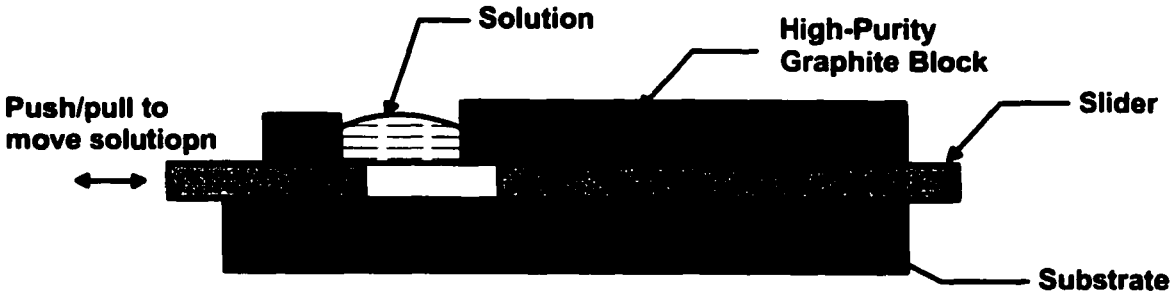

Figure 3.5. *Schematic of LPE "Sliding boat" crucible.*

The most important parameters in LPE are the starting temperature, which will determine the equilibrium concentration of the materials in the solution, and the cooling rate, which affects the growth rate and the quality (dislocation density, maximum height) of the grown crystal. Some other parameters of importance to achieve a high quality crystal growth using LPE are the temperature distribution in the solution, the crucible materials and geometry, and the level of impurities in the initial solution.

The growth temperatures in LPE range from about 350^oC to about 900^oC. In many cases, temperatures at which LPE layers are deposited are lower than corresponding temperatures in VPE processes. LPE growth rates are nevertheless high enough for efficient layer production. Growth rates usually few μ per min . A low temperature, combined with a moderately high growth rate, reduces the danger of contamination in the growing layer.

III-V Compounds, when grown by LPE, usually have fewer unwanted recombination centers for a given doping level than are present in $GaAs$ when it has been prepared by other growth techniques . The density of point defects, such as traps and nonradiative centers in luminescence, has been reported to be lowest in LPE material . This explains the high efficiency of many LPE-grown optoelectronic devices . High-purity LPE layers of $GaAs$ and InP have also proved successful in their application to microwave devices. Low growth temperature and high growth rate make LPE an economical means for the preparation of high-quality layers. These findings justify further efforts to develop LPE

techniques from small- scale laboratory a applications to large-scale commercial semiconductor growth operations.

3.5 Vapor Phase Growth

In vapor phase growth, the transport of the nutrient occurs through the vapor phase. Deposition from the vapor phase is in most cases the preferred technique for the fabrication of thin layers of high quality crystals, mainly because it offers maximum control of properties such as thickness and composition. The drawback of these techniques is their very low growth rate (under 1 μm per minute), which makes them unsuited for the growth of bulk crystal. Thus, they will not be discussed in detail in this study.

3.5.1 Metal Organic Chemical Vapour Deposition -MOCVD

This involves the forced convection of the metal organic vapour species over a heated substrate [33]. Those molecules striking the heated crystal release the desired species, resulting in crystal growth. The chemical process involved is quite simple in that an alkyl compound for the group III element and a hydride for group V element decompose in the 500^o to 800^o temperature range to form the III-V compound semiconductor.

Excellent uniformity in layer thickness, composition and carrier concentration are all achieved over a large area wafer using the MOCVD growth technique. This technique also easily lends itself to the growth of abrupt heterointerfaces. From a manufacturing / mass production perspective, MOCVD offers high through put while retaining the other desirable properties thereby making it a very promising choice [34].

3.5.2 Molecular Beam Epitaxy -MBE

At its simplest, MBE is a refined form of vacuum evaporation [34]. The molecular beams are produced by evaporation or sublimation from heated liquids or solids contained in crucibles. At the pressures used in MBE equipment, collision free beams from various sources interact chemically on the substrate to form an epitaxial film. The ability to start and stop a molecular beam by controlling the shutters attached to the vapour containing crucibles

in (typically 0.1 to 0.3 second) less than the time taken to grow a monolayer (typically 1 second) has led to the ability to produce complex multilayer structures.

MBE requires conventional ultra high vacuum (UHV) techniques and, in addition, the pressure in the system has to be low enough (usually 10-11 Torr) to ensure that no gas phase collisions occur. Thus homogenous reactions, which can occur in MOCVD, are completely avoided and the process is determined entirely by heterogeneous reactions on the substrate surface. The sample is held at a relatively low temperature (app. 500°C for $GaAs$) during epitaxy.

Despite the need for a sophisticated setup, the versatility offered by the MBE technique renders it attractive for many applications. In addition it offers precise control of film thickness, composition and doping. $AlGaAs/GaAs$ heterojunctions with atomically abrupt interfaces are readily obtained. However, the major disadvantages associated with MBE include high cost because films are usually grown one layer at a time. In addition, so called 'oval defects', which can be fatal for base- emitter junction of HBTs, are found at densities of a few hundred per cm^2; these defects are a primary factor limiting the yield of HBT circuits. Although extensive use has been made of MBE growth in HBT research, the quest for increased wafer through put and improved surface morphology continues [34].

Chapter 4

Liquid Phase Electroepitaxy (LPEE) and Existing Problems

4.1 Introduction

In liquid phase electroepitaxy, the set-up is quite similar to the one used by LPE, except that the growth is initiated and sustained by passing a direct electric current across the substrate-solution interface while the overall furnace temperature is kept constant. A major advantage of LPEE over LPE is that while the growth is limited to the amount of solute present in the solution in the latter, in the former the growth may be sustained by the incorporation of a source material. The source dissolves while the growth is performed on the substrate, thus developing into a pseudo-steady state process, driven by *DC* current.

The use of *DC* current adds somewhat to the complexity of the apparatus. Two electrodes are added to the system and a perfect electrical contact must be obtained between the bottom electrode and the substrate. The failure of achieving a uniform contact at this interface will result in non-uniform growth. Also, electrical insulation between the various parts of the crucible must be thought of. Every other aspect of the growth apparatus can be similar to those used in LPE. A typical LPEE growth cell is shown in figures 4.2 and 4.4.

On top of the various factors influencing the growth for LPE, the results achieved in LPEE are closely related to the intensity of the current applied to drive the growth. The current is the source of electromigration for solute species, and also causes Peltier cooling and Joule heating, both of which result in temperature differences within the solution, thus determining the flow patterns caused by convection. The current intensity influences the growth rate, the quality of the epitaxial layers, the doping level, and the maximum thickness obtainable before losing the integrity of the crystal.

4.2 Liquid Phase Electroepitaxy: Methods, Apparatus, Literature Reviews and Procedure

Liquid Phase Electroepitaxy (LPEE) is a relatively new, very promising technique successfully used to grow bulk compound and alloy semiconductor crystals with encouragingly good structural and chemical properties [35, 36, 37, 38]. It is a solution growth technique, in which a solution is sandwiched between a source (usually a low quality polycrystalline semiconductor), and a substrate (usually a high quality single crystal semiconductor). Crystallization on the substrate, simultaneous with the dissolution of the source, is initiated and sustained by applying a direct electric current across the substrate-solution interface while the temperature of the overall system is kept constant, well below the melting point of the semiconductor (in the order of $750 - 900^0$C). The applied DC current is the sole driving force of the growth process.

Procedure

In a typical LPEE growth system, graphite electrodes are placed at the top and bottom of the growth cell (figure. 4.1). The substrate is placed at the bottom of the solution and the source material is placed between the solution and the upper electrode. The contact zone located below the substrate provides a uniform, low resistance electrical contact between the lower face of the substrate and the lower electrode, which is essential for satisfactory growth. The boron-nitride "jacket" around the horizontal sandwich layers forms the cell and acts both as a heat conductor and as an electric insulator.

The furnace is heated to a growth temperature in the range of $750^oC - 900^oC$. After the system reaches a thermodynamic equilibrium, the electric current is turned on and the growth is initiated. During the growth process, the furnace temperature is kept constant. The applied electric current is the sole external driving force and the controlling element of the growth, and makes it possible to achieve high growth rate and precise control of the process. The electric current passes through the lower electrode, contact zone, substrate, but may bypass the source material into the upper electrode (depending on the setup, see figure 4.2). In SETUP 1 the electrical current pass through the source material. In this case the Joule heating is high. This will affect the intensity of the convection in the solution

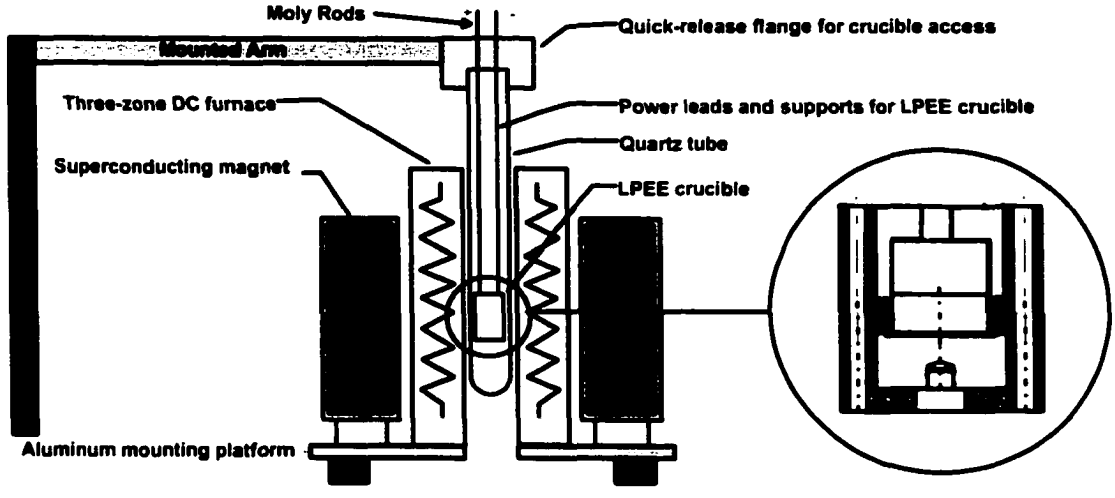

Figure 4.1. *Schematic view of platform for LPEE growth under magnetic field.*

which can limit the thickness of the grown crystal. In the second configuration (SETUP2) the electric current bypasses the source material. In this setup the electric current

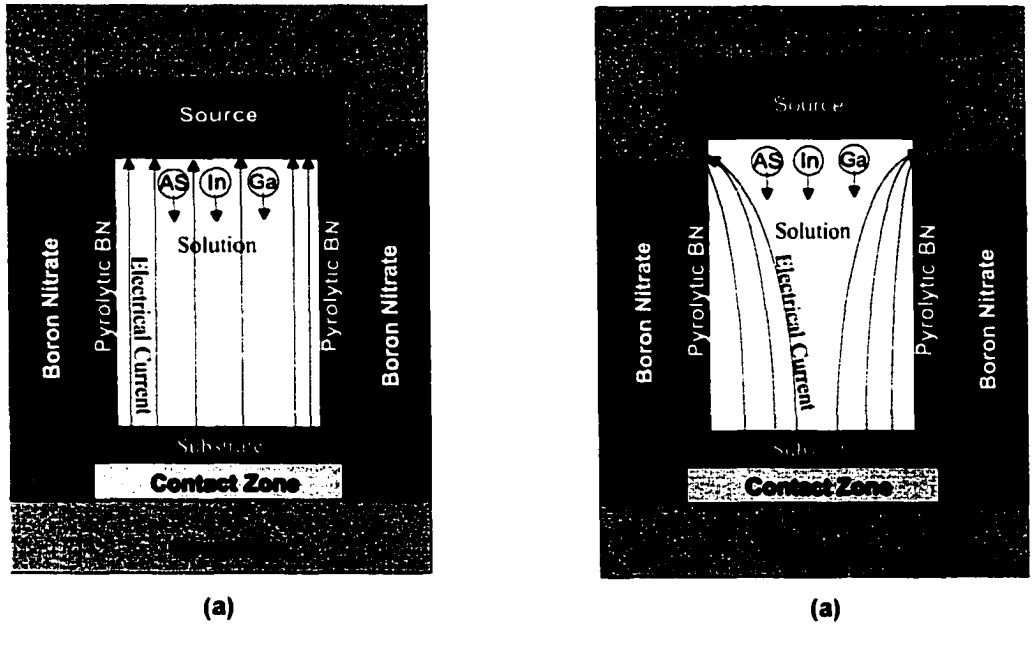

Figure 4.2. *Schematic view of an LPEE growth cell. a) Electric current passes through the source, b) electric current bypasses source.*

in the solution is not uniform, causing non-flat growth layers.

Literature Review

The use of electric current to generate growth in LPE was introduced in the early seventies. At that time, the study in [39] was the first to experiment it on a system in which the solution-substrate interface was crossed by a direct current up to 5.5 A/cm^2. High density current pulses were also used to produce striations in the crystal, useful for determining the growth rate of the crystal experimentally. No source material was used, and crystals of a maximum of 25 μm in thickness were achieved.

In its first stages of development, LPEE was referred to as the Peltier cooling induced LPE, since it was believed that this cooling was the sole mechanism responsible for the growth. Because of that, much attention was given to Peltier heating and Joule heating, both of which can counteract the Peltier cooling. In cases where the substrate is too thin, the Peltier heating at the back of the substrate can offset the Peltier cooling at the growth interface [40]. Where the substrates are too thick, an excessive amount of Joule heating will take place. [41] have developed an AC/DC method to neutralize this effect. In this method, an AC current is applied to provide a constant Joule heating, while a DC current is superimposed to provide the cooling at the interface.

Later on, the emphasis was placed on the geometry and materials of the LPEE crucible. Concerning the geometry, [41] argued that if the current is fed from the sides of the solution well, instead of on top of it, the density of current in the middle of the substrate will be lower, thus resulting in an uneven crystal growth. Lawrence et al.[41] insisted that the surface quality is subject to two conditions: i) a uniform substrate conductivity, and ii) a uniform electrical contact on the back of the substrate. A thicker substrate lowers the importance of this second condition. Jastrzebski et al. [42] studied the effect of the size of the graphite pedestal for the substrate. Pedestals of smaller diameter than the solution well cause an increase in thickness in the center of the crystal, with an opposite effect for larger pedestals. The position of the electrodes also influences the shape of the grown crystal. For example, in the case of the crucible shown in figure 4.3, the growth will be thicker on the right-hand side of the substrate, due to the electrodes being on that side.

As for the crucible materials, most researchers have used boron nitride (BN) for the electrically insulating parts of the crucible, and high density graphite for its conductive parts [43, 42, 40]. [44, 45] have use pyrolytic boron nitride (PBN) for the insulating parts

of the crucible that were in contact with the solution. PBN is not porous as is the case for BN, thus limiting the amount of impurities transferred from the crucible to the melt. The use of a quartz tube containing the crucible and a purified hydrogen atmosphere is also standard procedure.

The electrical contact at the back of the substrate has often been noted to represent a problem. This contact must be uniform in order to achieve a quality growth. Many researchers have found that the use of a liquid contact zone was the best alternative to this problem. [40, 42] propose to use molten Ga, with a thin foil of tantalum to prevent As migration and back dissolution of the substrate (see Figure 4.3). Later on, [40] used a molten alloy of Ga (90% weight) and Al to achieve the same purpose. The presence of Al in the Ga inhibits the back etching of the substrate by lowering the saturation level of the As species in the contact zone.

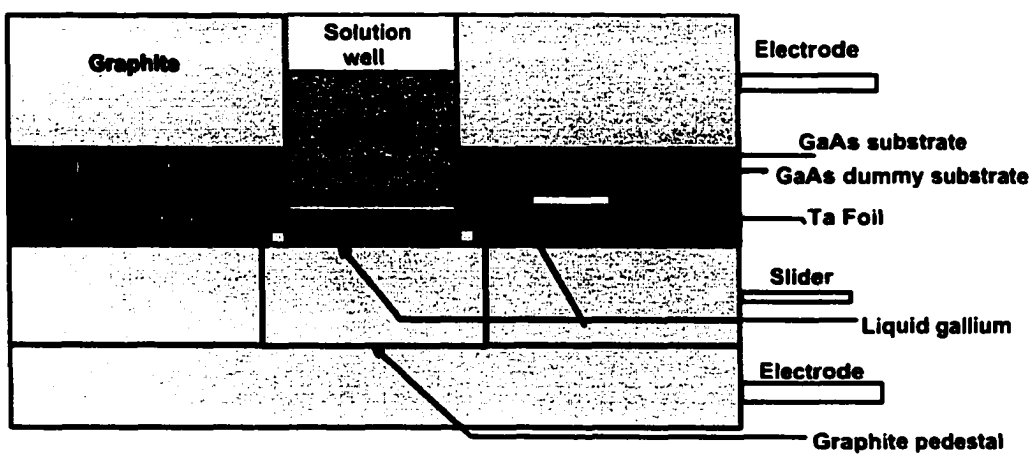

Figure 4.3. *Schematic of LPEE crucible.*

To prevent supersaturation or undersaturation conditions when the substrate is placed in contact with the growth solution, many apparatus were designed with a dummy substrate [44, 46, 42]. In these cases, the solution would first be equilibrated at the growth temperature with the dummy substrate, and then moved over the other substrate at the start of the growth. Some researchers [46, 47, 48] argue that it is better to backmelt the substrate lightly by raising the temperature of the solution by 0.5 to 5.0°C prior to the growth. This is because the surface of the substrate might have lost arsenic atoms during the heating cycle, thus being non-stoichiometric.

An important development in LPEE came in 1978 when Bryskiewicz [49] proposed

to use a source material on top of the solution. Due to the Peltier heating at the source-solution interface, the temperature in the solution in the vicinity of this interface increases. This increase in temperature dissolves the source, providing the required material in the solution for a continuous growth at the substrate. Without this source material arrangement, growth of thick crystals by LPEE as is currently done would be impossible. It includes a slider and a set of solution wells, used to perform the electroepitaxial growth of multilayer structures.

It was noticed that Joule heating from the various contact regions within the crucible caused unwanted convection in the solution during the LPEE growth process [50] . To counter this, he positioned the solution well in the furnace so that the horizontal temperature gradient prior to the application of the current was of the same magnitude but opposing sign to that induced by Joule heating. This allowed a significant increase in the thickness uniformity of the grown crystal.

Most of the LPEE apparatus designed by 1986 were with a horizontal furnace configuration. Later, when it became more and more apparent that the Peltier cooling was not the only important growth mechanism involved in LPEE [49, 48], many vertical apparatus were developed [51]. The main reason for this was to maximize the temperature symmetry and uniformity, thus limiting the convection within the solution.

For the first time ever, in 1987, $GaAs$ single crystals of more than 2 mm in thickness were grown by LPEE [52, 53]. The apparatus used to achieve this is shown in Figure 4.3. In this setup, the substrate is placed at the bottom of the solution to provide a greater growth stability. The electrical contact is made out of a gallium and aluminum alloy which can withstand a current of up to 10 A/cm^2 for over 100 hours. It was suggested that the best current density to use for the growth is around 5 A/cm^2; higher current densities cause instabilities to appear at the crystal's surface. With the use of a heat pipe, placed between the furnace and the quartz tube to increase the stability and uniformity of the temperature, crystals of up to 5 mm thick and 25 mm in diameter were obtained. This same apparatus was later used to grow bulk ternary alloy crystals of $InGaAs$ ($0 < x < 0.09$) [54]. The source material used in this case was of the same composition as the grown crystal.

4.3 Thermoelectric Effects and Growth Mechanisms

In the LPEE technique three main solute transport mechanisms are responsible for crystal growth [55]: i) diffusion due to Peltier cooling at the substrate-solution interface, ii) electromigration due to the electrostatic field and momentum exchange between the electrons and the solute species [55], and iii) natural convection due to gravity and/or Marangoni effect [6]. Due to their importance in LPEE we discuss below some well-known definitions and concepts in detail.

In a well-designed LPEE apparatus, vertical and horizontal temperature gradients outside the crucible are effectively minimized. Thermal effects that may lead to temperature gradients in the solution (in the crucible) may then be assumed to be solely due to Peltier cooling/heating and Joule heating. Peltier cooling/heating is a thermoelectric effect caused by the electric current passing across the substrate-solution and the substrate-contact zone interfaces, refer to figure 4.4. This current causes heat absorption or heat evolution at the interfaces, depending on the current direction. In an equilibrated LPEE system with a positive polarity of the lower electrode, Peltier cooling occurs at the substrate-solution interface and is accompanied by Peltier heating at the substrate-contact zone interface. Thus heat transport across the substrate affects the amount of cooling at the growth interface. Indeed, the amount of cooling at the growth interface increases with increasing substrate thickness. Being a semiconductor, the substrate has a high electric resistivity. The electric current passing through the substrate induces Joule heating proportional to the square of current density and electrical resistivity (Joule heat produced in the solution and graphite electrodes is at least an order of magnitude lower because of the low electric resistivity). The effect of Joule heating in the substrate increases with increasing substrate thickness and becomes significant for bulk crystals.

One of the two main growth mechanisms of LPEE is known as "electromigration". In the growth of III-V compounds or alloys, the solutions are metallic conductors. In such solutions, electromigration takes place due to electron-momentum exchange and electrostatic field forces [56]. Under the influence of the electric field induced by the electric current, solute species migrate towards the anode with a velocity proportional to solute mobility and electric field. Thus, when the substrate has a positive polarity, the solution becomes supersaturated with solute near the substrate-solution interface, resulting in epitaxial growth.

The combined effects of Peltier cooling/heating and Joule heating result in an axial

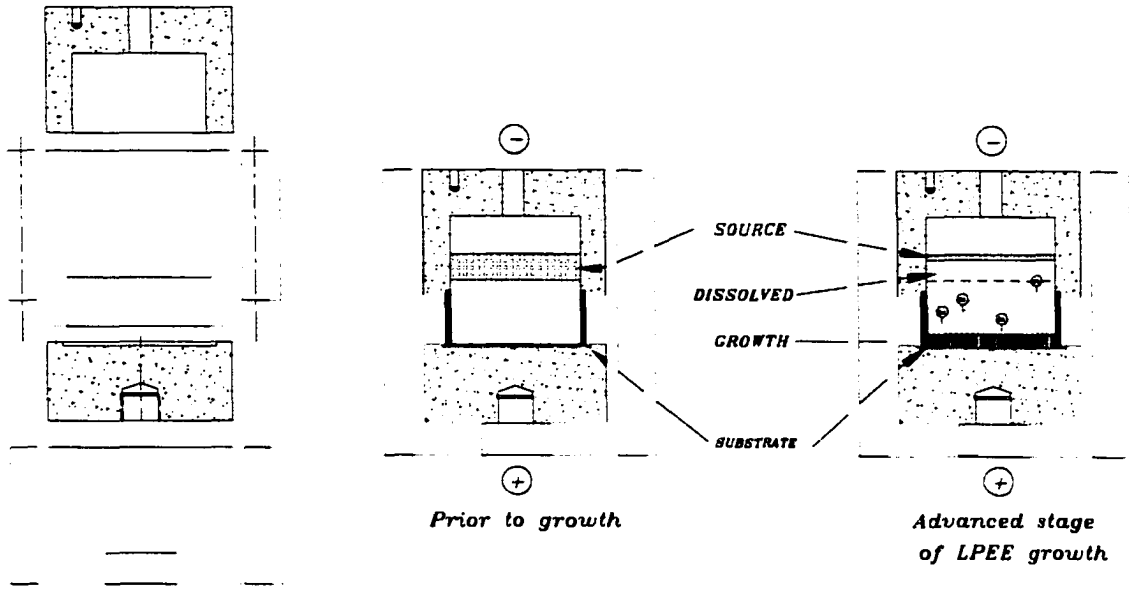

Figure 4.4. *Schematic representation of the growth cell.*

temperature gradient. This temperature gradient induces supersaturation of the solution in the vicinity of the substrate-solution interface, leading to further contribution to epitaxial growth. This is the second main growth mechanism in LPEE.

Electromigration and Peltier cooling are the two basic growth mechanisms. Either of these mechanisms can become dominant, depending on particular growth conditions [57, 58]. However, these contributions can be affected by the presence of natural convection in the solutions[59].

4.4 Convective Effects in LPEE

In crystal growth, convection influences growth kinetics, impurity incorporation, compositional homogeneity, morphological stability, and nucleation. An extensive review of the influence of convection on the growth of crystals from solution was presented by Wilcox [56]. Convection is believed to also play an important role in LPEE.

Verhoeven discussed convection in the presence of an electric current passing through a liquid metal [32, 60], and concluded that the primary source of convection results from

horizontal temperature gradients generated by Joule heating. Daniele [41] also discussed the possible effects of convection and boundary layer formation. Later, Jastrzebski et al. [61], proposed a one-dimensional theoretical model in which they incorporated the concept of a solute boundary layer caused by convection, and investigated the effect of this solute boundary layer on solute transport. They concluded that in the presence of significant convective flow, growth in LPEE is dominated by Peltier cooling. Jastrzebski et al. [43] performed a series of experiments from which they concluded that the growth process is not affected by convective flow until the Grashof number exceeds a value of the order of 10^4. Bryskiewicz et al. [21] conducted some experiments in a configuration where convection was intentionally introduced by superimposing a horizontal temperature gradient across the solution. They observed that the layers grown in such configuration exhibits noticeable compositional inhomogeneities along grown layers. Isozomi et al. [44] have observed experimentally that after the current density exceeds a particular value, the linear relation between growth and dissolution rates and current density is no longer valid. This was attributed to the convection caused by increased Joule heating.

In [62] where bulk $GaAs$ crystals were grown by LPEE, Bryskiewicz et al. observed the presence of a critical crystal thickness for a given current density above which the growth becomes unstable. They stated that the maximum achievable is limited by convection, and depends on Joule heating. Bryskiewicz et al. observed that the maximum thickness achieved in their experiment is much smaller than that calculated in [61], and pointed out that possibly convection was present in their system even before the Joule-heating-induced convection began.

This short review of historic developments in LPEE research shows that the relative contributions of electromigration, Peltier cooling, natural convection, applied current density, substrate thickness and diameters etc., are still not well understood.

The effects of convection have been observed in various experiments. It enhances the overall transport processes, and thus increases crystal growth rate, which is desirable. In the presence of significant convective flow, the growth in LPEE may be dominated by Peltier cooling [57, 59, 63]. However, it is well known that convection has often an adverse influence on growth kinetics, and the structure and quality of grown crystals [56]. It has been observed that convective flow, resulting from both thermal and solutal gradients, leads to the growth of $GaAs/InGaAs$ layers with non-uniform thickness profiles [64]. Further-

more, convection has been found to limit the maximum achievable thickness in bulk crystal growth experiments [65], due to a deterioration in the surface quality caused by unstable growth conditions.

In the growth of alloy semiconductors, convection adds another dimension to the difficulty of the problem [66]. In most alloys, densities of each component are significantly different. This difference in the presence of the gravitational field gives rise to the inhomogeneity in the composition of the liquid solution during growth. In other words, the gravity makes it difficult to maintain the solution with uniform liquidus composition. Less dense component(s) moving upwards leads to the depletion of the required component(s) in the vicinity of the growth interface, leading to unsatisfactory growth. For example, in the case of $GaInP$, phosphorus, with the smallest density, tend to float.

A number of techniques have been implemented to overcome difficulties caused by the gravitational field in ground-based experiments[67, 68]. One of these techniques is the applied magnetic field.

4.5 Application of External Magnetic Field

A number of experimental investigations have been conducted to reduce the adverse effect of convection by various means such as configuration stabilization [8], reduced gravitational field [9], and applied magnetic field [6, 10]. However, there are no published results that contain detailed experimental work on LPEE growth under magnetic field. Among the available techniques for suppressing natural convection, the application of external magnetic field seems the most feasible one. The application of an external magnetic field to an electrically conductive liquid solution induces an electromagnetic body force which tends to reduce the intensity of convection.

Simulation results from [69] without an external magnetic field are given in figure 4.5. The temperature difference in the growing direction (vertical) at the liquid zone center is higher than that at the crucible wall. The temperature gradient along the interface is higher near the wall. As a result, the convection flow pattern shown in figure 4.5 is observed in the region near the wall, given rise to stronger convection mass transfer there. In the center region of the liquid zone the effect of fluid flow is not significant, thus the mass transport in this region is almost driven by diffusion due to the temperature difference between the two

interfaces. Relatively different contributions from the diffusion and convection transports in different region bring about nonuniform growth across the growth interface. The results of the numerical simulation under external magnetic field of 20 KGauss are presented in figure 4.6. As can be seen from the figure, the convection was suppressed significantly, about 1000 time less. The velocity profile is almost uniform everywhere except at the wall. As a result, the shape of the grown crystal is almost perfect.

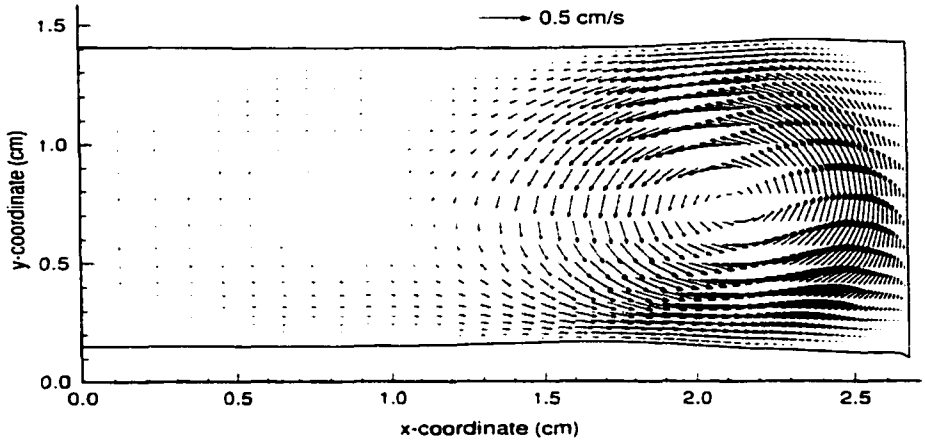

Figure 4.5. *Velocity field in the absence of external magnetic field (B=0).*

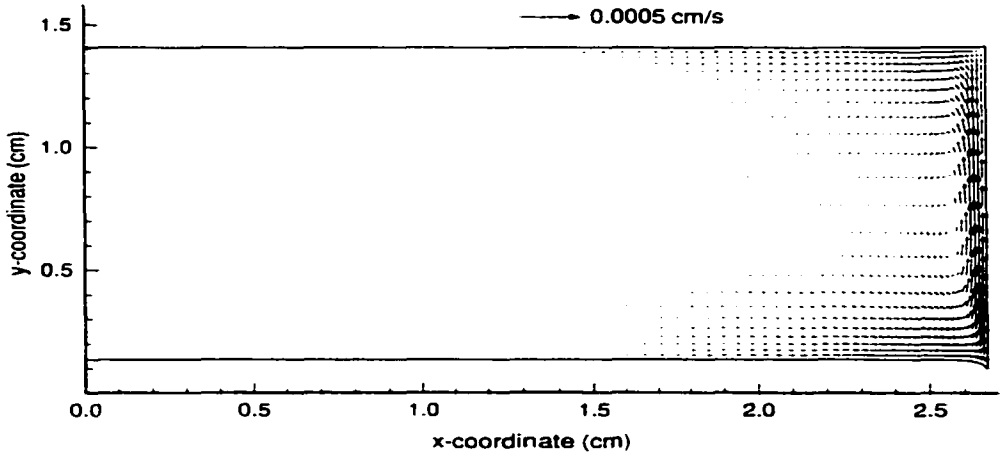

Figure 4.6. *Velocity field in the presence of external magnetic field (B=20 KGauss]*

Numerical simulations were carried out for the liquid phase electroepitaxial (LPEE) growth process of ternary alloy $InGaAs$ under external magnetic field [70]. The governing field equations together with appropriate interface and boundary conditions are solved numerically by the Finite Element Method for the growth cell configuration to be used in

our laboratory. Results show the feasibility of suppressing the natural convection in solution by the application of an external magnetic field. A field of 20 KGauss is sufficient to reduce the effect of gravity significantly.

4.6 Growth of Bulk Crystals by Liquid Phase Electroepitaxy

LPEE was used to grow thick epitaxial layers of $Ga_{1-x}Al_xAs$ (up to 1.4 mm) [71] for the first time. The experiments were performed in an apparatus similar to that described in [49] and [51], and it was observed that thick segments of epitaxial layers (up to 600 μm) of extremely uniform aluminum composition were produced.

LPEE experiments show that growth of bulk crystals is distinctly different from the growth of thin crystals. As Bryskiewicz et al. [51] pointed out certain additional problems were encountered in growth of bulk crystals which are not necessarily of significance in the growth of thin layers. For example, in scaling up the growth cell, convection interference (both solutal and thermal), must be maintained as low as possible. The electrical contact to the substrate should withstand current flow at high temperatures for extended periods of time, and the effects of Joule heating should be minimized. In their vertical apparatus, especially designed for bulk crystal growth, the furnace was equipped with a heat pipe to maximize the uniformity and symmetry of the temperature distribution within the process tube. The seed was positioned beneath the solution to reduce solutal convection, and in order to minimize Joule heating, a cell configuration with the $GaAs$ source being bypassed by an electric current was used. With this system, bulk $GaAs$ crystals with several millimeters thickness (up to 4 mm thick and 20 mm in diameter) and electrical properties comparable to those of thin LPE layers and far superior to those of melt-grown $GaAs$, were grown. They have also observed an upper attainable limit in thickness as a result of convective flow enhanced by thermal gradients introduced by Joule heating. Boucher et al. [52] have found no new dislocations generated during LPEE growth, as claimed in [62], and observed that the dislocation density, present in the substrates, is sharply reduced in LPEE bulk crystals. They stated that up to 95 % of the substrate dislocations do not propagate into the LPEE bulk crystals, and that the magnitude of dislocation removal is independent of growth parameters, but does depend critically on the thickness of grown crystal.

Thus, they pointed out that no dislocation removal takes place in crystals with thickness below 60 μm whereas for thicknesses larger than 60 μm rapid dislocation removal takes place. Bryskiewicz et al. [49], analyzing the surface morphology of the crystals grown by the LPEE system, have observed that in addition to the convection the wetting of the growth cavity by Ga-As solution provided another factor limiting the stable growth and the thickness of LPEE $GaAs$ bulk crystals. In these experiments, enhanced nucleation due to wetting, had caused the formation of polycrystalline edges and a dendritic growth. This problem was solved by modifying the growth cell to lower the growth velocity near the edges of the growth crystals, and it has been observed that in most cases, polycrystalline regions at the edges vanished completely. Thus, they achieved stable growth of one inch diameter high quality $GaAs$ bulk crystals thicker than 4 mm.

One must therefore examine the effect of such strong magnetic field on various phenomena involved in LPEE, through carefully designed experiments and to reduce the effect of Joule heating to minimum. This is the subject of this research. The aim is to determine the optimum growth conditions for reproducible high quality bulk ternary crystals for industrial applications.

4.7 Quality of Crystals Grown by LPEE

To the best of our knowledge, at this moment, no semi-insulating substrates have been grown by LPEE. The reason for this is quite simple: as we have seen, not until the results achieved by Briskiewicz et al. in 1986 was LPEE ever considered a possible method for the growth of bulk crystals [51]. LPEE was always used to grow epilayers on top of existing substrates grown by some other method, usually HB or LEC. And electronic applications and devices, as we have seen earlier, do not require the growth of a semi-insulating epilayers on top of a substrate; thus the use of LPEE is the only option to produce conductive layers.

Some advantages noted for the LPEE method include:

- Growth of highly homogeneous materials, with variations in impurity concentration within the crystal well under 10 % in most of the cases [48, 49].
- The absence of terracing or striations [49].
- Very low dislocation density, usually under 10^3 cm^{-2}, and often under 10^2 cm^{-2} [46, 52].

- Stoichiometric growth [52].
- Possibility to grow various geometries, not limited to a circular shape like in LEC. Bryskiewicz has growth rectangular shape 1.2 x 5.0 cm^2

On the other hand, some limitations are:

- A very low growth rate, from 60 to 240 μm per hour [51, 39, 68, 52, 40, 42].
- The quality of growth, mainly the dislocation density, is influenced by the quality of the substrate. Even if many dislocations are eliminated during the growth of thick layers, the final quality of the crystal is limited by the dislocation density in the original substrate [52]. Various recombination centers, often non-radiative, have also been noted to diffuse from the substrate to the epilayer [48].
- To date, maximum produced diameter of 25 mm, with thickness close to 5 mm [53].

The relative advantages and disadvantages of using LPEE to grow bulk crystals have already been discussed above. These considerations also apply in the case of conductive $GaAs$ grown by LPEE. This section will thus only focus on the diversity and quality of the conductive substrates grown by the LPEE technique.

For n-type crystals, a wide range of different dopants, such as Si, Te, and Sn have been used. With doping varying from under $10^{15}cm^{-3}$ to over 5 x $10^{18}cm^{-3}$, very good results have been achieved [48, 45, 53, 40, 47]. For low doping (under $10^{17}cm^{-3}$), electron mobilities of up to 8400 cm^2/V-s and carrier lifetimes in the high-$10^{-7}s$ range (compared to a $10^{-10}s$ range in most cases for crystals grown by a melt technique) have been recorded. For high doping, electron mobility is typically above $6300cm^2/V$-s.

For the p-type materials, Ge is usually the standard dopant used with LPEE, with Si being sometimes used for low-level doping (remember the amphoteric properties of Si, as discussed earlier). Doping levels for $GaAs$: Ge is typically, in the $10^{18}cm^{-3}$ range, with hole mobility above $100cm^2/V$-s [46, 52, 42]. In case of Si doping, around $10^{15}cm^{-3}$, the hole mobility is found higher than $300cm^2/V$-s [51, 53]. The favored growth direction in LPEE growth of $GaAs/InGaAs$ is $< 100 >$.

Chapter 5

Semiconductor Substrates and Devices of Interest for $GaAs$ and $InGaAs$

Ternary, III-V bulk single crystals are of interest as lattice-matched substrates for a variety of homo- and heteroepitaxial applications. Close lattice matching of the substrate to epilayers avoids the need for compositional grading of layers necessary for minimizing strain and misfit dislocations. $Ga_{1-x}In_xAs$ substrates with x=0.04 are of particular interest since they are closely lattice-matched to $ZnSe$ for the fabrication of blue-emitting lasers diodes.

Major applications of immediate interest for blue laser diodes include optical data storage, very high density compact disc players, and high resolution laser color printers for which efficient blue generation is required to complement the red and green currently available.

The study of $In_xGa_{1-x}As/GaAs$ material system has attracted a lot of interest because of basic physical and material issues as well as because of promising applications of optoelectronic devices.

For optoelectronic applications, devices fabricated within the $In_xGa_{1-x}As/GaAs$ material system have a number of attractive fractures for enhanced performance and/or improved device operation. First, the device can have convenient matching of optoelectronic light sources from 0.9 to 1.7 μm, including the 1.55 μm wavelength so important for fiber optic communication. An added feature of great practical importance is the fact that the $GaAs$ substrate is transparent to the longer wavelength resonant with the interband transitions of the quantum well system. This is not a feature, for example, of the $Al_xGa_{1-x}As/GaAs$ system. This property allows suitable advantages for optical applications and reduce costs in device fabrication. Another material property is the higher photoluminescence efficiency for interband transition in $In_xGa_{1-x}As/GaAs$ quantum wells as

compared to the $Al_xGa_{1-x}As/GaAs$ material system. This last feature indicates that carrier collection is highly efficient in this pseudomorphic quantum well material system. This property is promising because it translates into high quantum efficiency for semiconductor laser and light emitting diodes (LED). Since the effective mass of $InAs$ is relatively small ($m_e = 0.027m_o$), (for comparison, $AlAs$ has $m_e = 0.10m_o$) the $In_xGa_{1-x}As/GaAs$ material system could turn out to be very important for high-speed electronic devices. Due to all these suitable advantages the $In_xGa_{1-x}As/GaAs$ material system has a high potential for novel optoelectronic devices, such as lasers, switches, detectors, and spatial light modulators, which are considered key elements for optical communication and processing.

5.1 Alloy Semiconductor Substrates for Novel Devices

Alloy semiconductors, such as $GaInAs$, $GaInP$, $GaInSb$, etc., grown on commercially available $GsAs$, $GaSb$, etc. substrates, are of interest as lattice-matched substrates for novel, semiconductor devices in optoelectronics. For instance, $Ga_{0.47}In_{0.53}As$ ternary alloy grown epitaxially on the lattice matched InP substrate has been used as active layer in lasers and photodetectors in optical communication systems [72, 73]. It is a very good candidate for high speed transistors because of its high carriers mobility. $GaInAs$ epitaxial layers-grown on $GaAs$ substrates have also been used for High Electron Mobility Transistors (HEMT) structures with significantly improved performance, and for strained-layer lasers, modulators, and detectors operating in the near infrared region [74]. For this ternary material however, only thin layers can be grown due to lattice mismatch. As a result, many problems have been observed in lasers fabricated on such substrates, and are restricted to the 0.8-1.1 μm region [75].

High performance semiconductor lasers operating in the 2-5 μm range are highly desirable in optical fiber communication systems employing low-loss fluoride-based fibers, laser radar, remote sensing of atmospheric gases, and molecular spectroscopy [76, 77]. However, currently available alloy layers exhibit a miscibility gap in the range of 2.4-4 μm [78, 55]. Availability of $InAsP$, $InGaAs$ and $GaInSb$ substrates with desired thickness and quality would overcome this difficulty. These materials and many other desired alloy semiconductors either can not be grown commercially, or grown with inadequate thickness and quality, or cannot be grown reproducibly. LPEE has proven to have the potential for

growing such crystals with desired properties.

The number of novel, high performance optoelectronic and microwave devices would increase significantly should high quality alloy substrates be available commercially. Some alloy materials which can be grown by LPEE are summarized in table 5.1 below [79].

Table 5.1. *Applications of Semiconductors.*

Semiconductor Alloys	Potential Applications
$In_{0.97}Ga_{0.03}As$ substrate	Lattice Matched $ZnSe$ Based Blue Emitters.
$In_xGa_{1-x}As$ Substrate ($0 < x < 0.30$)	Reflectance Modulators: $1.06\mu m$, $1.3\mu m$, $1.5\mu m$.
	VCSEL's: $1.3\mu m$, $1.5\mu m$.
	HEMT Structures: High Efficiency, > 2.
	FET's: Improved Power.
	Solar Cells: Improved Efficiency.
$In_xGa_{1-x}P$ Substrate ($0 < x < 0.70$)	Visible Emitters: 560-900 νm.
InP_xAs_{1-x} Substrate ($0 < x < 0.20$)	$(In.Ga)$ As Mid-IR Laser: ($> 2.1\mu m$).
$In_xGa_{1-x}Sb$ Substrate ($0 < x < 0.30$)	Sb Based Laser: ($> 3\mu m$.)
$InAs_xSb_{1-x}$ Substrate ($0 < x < 0.10$)	$ZnTe$ Based Visible Emitters.
$Hg_{1-x}Cd_xTe$ substrate	Mid- and Far-infrared detectors and lasers.
$Si_{1-x}Ge_x$ substrate	n-channel Field Effect Transistors (FETs).

5.2 Semiconductor Devices and Substrates of Interest for $InGaAs$ / $GaAs$

The real drive behind the study of the growth of $InGaAs/GaAs$ single crystals is the demand in recent applications that require the special characteristics of $GaAs$. The ap-

plications and devices, in the wide field of electronics, range from simple light emitting diodes (LED), to much more sophisticated metal-to-semiconductor field-effect transistors (MESFET) or digital integrated circuits (IC). In other fields, one can also mention the impact of GaAs on solid state lasers, medium power devices, magnetic bubble memory, and electro-acoustic devices.

$Ga_{1-x}In_xAs$ substrates with x=0.04 are closely lattice-matched to $ZnSe$ for the fabrication of blue-emitting lasers diodes. The Light Emitting Diode (LED) is one of the simplest optoelectronic devices which has found important applications as a display device as well as an optical signal generator for optical communication . We will briefly outline some of the important considerations for LEDs or Laser Diodes (LD).

To make sure there is no confusion, by substrate we mean the starting crystal upon which the other epilayers (or doped regions, using ion implantation, for example) needed to manufacture the device are then added.

5.2.1 Light Emitting Diode (LED)

A LED is made out of a simple p-n junction under forward-bias. The idea is to generate as many minority carriers as possible (electrons in the p side, and holes in the n side), and then to have them to recombine with the majority carriers. By doing so, in the case of $GaAs$, a photon of 0.85 μm (near infrared) will be emitted. $GaAs$ LEDs cannot be used for display since the wavelength is beyond the visible range. The whole spectrum from 0.85 to 0.55 μm (visible yellow) can be obtained if some of the Ga is replaced by either aluminum or phosphorus.

The substrate used for this device must be conductive, and can be of either n- or p-type (10-50x$10^{17}cm^{-3}$). To obtain a high density of emissions, it is important to achieve the highest recombination rate as possible (long lifetime would allow the carriers to drift way past the p-n junction before recombining, thus lowering the intensity of the emission), and to minimize the amount of non-radiative recombination centers. Also, to insure high reliability of the diode, and to allow a high quality growth of epitaxial layer, a low dislocation density is needed (under 10^4cm^{-2})

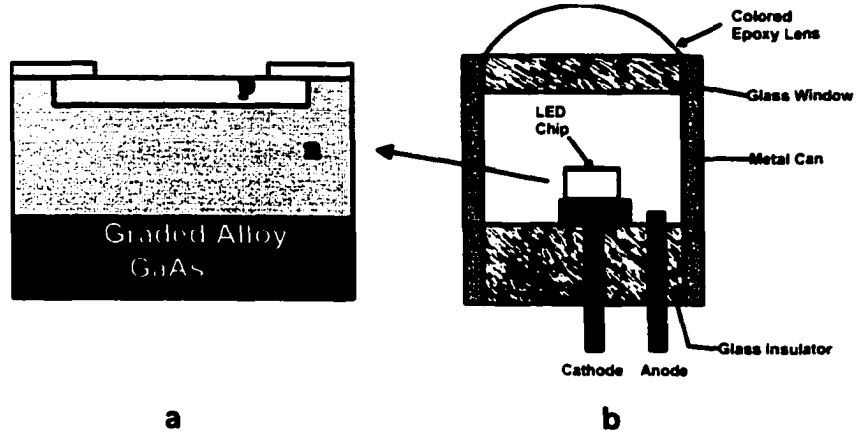

Figure 5.1. *Basic GaAs LED structure.*

5.2.2 Substrate Availability

Almost all optoelectronic light sources depend upon epitaxial crystal growth techniques where a thin active layer (a few microns) is grown on a substrate. (which is$\sim$ 200 μm). The availability of a high quality substrate is extremely important in epitaxial technology. If a substrate that lattice matches to the active device layer is not available, the device layer may have dislocations and other defects in it. These can seriously hurt the device performance. The important substrates that are available for light emitting technology are $GaAs$ and InP. A few semiconductors and their alloys can match with these substrates.

Semiconductors that cannot lattice match with $GaAs$ or InP have an uphill battle for technological success. The crystal grower must learn the difficult task to grow the semiconductor on a mismatched substrate without allowing dislocations to propagate into the active region.

Important semiconductor materials exploited in optoelectronics which are lattice matched very well to $GaAs$ substrates are the alloy $Ga_xAl_{1-x}As$; $In_{0.53}Ga_{0.47}As$ and $In_{0.52}Al_{0.48}As$ which are lattice matched to InP; $InGaAsP$ which is a quaternary material whose composition can be tailored to match with InP and can emit at 1.55 μm; and $GaAsP$ which has a wide range of bandgaps available. Recently there has been considerable interest in large bandgap materials such as $ZnSe$ and ZnS to produce devices that emit green light. The motivation is for superior display technology and for high density optical memory applications (a shorter wavelength allows reading of smaller features). $Ga_{1-x}In_xAs$ substrates with x=0.04 are closely lattice-matched to $ZnSe$ (refer to figure. 2.2)

It is important to keep in mind that alloys like $GaAlAs$ and $GaAsP$ become indirect at certain compositions . The band structure of $In_xGa_{1-x}As$ is direct over the entire range of composition. For efficient light emission, one needs to work in the direct gap region.

Chapter 6

Models for LPEE Growth

The growth process in LPEE is quite complex, and involves the interactions of various thermomechanical and electromagnetic fields. These include fluid flow, heat and mass transfer, electric and magnetic fields, various thermoelectric effects and their interactions in the liquid phase, and the heat and electric conduction with various thermoelectric effects and mass transport by diffusion in the solid phase. In addition, the moving growth and dissolution interface with possible finite mass transport rates complicate the process further. To gain a better understanding for the growth process of LPEE, over the past seven years a number of modelling studies have been carried out [80, 66, 81, 69].

A rational macroscopic continuum model, which includes all the above mentioned fields and interactions, has been developed in [7]. This is the first comprehensive model developed for the LPEE growth process of binary semiconductors. In the model the governing equations were obtained from the fundamental principles of electrodynamics and thermomechanics of continua. The constitutive equations for the solid and liquid phase were derived from an irreversible thermodynamics theory. The model takes into account electromigration and the well-known thermoelectric effects such as Joule and Peltier.

6.1 Basic Equations

In this section, we briefly introduce the governing equations of the LPEE growth process of ternary alloys as were introduced in [7].

6.1.1 Maxwell's Equations

The nonrelativistic electromagnetic balance laws, namely the Gauss law, the Faraday law, the conservation of magnetic flux, the Ampere law and the conservation of electric charge, yield the local electromechanical equations of the electrodynamics continua (liquid phase). These equations are known as the Maxwell equations. These equations under the assumption of the classical magnetohydrodynamic (MHD) approximation take the following forms:

$$\nabla \times \mathbf{E} + \frac{\partial \mathbf{B}}{\partial t} = 0. \qquad \nabla \cdot \mathbf{B} = 0 \tag{6.1}$$

$$\nabla \times \mathbf{H} = J. \qquad \nabla \cdot \mathbf{D} = 0 \tag{6.2}$$

where **E, B, H, D,** and **J** denote the electric field, magnetic induction, magnetic field, electric displacement and total current, respectively. In the same frame the electric displacement per unit volume and the magnetization per unit volume are given by

$$\mathbf{D} = \epsilon_0 \mathbf{E}. \qquad \mathbf{H} = \mu_0^{-1} \mathbf{B} \tag{6.3}$$

where ϵ_o and μ_o are the dielectric constant of vacuum an the permeability of vacuum, respectively. The conservation of charge equation takes the form

$$\nabla \cdot \mathbf{J} = 0 \tag{6.4}$$

In co-moving frame, the electric field and the total current are transformed according to

$$\mathcal{E} = \mathbf{E} + \mathbf{v} \times \mathbf{B}. \qquad \mathcal{J} = \mathbf{J} \tag{6.5}$$

The associated jump conditions on a surface of discontinuity σ, moving with velocity **v**, becomes

$$\mathbf{n} \times [\mathbf{E}] - \mu_0 \mathbf{v} \cdot \mathbf{n}[\mathbf{H}] = 0.$$

$$\mathbf{n} \cdot [\mathbf{H}] = 0. \quad \mathbf{n} \times [\mathbf{H}] = 0. \quad \mathbf{n} \cdot [\mathbf{J}] = 0 \tag{6.6}$$

where **n** is the unit normal to σ, and $[\cdot]$ denotes the jump defined for quantity A by

$$[A] = A^+ - A^-$$

where A^+ and A^- denote the values of A on σ approached from the positive and negative sides of the normal **n** of σ, respectively.

6.1.2 Thermomechanical Balance Laws

These laws are the conservation of mass, the balance of linear momentum, the balance of angular momentum, the balance of energy, and the second law of thermodynamics. The local forms for these fundamental laws including the electromagnetic contribution are given.

Conservation of mass

$$\frac{\partial \rho}{\partial t} + (\rho v_k)_{,k} = 0 \qquad V - \sigma. \tag{6.7}$$

$$[\rho(v_k - u_k)]n_k = 0 \quad on \quad \sigma. \tag{6.8}$$

where ρ is the mass density and a comma denotes the partial differentiation with respect to spatial coordinates.

Balance of linear momentum

$$t_{kj,k} + \rho f_j + f_j^{em} = \rho\left(\frac{Dv_j}{Dt}\right) \quad in \quad V - \sigma \tag{6.9}$$

$$\left[\rho v_j(v_k - u_k) - (t_{kj} + t_{kj}^{em})\right] n_k = L_j \quad on \quad \sigma \tag{6.10}$$

where t_{kj} is the stress tensor, f_j is the body force, f_j^{em} represents the so-called ponderomotive force, L_j is used to denote the effective surface tension acting on $\sigma(t)$, t_{kj}^{em} is the Maxwell stress tensor defined by

$$t_{kj}^{em} = E_k E_j + B_k B_j - \frac{1}{2}(E^2 + B^2)\delta_{kj} \tag{6.11}$$

and $\frac{D}{Dt} \equiv \frac{\partial}{\partial t} + v_k \frac{\partial}{\partial x_k}$ is the material time derivative.

The energy balance yields the following energy equation

$$\rho \frac{D\varepsilon}{Dt} = t_{kj} v_{j,k} + q_{k,k} + \rho h + J_k E_k \quad in \quad V - \sigma \tag{6.12}$$

$$\left[\left\{\rho(\varepsilon + \frac{1}{2}v^2) + \frac{1}{2}(E^2 + B^2)\right\}(v_k - u_k]n_k)\right] - \left[(t_{kj} + t_{kj}^{em})v_j - q_k\right] n_k = 0 \quad on \quad \sigma \tag{6.13}$$

where ε is the internal energy density per unit mass, q_k denotes the heat flux per unit area and h is the heat source per unit mass.

Entropy Inequality

$$\rho\frac{D\eta}{Dt} - \left(\frac{q_k}{\theta}\right)_{,k} - \frac{\rho h}{\theta} \geq 0 \quad in \quad V - \sigma \tag{6.14}$$

$$\left[\rho\eta(v_k - u_k) - \frac{q_k}{\theta}\right] n_k \geq 0 \quad On \quad \sigma \tag{6.15}$$

where η represents the entropy production density per unit mass and θ is the absolute temperature.

The equations in $V - \sigma$ are the local balance laws everywhere except at the surface of discontinuity, and the remaining equations are the jump conditions across the surface of discontinuity, which will give the boundary and interface conditions.

6.1.3 Equations of the Liquid Phase

In the present model the liquid phase is considered as a mixture of three viscous, heat and electric conducting fluids, and assumed to be a dilute, ternary metallic solution where one of the components is the solvent and the others are the solute. For a $Ga_xIn_{1-x}As$ ternary alloy crystal of III-V system, $x_A = x_{Ga}$, $x_B = x_{In}$ and $x_C = x_{As}$ are respectively the mole fractions of elements of Ga, In and As in the liquid phase, and x_C^s is the mole fraction of element As in the solid. Since $x_A + x_B + x_C = 1$, x_A and x_C are selected as the two independent compositional variables in the liquid phase, and in the solid, since the atoms of As are always 50% if the solid-state defects are neglected, we have one variable (x_A^s) since

$$x_A^s = \frac{x}{2}, \quad x_B^s = \frac{(1-x)}{2}, \quad x_C^s = \frac{1}{2} \tag{6.16}$$

The mass conservation, balance of linear momentum, balance of energy an the Maxwell equations yield the governing equations in the liquid phase [81]. Below we present them in Cylindrical coordinates.

Incompressibility condition

The solution is assumed to be an incompressible, Newtonian fluid. In this case, the liquid phase density is assumed constant, and thus the continuity equation is satisfied iden-

tically and replaced by the incompressibility condition

$$\frac{\partial u}{\partial r} + \frac{u}{r} = \frac{\partial v}{\partial v} = 0 \tag{6.17}$$

where u and v are the flow velocity components in the r and z directions, respectively.

Momentum equations

In the momentum balance, the well-know Boussinesq approximation is adopted. This allows us to take into account the buoyancy forces due to density change induced by temperature and concentration gradients in the solution. The momentum equations become

$$\begin{aligned} -\frac{1}{\rho_L}\frac{\partial P}{\partial r} + \nu\left(2\frac{\partial^2 u}{\partial r^2} + \frac{2}{r}\frac{\partial u}{\partial r} + \frac{\partial^2 u}{\partial z^2} + \frac{\partial^2 v}{\partial r \partial z} - \frac{2u}{r^2}\right) - \sigma_L B^2 u &= \frac{\partial u}{\partial t} + u\frac{\partial u}{\partial r} + v\frac{\partial u}{\partial z} \\ -\frac{1}{\rho_L}\frac{\partial P}{\partial z} + \nu\left(2\frac{\partial^2 v}{\partial z^2} + \frac{1}{r}\frac{\partial v}{\partial r} + \frac{1}{r}\frac{\partial u}{\partial z} + \frac{\partial^2 v}{\partial r^2} + \frac{\partial^2 u}{\partial r \partial z}\right) - F_B &= \frac{\partial v}{\partial t} + u\frac{\partial v}{\partial r} + v\frac{\partial v}{\partial z} \end{aligned} \tag{6.18}$$

where ν is the kinematic viscosity, ρ_L is the mass density of the solution, P is the pressure, and F_B represents the buoyancy force due to temperature and concentration gradients, expressed by

$$F_B = g\left[\beta_A(x_A - x_A^o) + \beta_C(x_C - x_C^o) + \beta_T(T - T^o)\right) \tag{6.19}$$

where g is the gravitational constant, β_A and β_C are the solutal expansion coefficients related to components A and C, β_T is the thermal expansion coefficient, x_A^o and x_C^o are respectively the initial mole fractions of components A and C in the solution, T^o is the initial temperature.

Energy equation

The liquid phase is a good electric conducting metallic solution. Its electrical resistivity is very small compared to the solid phase. Since the Joule heating is proportional to the current density and the electric resistivity, its magnitude in the solution is at least one order lower than that in the solid. Therefore, the effect of Joule heating was neglected in the solution. The energy equation then becomes

$$\frac{K_L}{\rho_L \gamma_L}\left(\frac{\partial^2 T}{\partial r^2} + \frac{1}{r}\frac{\partial T}{\partial r} + \frac{\partial^2 T}{\partial z^2}\right) = \frac{\partial T}{\partial t} + u\frac{\partial T}{\partial r} + v\frac{\partial T}{\partial z} \tag{6.20}$$

where T is the temperature at a point in the solution, K_L and γ_L are the thermal conductivity and specific heat of the solution, respectively. In Eq. (6.20), we have also neglected the effects of concentration and density changes on the temperature field.

Electric field equation

In this special axisymmetric model, the Maxwell equations Eq. (6.1)-(6.5) simplified significantly [81]. The electric field is non-uniform in the solution since the electric current bypasses the source material in the growth configuration under consideration. However, the change of the electric field in time is slow and thus the assumption of quasi-steady electric field in the solution is reasonable. Under these conditions, the Maxwell equations reduce to the following single electric field equation

$$\frac{\partial^2 \phi}{\partial r^2} + \frac{1}{r}\frac{\partial \phi}{\partial r} + \frac{\partial^2 \phi}{\partial z^2} = 0 \tag{6.21}$$

where ϕ is the electric potential, and the associated field components E_r and E_z will be calculated by

$$E_r = -\frac{\partial \phi}{\partial r} \qquad E_z = -\frac{\partial \phi}{\partial z} \tag{6.22}$$

Mass transport equations

Mass conservation for solutes yields two transport equations [81], which include electromigration, diffusion and convection. In Cylindrical coordinates they become

$$\begin{aligned}
\mu_A E_r \frac{\partial x_A}{\partial r} + \mu_A E_z \frac{\partial x_A}{\partial z} + D_A \left(\frac{\partial^2 x_A^s}{\partial r^2} + \frac{1}{r}\frac{\partial x_A^s}{\partial r} + \frac{\partial^2 x_A^s}{\partial z^2} \right) &= \frac{\partial x_A}{\partial t} + u\frac{\partial x_A}{\partial r} + v\frac{\partial x_A}{\partial z} \\
\mu_C E_r \frac{\partial x_C}{\partial r} + \mu_C E_z \frac{\partial x_C}{\partial z} + D_C \left(\frac{\partial^2 x_C^s}{\partial r^2} + \frac{1}{r}\frac{\partial x_C^s}{\partial r} + \frac{\partial^2 x_C^s}{\partial z^2} \right) &= \frac{\partial x_C}{\partial t} + u\frac{\partial x_C}{\partial r} + v\frac{\partial x_C}{\partial z}
\end{aligned} \tag{6.23}$$

where μ_A and μ_C are the mobilities of elements A and C, respectively, and D_A and D_C are the diffusion coefficients of elements A and C in the solution, respectively.

6.1.4 Equations of the Solid Phase

Mass diffusion takes place between elements A and B in a III-III-V ternary crystal. Therefore if one neglects the defect of the solid, then the element C sublattice must be filled, and thus

$$\frac{\partial x_C^s}{\partial r} = \frac{\partial x_C^s}{\partial z} = 0 \tag{6.24}$$

Solid diffusion is governed by only one mass transport equation:

$$\frac{\partial x_A^s}{\partial t} = D_A^s \left(\frac{\partial^2 x_A^s}{\partial r^2} + \frac{1}{r}\frac{\partial x_A^s}{\partial r} + \frac{\partial^2 x_A^s}{\partial z^2} \right) + \frac{D_A^s}{\omega^s} \left(\frac{\partial \omega^s}{\partial r}\frac{\partial x_A^s}{\partial r} + \frac{\partial \omega^s}{\partial z}\frac{\partial x_A^s}{\partial z} \right) \tag{6.25}$$

where D_A^s is used to denote the diffusion coefficient of element A in the solid and ω^s denotes the mole density of the solid. Note that the last term in Eq (6.25) represents the change in mole density.

In the solid phase the energy equation is the only field equation.

$$\rho_s \gamma_s \frac{\partial T}{\partial t} = K_s^r \left(\frac{\partial^2 T}{\partial r^2} + \frac{1}{r}\frac{\partial T}{\partial r} \right) + K_s^z \frac{\partial^2 T}{\partial z^2} + \frac{1}{\sigma_s} J^2 \tag{6.26}$$

where T is the temperature at a point in the solid, K_s^r, K_s^z, ρ_s and γ_s are the thermal conductivities in the r- and z-directions, mass density and specific heat of the solid, respectively, and **J** is the applied current density and σ_s is the electrical conductivity of the crystal.

6.1.5 Phase Diagram

Mass transport equations at the interface and phase diagram must be solved simultaneously for concentrations x_A, x_C, x_A^s, and growth rate v^g. The phase diagram for ternary III-V alloy system $A_x B_{(1-x)} C$ can be described by the following expressions [82]:

$$\gamma_{AC}^s x = \frac{4\gamma_A \gamma_C x_A x_C}{\gamma_A^{sL(AC)} \gamma_C^{sL(AC)}} exp\left[\frac{\Delta S_{AC}^F \left(T_{AC}^F - T \right)}{RT} \right] \tag{6.27}$$

and

$$\gamma_{BC}^s (1-x) = \frac{4\gamma_B \gamma_C x_B x_C}{\gamma_B^{sL(BC)} \gamma_C^{sL(BC)}} exp\left[\frac{\Delta S_{BC}^F \left(T_{AC}^F - T \right)}{RT} \right] \tag{6.28}$$

where $\gamma's$ are the activity coefficients, ΔS_{AC}^F and ΔS_{BC}^F are the entropies of fusion, T_{AC}^F and T_{BC}^F are the melting points, R is the gas constant, and T is the growth temperature. The activity coefficients and the numerical value of related interaction parameters can be found in [82].

6.1.6 Numerical Modelling

In parallel with theoretical studies, the numerical simulations are carried out in [81, 69] to gain insight of LPEE growth of ternary semiconductor crystal under normal and magnetic

field conditions. The number of modelling studies accounting for convection, however, is small. Many researchers have either neglected this effect or handled it in a simple empirical manner. This is understandable since the inclusion of convective effects makes the associated governing equations highly nonlinear and analytically intractable. The aim in this part is to simulate the experiments; growth conditions using the developed model [69]. Dost [70] presented a model for the LPEE growth process of $InGaAs$, for which the growth cell is assumed to be subjected to an external applied magnetic field in order to reduce the effect of natural convection induced by the temperature and solute concentration gradients in the liquid phase.

A rational mathematical model for LPEE growth process of alloy semiconductors has been developed in [81]. The fundamental equations are the well-known Maxwell equations of electrodynamics, and the thermomechanical balance equations of the continuum including the electromagnetic interactions with the continuum. The solution (liquid phase) is considered as a ternary fluid mixture, and the solid phase is a rigid electric and heat conducting material allowing solid diffusion. The constitutive equations for both the liquid mixture and the solid phase are derived from a rational thermodynamic theory so as not to violate the second law of thermodynamics. The boundary and moving interface conditions are obtained from the jump conditions associated with the corresponding fundamental equations. For their detailed derivations, refer to [80].

The use of a magnetic field as an additional control parameter in LPEE crystal growth has yet to be understood and more research is needed to elucidate its true potential.

Chapter 7

Experimental Apparatus Design

A state of the art LPEE crystal growth facility was recently developed at the University of Victoria. This facility was built to achieve the reproduction of conditions assumed in the theoretical models [83]. Correlations between the results achieved experimentally and numerically would provide the validation of the theoretical models. A platform was designed and constructed for this study. The major considerations for the design are the accommodation of the magnet and crucible. The external magnet had to be designed horizontal and stationary due to the physical limitations. It could not have the rotation capability similar to the existing LPEE facility in the Crystal Growth laboratory. In order to compensate for the lack of rotation of the growth platform, a novel LPEE crucible was designed and built. This crucible would allow for the growth of crystals of up to 11 mm thick and 25 mm in diameter .

A sketch of the LPEE apparatus is presented in figure 7.1. The first element in the apparatus consists of a crucible, in which the substrate, the solution, and the source material are contained. The crucible is held within a reactor tube, made out of quartz, by four molybdenum rods. Two of these rods act as electrodes. The reactor tube is needed to contain the high purity hydrogen atmosphere required during the growth process. At one end, the rector tube is constrained by vacuum-tight sealed flange, through which electrodes are inserted. These electrodes reach the crucible, and allow the DC current from a power supply to flow through the growth cell within the crucible. Also through the flange, a thermocouple (TC) is inserted and extends to the crucible. The direct current needed to sustain the growth is provided by a 100A, 10V power supply.

The reactor tube sits inside a three-zone furnace with independent controllers. The furnace and magnet rest on an aluminum platform. The platform base rests on four feet. These feet take the form of M20 screws, allowing the leveling of the platform. The reactor

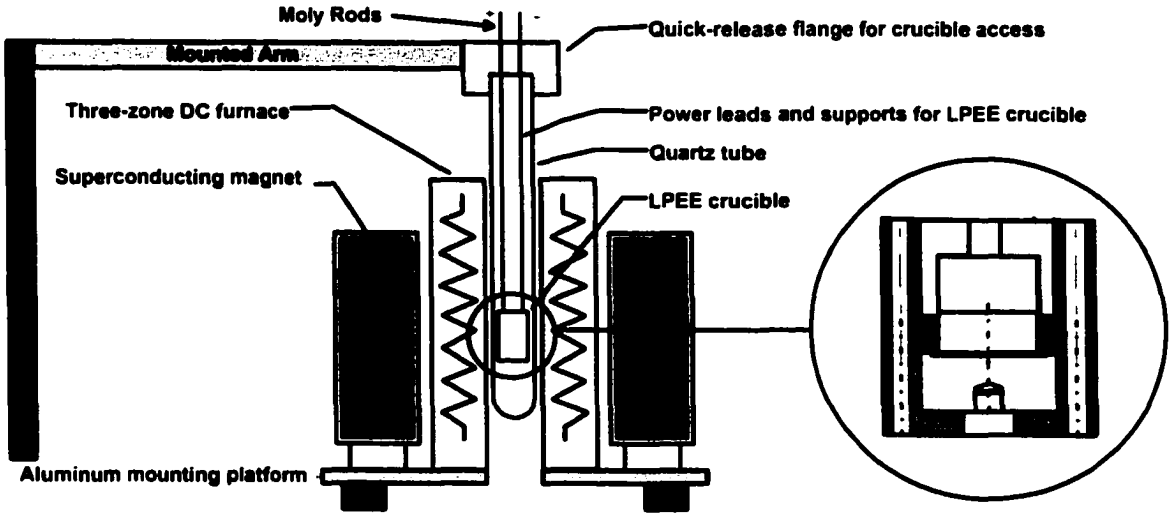

Figure 7.1. *Schematic view of platform for LPEE growth under magnetic field.*

and end flange are fixed on a horizontal aluminum arm. This arm is mounted on a horizontal wall. This prevents the crucible from being subjected to the vibration generated from the magnet.

During the LPEE growth process, hydrogen is constantly flown through the reactor tube to insure that there is no accumulation of impurities. Between the hydrogen supply cylinder, and the reactor tube, the hydrogen is first purified to lower the amount of impurities in the stream to under 10 PPB levels, and then filtered to remove unwanted particles. Hydrogen enters the reactor tube through the end flange and exits at the outlet. A turbomolecular pump (TMP) is also connected to the reactor via the same end flange. This pump is used at the start of the experiment, to remove as much of gas present in the reactor tube as possible. Hydrogen is inserted in the tube only after high vacuum gas been reached.

In a typical LPEE experiment, the feed (source) material's placed in the top of the solution, while the seed (substrate) is placed under it. To provide uniform current distribution throughout the seed during growth, a liquid contact made out of a gallium-aluminum alloy (gallium-rich) is inserted between the backside of the seed and the graphite from the crucible. The solution is prepared separately outside the growth cell, then inserted into the system. The furnace is heated to the growth temperature in the range of $780 - 900^{o}C$. After the system reaches thermodynamics equilibrium, the electric current is turned on and growth is initiated. During the growth process, the furnace temperature is kept constant.

The applied electric current passing through the growth cell is the sole driving force for growth. The system is also subjected to a steady state external magnetic field in the vertical direction, to suppress the adverse affects of convection on the growth process [84].

The field generator was designed in conjunction with the Cryofuel research group to provide a region where crystal can be grown by LPEE in the presence of magnetic fields up to 5 Tesla.

7.1 LPEE Crystal Growth System Design

In the above section, an overview of the facility and services was given in general terms. More specific information on the design and specifications for each of the facility components are given in following sections.

7.1.1 Crucible

The most critical part of the LPEE crystal growth apparatus is the crucible structure. It has a major impact on the quality of the growth crystals, determines its surface dimensions and shape, and dictates what types of experiments can be performed, as well as how successful they will be. There are many considerations to be taken into account in the development of a novel LPEE crucible. For instance, a crucible must:

- Provide electrical insulation between the two electrodes, except through the solution-substrate interface.
- Allow for thermal expansion of its parts.
- Provide uniform electrical contact at the back of the substrate.
- Prevent solution leaks.
- Minimize the amount of impurities released from the crucible to the solution.
- Permit the easy removal of materials at the end of the growth experiment.
- Allow the crucible to be reusable.
- Provide a system for temperature monitoring within the crucible.

Taking each of these points into consideration, the crucible shown in figure 7.2 was designed and constructed. High density, high purity graphite is used for the electrically

conductive parts of the crucible, while boron nitride is the material of choice for the insulating components, and pyrolytic boron nitride was used for the growth cell. The crucible has a cylindrical symmetry with an out side diameter of 50.0 mm. The crucible has two main parts. the bottom part, used to contain the substrate, is referred to as the substrate holder (SH). The top portion which fit in the SH by means of its own weight, called the source and solution holder.

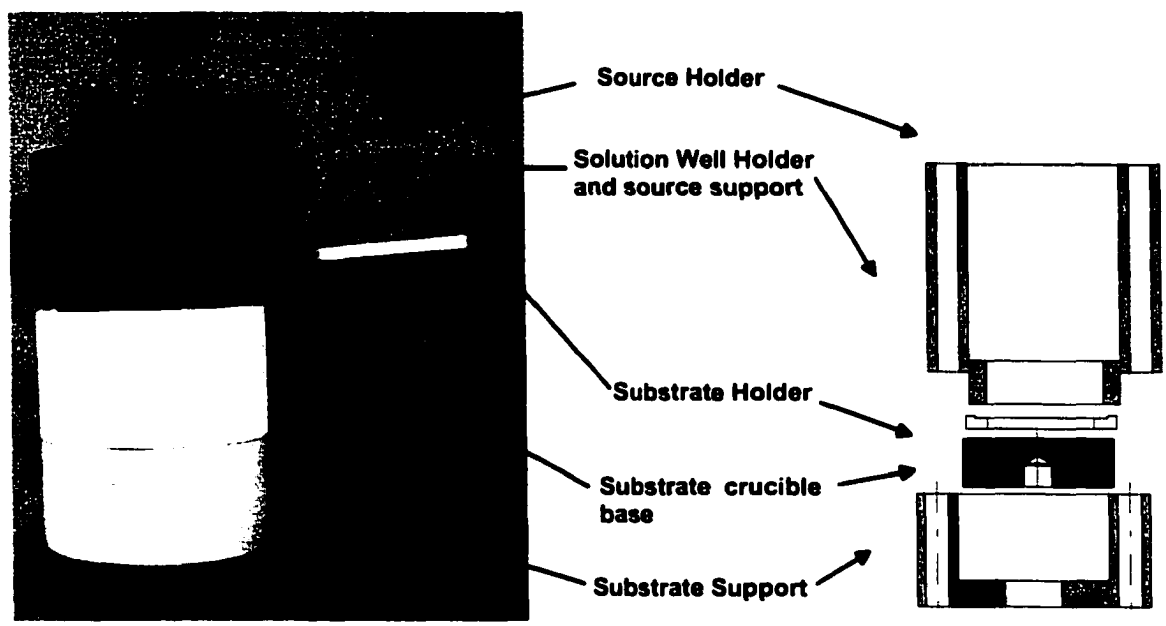

Figure 7.2. *Photograph and schematic of LPEE crucible.*

The substrate crucible accommodates the substrate and the contact zone material. For the contact zone, an alloy of gallium and aluminum, with aluminum at about 10% in weight, is used [51]. More detailed discussion about the contact zone will be given in Chapter 8. This alloy is solid at room temperature, and melts completely at temperatures above 250°C. The contact zone is confined between the back surface of the substrate, and a high density graphite base which is threaded to the positive molybdenum electrode. The substrate and contact zone alloy are held in place by a boron nitride substrate support.

The most important properties of BN, which are of use in this application are: i) high thermal conductivity, ii) low thermal expansion, iii) electrically insulating, iv) high fusion temperature, and v) hygroscopic, thus protecting the solution from humidity. In the present configuration, the BN substrate support is made to accommodate 27 by 27 mm square

substrates and from 400 to 1200 μm in thickness.

The solution well was made of pyrolytic boron nitride (PBN). PBN is used because, in addition to all the qualities of BN, it does not have its porosity problem which could lead to an increase in the contamination level of the solution. Also, PBN is not wetted by the $InGaAs$ solution [85, 86], which represents an advantage when removing the solution at the end of the growth process. The PBN ring is restrained into its position by a graphite holder. The substrate crucible is held into position by two BN jackets and two molybdenum rods that reach it from the reactor top flange.

The source crucible is designed to handle 28 by 28 mm square source materials ranging from 3.0 to 4.0 mm in thickness, and it can be easily modified to accommodate source up to 10 mm, if needed in the future . The source material is held in a cavity graved in graphite part. This was designed to reduce the Joule heating in the growth cell, which can limit the thickness of the grown crystal. This was done through a major change in the construction of the traditional growth cell. The new design was made to accommodate the advantage of both SETUP1 and SETUP2 (see figure 4.2). The graphite part is connected to the negative electrode, and forming a reservoir in which the solution will be contained during the warm-up and equilibration phases of the growth experiment (see figure 7.3).

Two BN jackets hold all these components together. The bottom jacket acts as an electrical insulator for the whole system. All these last components are free to move and expand axially, there is no threading between any part of the crucible. The axial positioning of this assembly is controlled by the source and substrate electrodes, which extend to the flange at the top end of the reactor tube (see figure 7.3). Also these rods are used to fix the crucible into position. These rods, going past the source crucible BN jackets, extend through the substrate crucible, offering a first step in the alignment of the crucible. The BN jacket is also used to restrain two ceramic protection tubes containing one K-type thermocouple each. These tubes are not permeable to gases, and free to slide within the outside of the crucible. Thus they provide the possibility of measuring the temperature distribution within the reactor tube at any given time during a crystal growth experiment.

Crucible's Operation

In figure 7.4, we describe the crucible's operation during a typical LPEE experiment. In

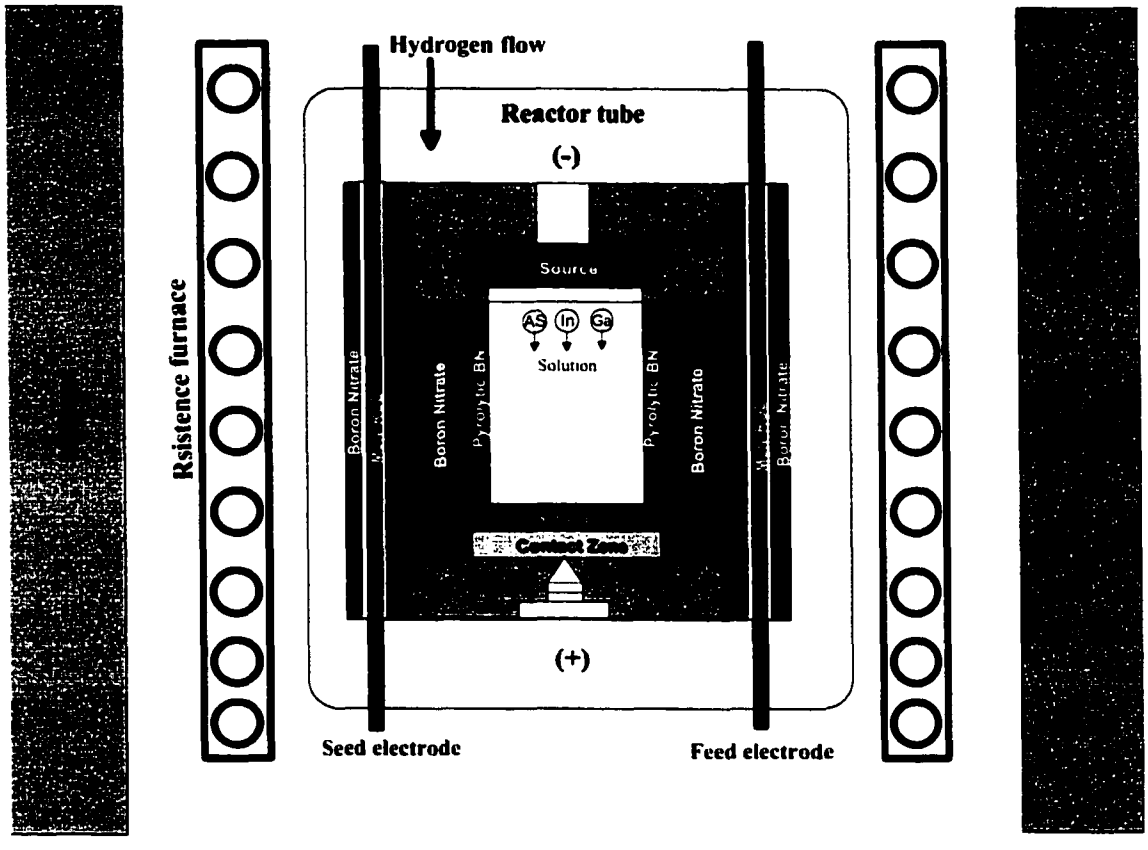

Figure 7.3. *Schematic view of the growth platform.*

stage one, the growth materials are already within the crucible. This was done by first introducing the substrate holder, containing the substrate and the contact zone alloy, inside the BN bottom half jacket. The contact zone material introduced first. The contact zone material's was originally in a solid state, but melted before the introduction of the substrate. Then, the source materials are fitted in the source holder and the solution material in the reservoir. There is no restraint on the chips of solution material, solid at RT. Up to this stage, there is no contact between the solution and the substrate. This situation prevails until the solution melts and thermally equilibrates with the source once growth temperature will have been reached.

To prevent supersaturation or undersaturation conditions when the substrate is placed in contact with the growth solution, many apparatus were designed with a dummy substrate. In these cases, the solution would first be equilibrated at the growth temperature with the dummy substrate inside the crucible, and then moved over the other substrate at the start of

the growth. This procedure can not be followed in our setup, because we are limited by the size of the core of the magnet, which already exists and is small. The solution is prepared separately outside the solution well, then inserted into the system.

In the second stage, the temperature is raised, and the molybdenum rods supporting the crucible, as well as the crucible parts, expand freely in length. This freedom in expansion prevents any cracks in the crucible. After the solution and contact zone material have reached equilibrium at the growth temperature, the solution must now be placed in contact with the substrate. This was made by unplugging the graphite rod, taking advantage of gravity. This is shown in the third stage. Tight tolerances between the the crucible parts insures that the solution flows from the source reservoir to the solution well in the substrate crucible without leakage.

To insure complete wetting of both the substrate and the source by the solution, an excess solution being introduced over the edge of the solution well. The excess solution is caught in the source reservoir.

At this time, the DC current can now be applied, by-passing and passing through the source material, at the same time, to minimize the Joule heating and insure the uniformity of the electrical field in the solution, at the same configuration. The configuration of the growth cell, at this time, is given in figure 7.4, last figure. To correspond with the geometry used in the numerical simulation performed by the UVic crystal growth research group, the growth cell was chosen to be 25 mm in diameter, by 10 mm in height, refer to table 7.1 for more dimensions .

At the end of the growth, the DC current is shut-off. Finally, the temperature is lowered, and the furnace let cool down. This corresponds to the final stage.

7.1.2 Furnace, Reactor Tube, End Flange, and Platform Base

The preliminary investigations and results of the experiments, showed that a three-zone tubular furnace is needed, to allow for a good control of the temperature profile along the length of the crucible. Because of the vertical orientation of the crucible, a furnace with independent heating zones is required to compensate for the temperature gradient induced by the convection generated at high temperature. Figure 7.5 shows a photograph of the furnace.

The furnace is to fit within the magnet bore. As such, three precautions were taken: i) it

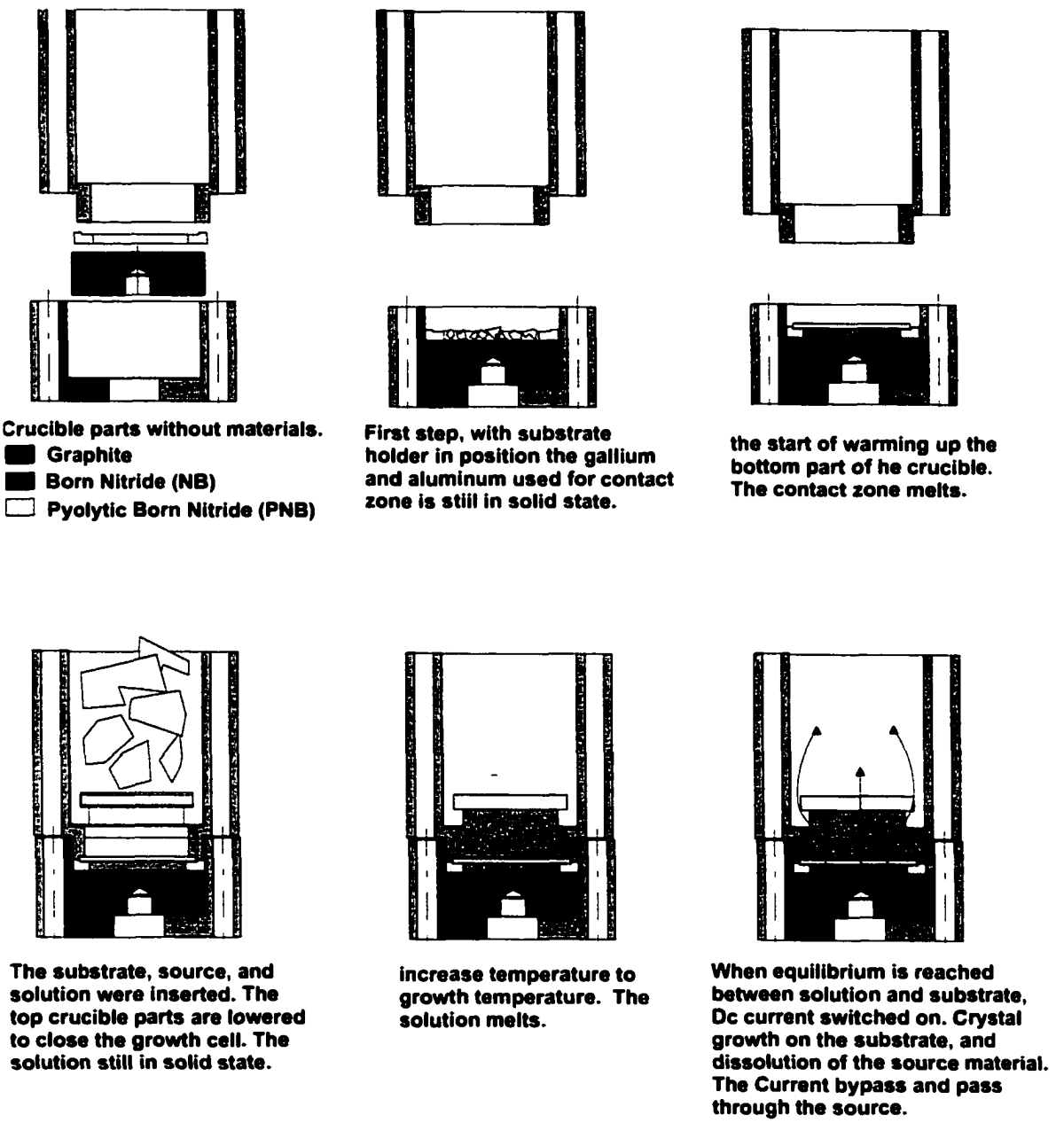

Figure 7.4. *Schematic of crucible operation during LPEE growth experiment.*

was powered by direct current, to avoid induction related problems that would result from using an alternating current within the strong magnetic field, ii) since the inner wall of the magnet has to be kept at RT, a cooling ring is incorporated along the length of the furnace, to keep the temperature at the outside wall of the furnace at RT during the growth, and iii)

Table 7.1. *Dimensions of various crystal growth platform components.*

Item	Specification	Dimension (mm)
Growth cell	Height	10
	Diameter	25
Crucible	Outside diameter	51
Reactor tube	Overall length	540
	Inside diameter	55
	Outside diameter	59
Furnace	Overall length	550
	Length of zone2	152
	Inside diameter	63
	outside diameter	183

all the materials used to build the furnace and its components are nonmagnetic materials, to minimize the external effect on the magnetic field distribution.

The crucible is contained within a reactor tube made out of quartz (see figure 7.3). The tube is open from one side only. This tube is necessary to contain the high purity hydrogen that flows around the crucible during the growth process. Quartz is the material of choice because of its following features: high melting point, low thermal expansion coefficient, high resistance to both oxidizing and reducing atmospheres within the growth temperature range, and transparency.

The reactor tube is held in place by aluminum supports, as shown in figure 7.6, along with the other components forming the end flange. The quartz tube was designed to hold its own weight. To allow for thermal expansion of the reactor tube, which should be under 1 mm at a growth temperature of 1000°C, the tube was held hanging only from the top. The reactor tube is restrained at the top end by an aluminum cap and viton o-rings. These o-rings also provide a vacuum-tight seal and a light over-pressure seal when covered with vacuum grease and compressed adequately. Note that the vacuum grease used here, as is the case for all vacuum grease used elsewhere on this growth platform, is silicon-based. This type of oil has a very low vapor pressure, thus minimizing contamination within the reactor tube.

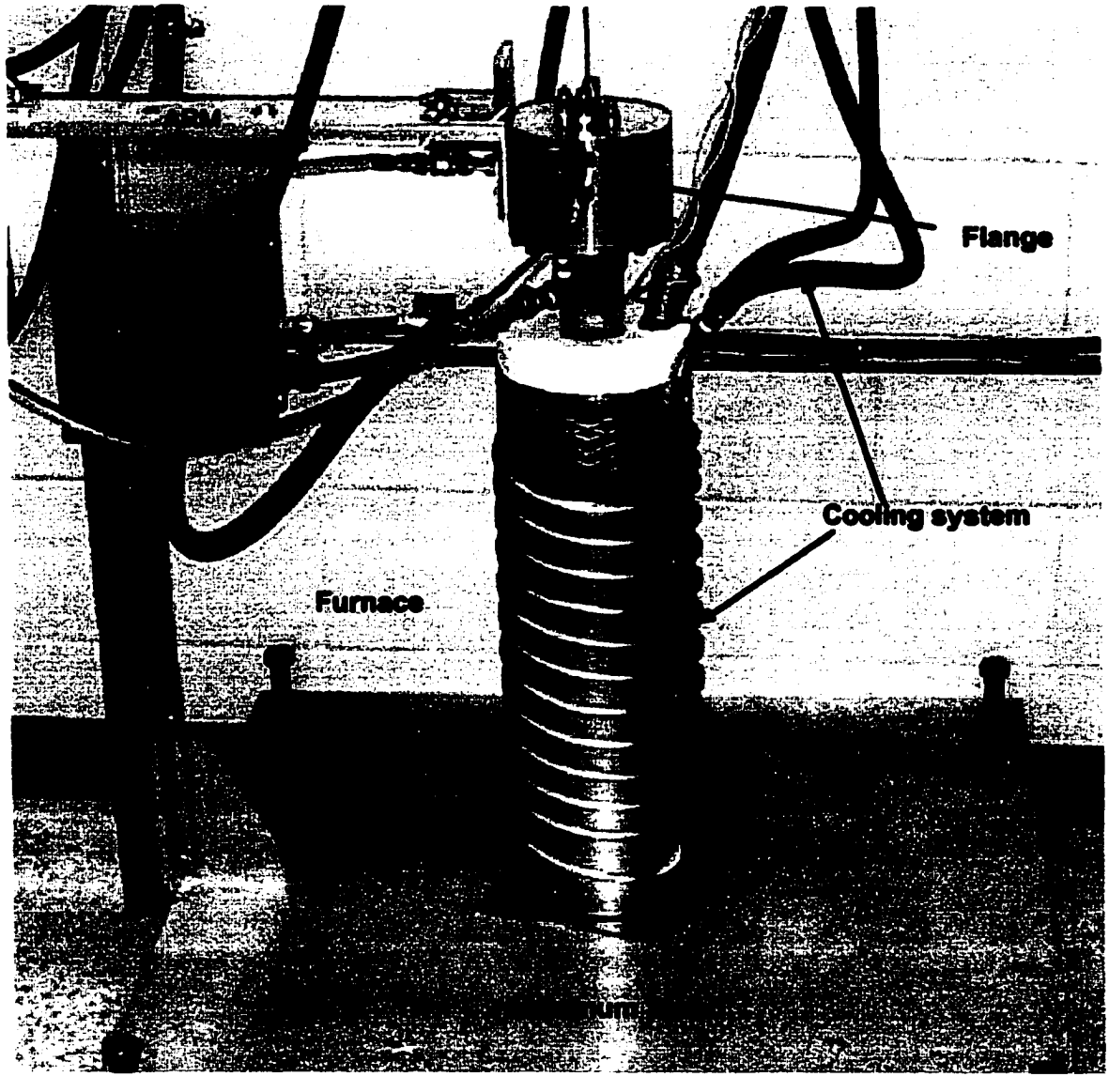

Figure 7.5. *Photograph of the furnace and its components*

Viton o-rings are also used to seal the reactor tube end support to the cover plate. The cover plate is the part of the support which is removed to access the crucible, see figure 7.6. Because the viton o-rings do not resist well to temperatures above 150° C, two precautions were taken to protect them: i) the end of the reactor tube is sticking out of the furnace, thus allowing the tube end to be at a low temperature even when its center portion is at the growth temperature, and ii) a cooling ring is incorporated at near the o-ring. When the furnace is

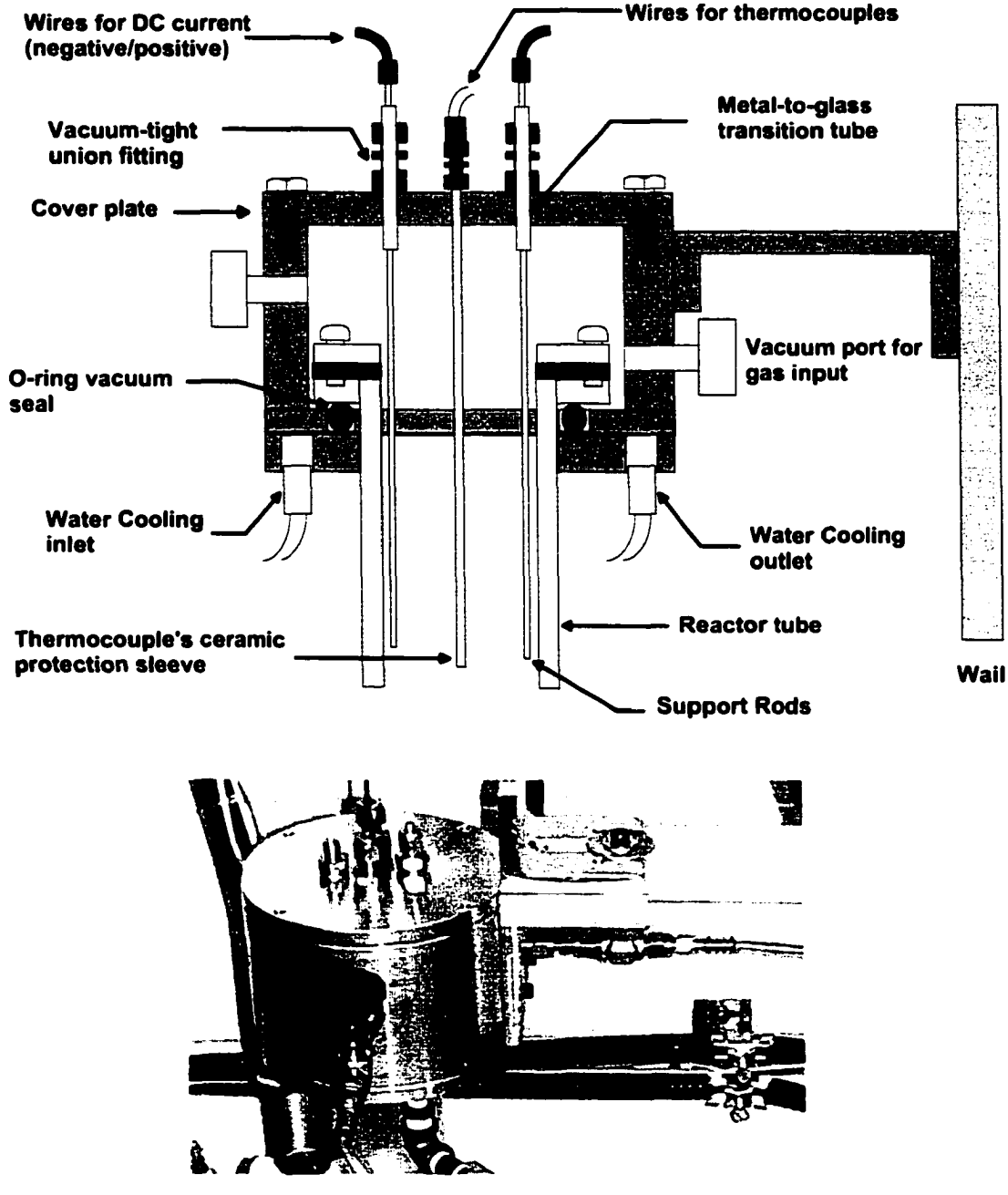

Figure 7.6. *Schematic view and photograph of the reactor tube end flange.*

on, cold water is flowed through these rings to remove the heat that reaches the flange from convection within the hydrogen, conduction from the quartz tube and molybdenum crucible support rods. Most of the flange components are made out of aluminum, so that the excess heat can be rapidly conducted to the cooling rings, thus preventing the temperature

becoming high in the region of the flanges.

Vacuum-tight union fittings are used to hold both the TCs ceramic protection sleeves, and the source electrode, as seen in figure 7.6. The source and substrate electrodes, in the region of the flange, are covered by a glass tube. This tube provides electrical insulation between the electrode and the cover plate of the flange. By loosening the union fittings, it is possible to slide the ceramic sleeves and/or electrode, thus providing axial displacement mentioned in the previous section. At a later stage of the thesis work a simple vacuum electrical feedthrough was used instead of the glass tube to allow the passage of the current through the cover plate. This was done because electrodes do not require axial translation.

Valve fittings for gas input/output to or from the reactor tube are connected to the end flange. KF small flange connections consist of two symmetrical small KF flanges of the same diameter, linked together by a clamping ring [87]. A centering ring with an o-ring gasket insures a proper alignment and a high-vacuum seal. A smaller fitting would increase time required to reach the desired vacuum level to start the experiment . The KF types of fittings were chosen over ISO-K or CF fittings, because of the ease with which they can be handled without the need of any tools, while they offer a satisfactory performance to the high vacuum requirements of this application. Viton o-rings insure vacuum connections between these KF fittings and the tube end flanges.

The crucible support rods are threaded in the flange cover plate. The flange cover plate is threaded in the main flange. Thus, removing the cover plate also pulls out the crucible. The reactor and end flange are fixed on a horizontal aluminum arm. This arm can be adjusted in the vertical and horizontal directions, which can provide the flexibility of adjusting the height of the crucible, and it is mounted on a vertical wall, that gives the flexibility to adjust the crucible height for the desired location. This prevents the crucible from being subjected to the vibration generated by the magnet. The furnace and magnet rest on an aluminum platform. The platform base rests on four feet. These feet take the form of M20 screws, allowing the leveling of the platform.

7.1.3 Magnet

The field generator was designed and built in collaboration with the Cryofuel Research Group to provide the required magnetic field of up to 5 Tesla to grow crystals by LPEE. The magnet has a bore of 203 mm in diameter and 540 mm in height. The magnetic field is

static and vertical. The magnet is conduction cooled by a single two-stage GM cryocooler, see figure 7.7.

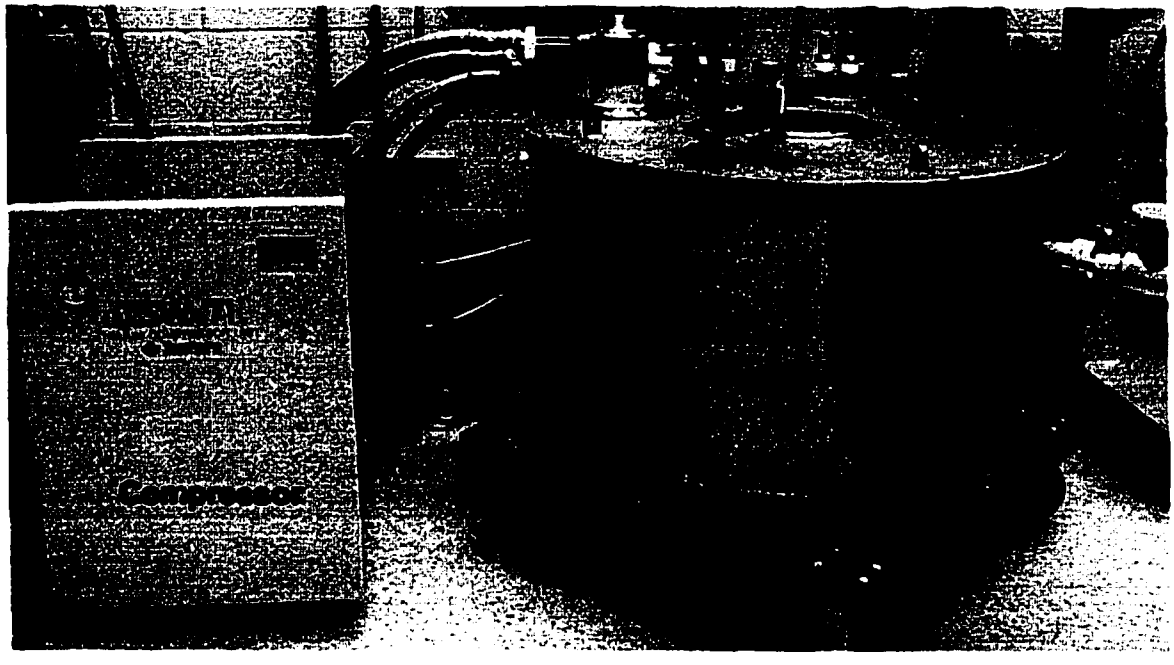

Figure 7.7. *Field generator*

7.2 Apparatus Design

The assembly of a DC power supply, controllers for the pumping system and the furnace, temperature indicators, and components to control the flow and even the quality of the various gases, these outside components, interconnected to the growth platform, is what will be looked at the present sections. This section focuses on the design of the components, not included in the growth platform, which form the LPEE apparatus, refer to figure 7.8.

The pumping system is an important part of the LPEE growth system. It is required to remove of the air from the reactor tube prior to the admittance of hydrogen. A vacuum in the order of 10^{-5} mbar would provide a reduction in the number of gaseous particles in the reactor tube by a factor of 10^{8} from atmospheric pressure. Since the growth process is performed at pressures slightly above the atmospheric pressure, 10^{-5} mbar of air within the tube at the moment of the hydrogen input would result in 10 PPB of impurities; a value

similar to the background contamination level of the hydrogen provided by the purifier.

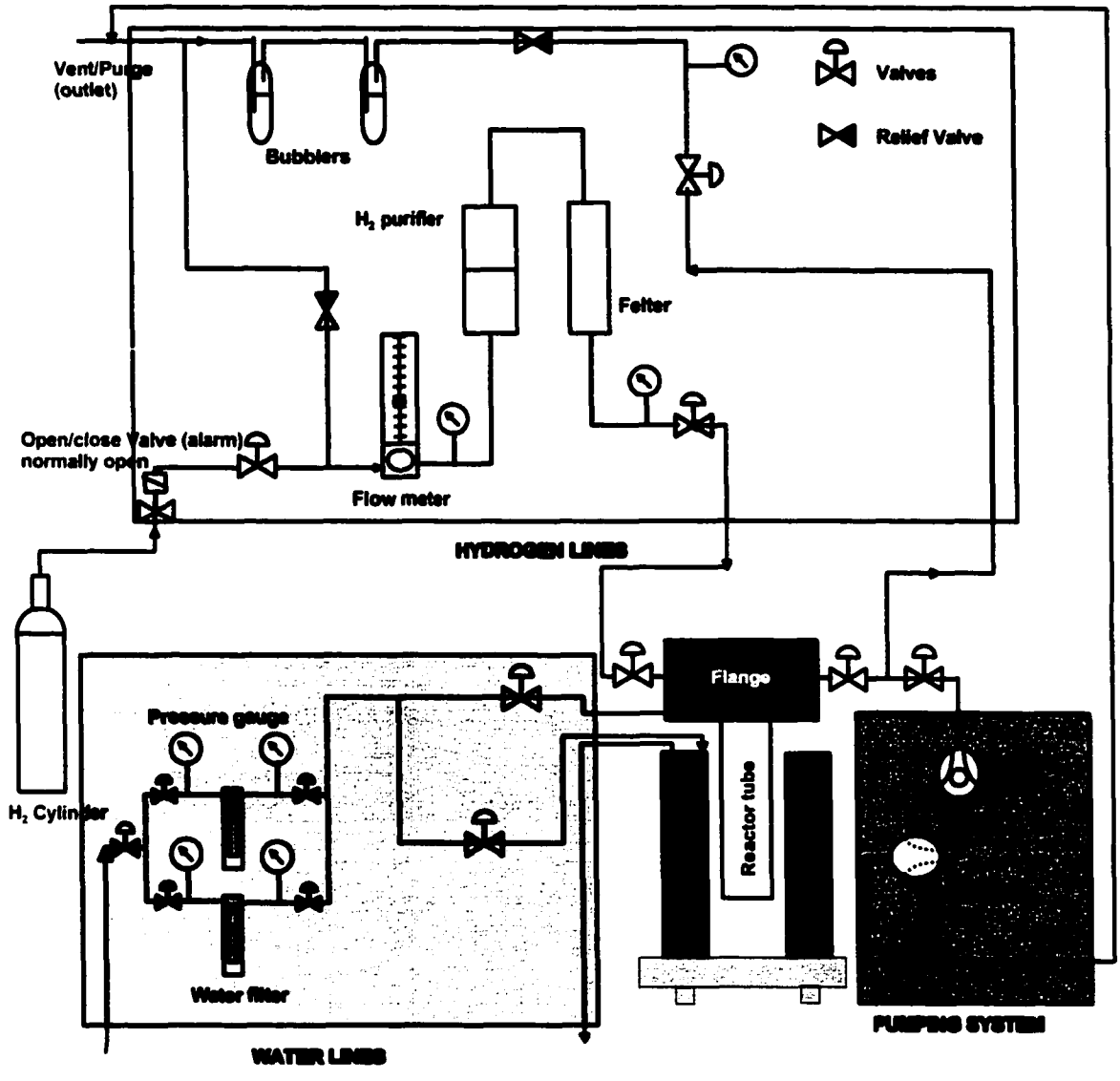

Figure 7.8. *Flow Diagram.*

7.2.1 Pumping System

In this facility, when the pump is in operation, the vacuum level can be measured directly from the intake flange of the turbomolecular pump (TMP). Pressures down to 10^{-3} mbar are read by a Pirani type sensor, while pressures under this value are determined using a hot

cathode filament ion sensor. The signals sent by these sensors are processed by a vacuum gauge, which then indicates the vacuum level on its front panel. Needed for the operation of the TMP are a frequency controller and a backing pump. The frequency converter produces a three-phase signal needed to take the TMP to its steady state rotational speed of 72000 RMP. As for the backing pump, the one used is of rotary vane type, with an anti-suckback valve isolating the pump from the rest of the system when its motor stops or slows down. This prevents oil vapors from diffusing into the TMP and the reactor tube.

7.2.2 Gas and Water Network

A series of different elements are required to direct and control the flows of the gases and water used in the facility. A water system is needed to cool the outside of the furnace, the flange holding the quartz tub, and the compressor used with the field generator. A diagram representing the gas lines network, and its various components, is given in figures 7.8 and 7.9 . A Hydrogen inlet line to carry the hydrogen from the hydrogen gas cylinder to the reactor tune is needed.

Components of the hydrogen line include a flash arrestor inserted near the cylinder, and a purifier installed towards the end of the line. Hydrogen flows through the purifier before entering the growth system..

To limit the contamination between the purifier and the reactor tube, only a cleaned high quality SS tubing was used in that section. The standard copper tubing is used practically in all other sections of the gas network. It is also worthy to mention the addition of a filter that traps particles down to 0.2 μm in diameter in the hydrogen line, just before the inlet to the reactor tube. This filter is added to pick up any SS dust that might be generated inside the flexible tubing.

Because of possible fire and explosion hazards associated with hydrogen, particularly at high temperature, a few preventive measures were taken. First, on the vent/purge outlet line, a bubbler is added to visualize the flow. This feature should help the facility users to notice major gas loses within the system, and then react accordingly. Second is the use of solenoid valves in case of an alarm signal. When the signal is given, a solenoid valve shuts off the hydrogen flow. The instances when this alarm signal is given are presented in the next paragraphs.

For this laboratory, two alarm levels have been defined. The first one, the low-level

alarm, or LLA, represents a situation when at least one of the measured parameters in the facility is beyond its acceptable limit, but is not a source of immediate danger. The second alarm level, the high-level alarm, or HLA, is present when at least one of the measured parameters in the facility is beyond its acceptable limit, but this time representing a real threat to the safety of the personnel within or around the facility.

The LLA is generated by any of the five following conditions: i) if the pressure within the water cooling line drops under 30 psig, ii) if the temperature within the furnace, read by three over-temperature TCs, goes beyond a pre-determined temperature, presently set at 980°, iii) if the furnace emergency manual switch is turned off, iv) if the manual switch on the safety switchboard is turned off, or v) if a HLA is in effect.

There are three mechanisms to provoke the HLA: i) if the hydrogen level within the facility exceeds 10 % of the hydrogen LEL, ii) if any flames are detected in the area of the growth platform, and iii) if the rate of the increase of temperature within the facility surpasses the standard acceptable level. The hydrogen level sensor, or sniffer, the infrared flame detector, and the temperature increase rate sensor, are all situated in the ceiling of the laboratory, in a position above the growth platform.

7.2.3 Furnace, Controllers and DC Power Supply

Furnace

The preliminary investigations and results of the experiments showed that, as mentioned in the previous section, a three-zone furnace was necessary to provide the required uniform temperature distribution in the system. With a single zone furnace, and mainly due to convection, it would not have been possible to provide a relatively uniform temperature profile within the crucible. Zones more than three would not have been justified because of the very limited dimensions of the growth cell, and because the Indium gallium arsenide solution is such a good heat conductor. Small temperature gradients along the crucible length will not affect significantly the temperature uniformity within the growth cell.

The furnace was powered by a direct current, to avoid induction related problems that would result from using an alternating current within the high magnetic field. Since the inner wall of the magnet has to be kept at RT, a cooling ring is incorporated along the length of the furnace, to keep the temperature outside the furnace at RT during the growth. All the

power connections and thermocouples inlet and outlets were designed to fit from the top of the furnace. Such a connection allows us to fit the furnace into the magnet opening with no difficulty.

Controllers

In order to take full advantage of the three heating zones, we have opted for independent PID, phase angle fired, SCR controllers for each zone, connected to type-K thermocouples. These thermocouples can be used for temperatures up to 1250° C, significantly higher than the furnace upper limit (1200° C), or the upper useful limit of LPEE for $GaAs$ (980° C), refer to figure 7.10.

The middle zone controller is programmable, with a limit of 12 segments of ramps and soaks per program. The controller for the furnace middle zone, which corresponds to the zone in which the crucible is positioned, can be used as a master controller over the other two. In this case, the two slave controllers follow the SP determined by the master controller.

DC Power Supply

Numerical simulations [88, 89] have shown that the desired electric current density is about 10 A/cm^2. At very low current densities the growth rate is too small, whereas an excessively high current density will cause an increase in the intensity of the convection cells within the solution, and lead to a loss of coherence at the crystal's surface. In both cases, the maximum thickness of the monocrystalline grown layer is limited. Current intensities under 15 A/cm^2 are typically used in LPEE of $GaAs$ and $InGaAs$, with the region from 2 to 10 A/cm^2 seemingly being the most promising [51, 52, 53, 89, 90, 91, 92].

If 15 A/cm^2 is assumed to be the maximum current density required for the growth, and a maximum growth cell diameter 30 mm, the voltage output requirement is now determined by the resistivity of the system at the growth temperature.

The resistivity of the system can be estimated by adding the resistivity of all the elements, in series, though which the DC current will flow. These elements are referred to as the conductive media. Knowing the geometry of the elements forming the conductive me-

Table 7.2. *Electrical sensitivities for various material at* 850° *C.*

Material	Resistivity ($\mu\Omega.cm$)
Copper 45	7
Moly	350
Graphite, grade Poco SFG-2	4000
Gallium solution [92]	50
Indium solution	40
$GaAs$ substrate, semi-insulating or lightly doped [92, 1]	25000
Contact zone alloy, Ga-Al [92, 93]	40

dia and the resistivity of the constituent materials of each element, the electrical resistivity of each element was calculated. The results are presented in Table 7.3, with the material resistivity given in Table 7.2.

As it can be seen from Table 7.3, the estimated resistivity of the system is 0.037 $\Omega.cm$ at a temperature of 850° C. This does not include the contact resistance at each of the connections between these elements, which are the values difficult to estimate. It seems improbable that the total resistivity of this system will exceed 0.1 Ω, even towards the end of the growth process, at epitaxial layers of a few millimeters in thickness.

With 0.1 Ω accepted as the maximum resistivity of the system, it follows automatically that the DC power supply is required to provide up to 10 V as the output voltage, for a maximum current of 100 A.

Temperature Monitoring System

At all time during an experiment, the temperature within the crucible can be determined. This is done using two type-K thermocouples, each protected by a separate ceramic tube. These Tcs are connected to digital panel indicators, with a 0.1^o resolution and a 0.2^o accuracy within the growth temperature range.

Table 7.3. *Electrical sensitivities of the conductive media elements at* 850° *C.*

Component	Resistivity (Ω)
Copper wire from DC power supply to growth platform, source side	0.008
Glass-to-metal transition tube	0.004
Moly electrode, source side	0.006
Graphite electrode, source side	0.002
Gallium solution [92]	.00003
Indium solution	.00006
Substrate	0.0009
Graphite electrode, substrate side	0.002
Moly electrode, substrate side	0.006
Copper wire from DC power supply to growth platform, substrate side	0.008
Contact zone alloy, *Ga-Al* [92, 93]	0.00001
Total	~ 0.037

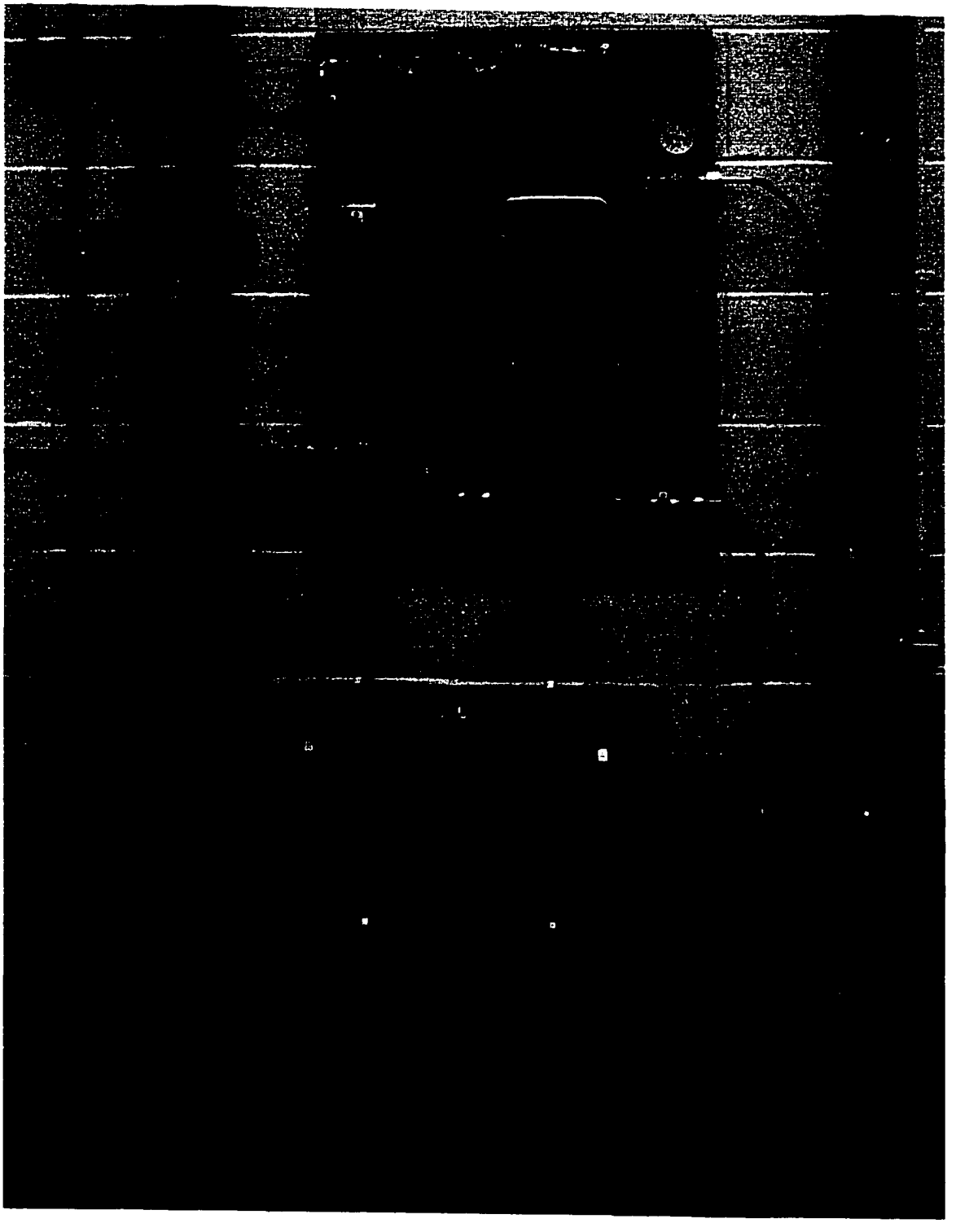

Figure 7.9. *Photograph of Gas and Water network.*

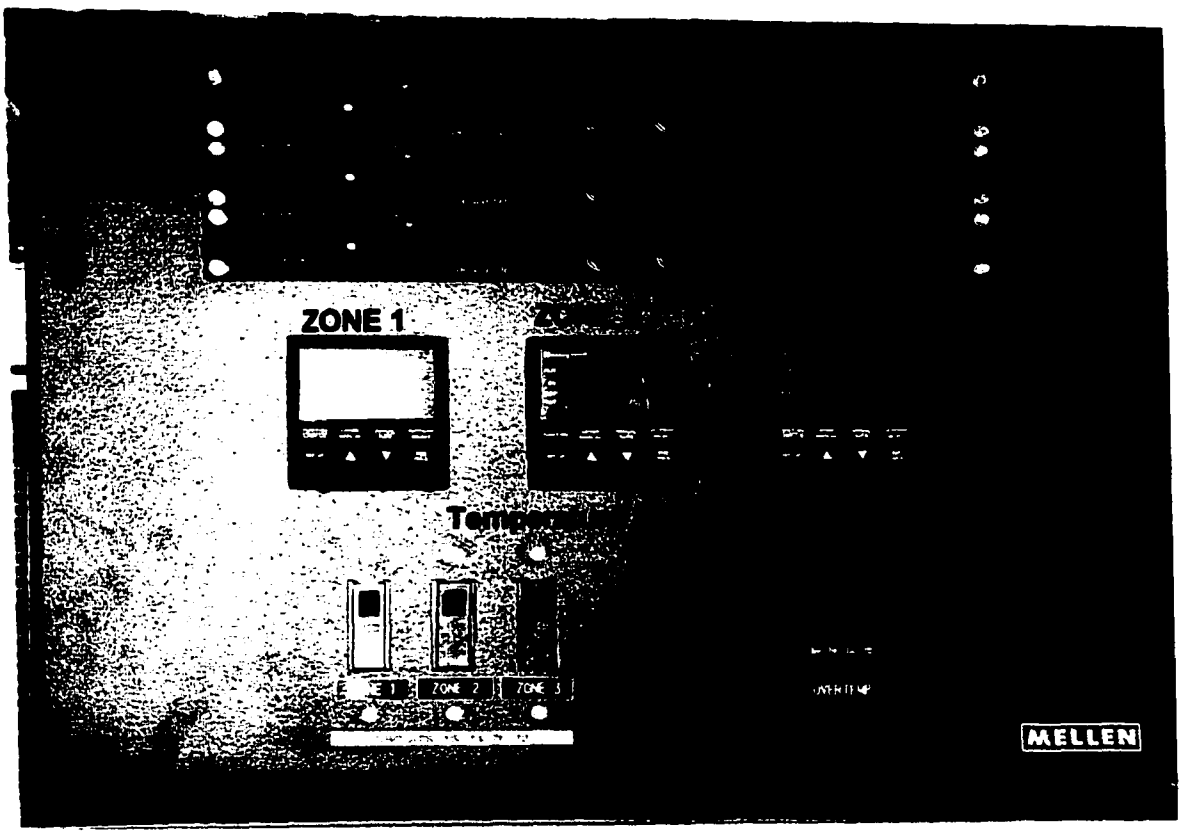

Figure 7.10. *Photograph of controllers.*

Chapter 8

Experimental Procedure and Preliminary Results

8.1 Furnace Temperature Profile and its Effect on Growth

A furnace temperature profiling was performed to determine as accurately as possible the axial temperature distribution along the column where the growth crucible is positioned. Two thermocouples (TC) enclosed in ceramic tubes were used. It is possible to slide the TC along the axial direction. The first thermocouple is positioned inside the crucible with all components present. The second was positioned just outside the crucible. Temperature profiling was done with no material in the crucible.

Plots showing temperature versus distance along the crucible helped determine the temperature gradient between the source and the substrate. This was facilitated by using a dummy graphite crucible to accommodate the thermocouples. Thermocouple readings were taken at locations where the actual crucible would be positioned. Measurements were performed twice at each location, one during the TC extraction and the other one during its insertion. The average reading was used as the data points for plotting. Measurements were performed at 1 to 5 mm intervals until the entire crucible range was covered. Measurements were performed for different controller set points. System pressure was maintained at the same pressure of the growth experiment. Hydrogen was flowing during the profiling measurement. The profiles help in understanding the thermal behavior of the system for a particular external set temperature. All zones (Z1, Z2, and Z3) were utilized during growth. The positions of the substrate and the source relative to the temperature profiles as well as the position of zones are shown in figure 8.1.

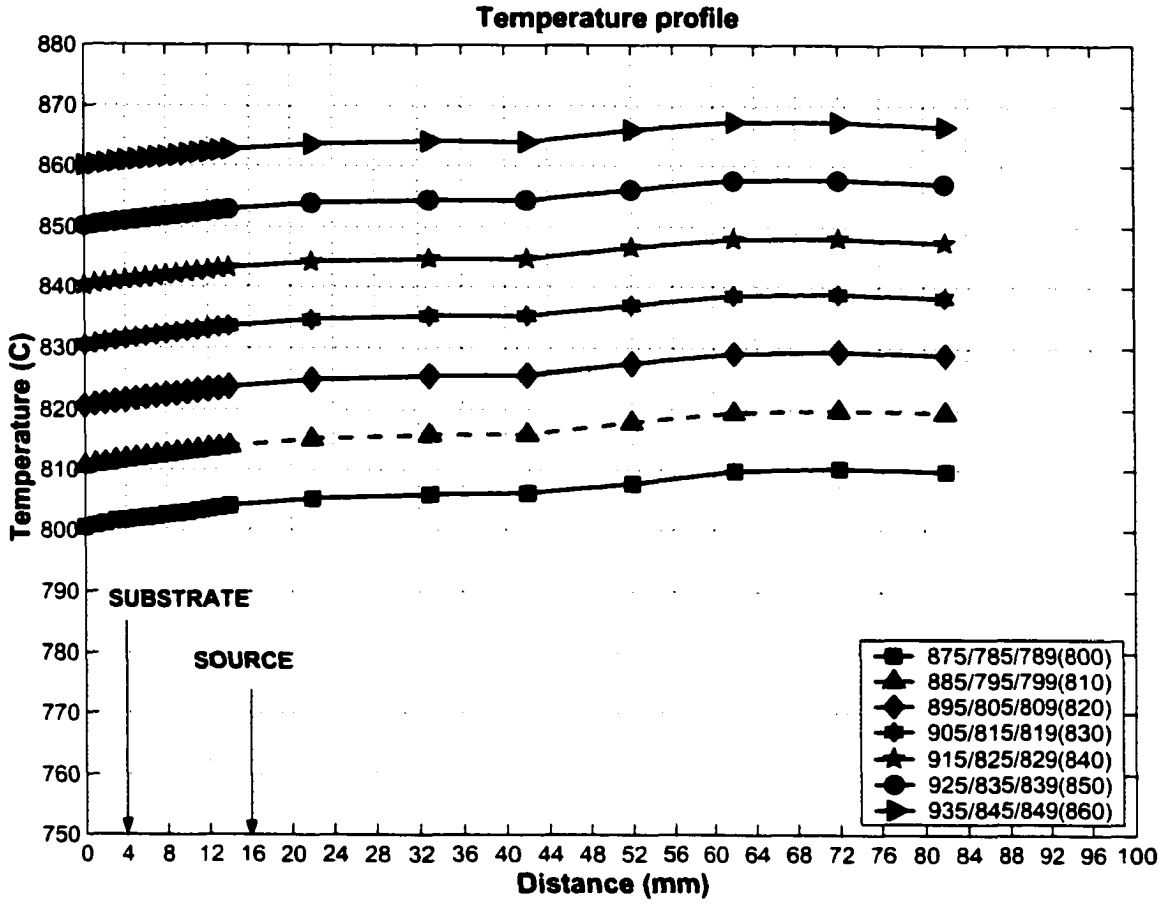

Figure 8.1. *Temperature profiles*

8.2 Contact-zone

One of the most crucial parameters of the LPEE growth experiments is the uniformity of the contact-zone (substrate-graphite). It must provide the passage of a uniform current through the interface. It must be stable and sustain the electric current for long periods of time at high temperatures.

It was first thought that it is possible to achieve such a contact with gallium and tantalum foil. This was done by placing the layer of Ga on the substrate, then a Ta foil, and then a second thin layer of Ga which served as the contact between the Ta layer and the graphite. The Ta foil, being not completely dissolved, stopped the upward diffusion of gallium ions into the substrate under the action of the electric current, and resulted in se-

vere dissolution of the back of the substrate by gallium. Experiments showed that it is not possible to achieve these requirements. Because of the hydrogen environment during the LPEE experiments and the reaction between the tantalum foil and hydrogen, the tantalum foil disintegrated. The tantalum foil was too thin to handle the electric current. After a large number of contact-zone trials, it was finally decided to use a liquid contact zone that can withstand a prolonged growth (3-8 days at the beginning of the project) at high temperatures. After a large number of trials, a liquid contact zone that consists of an alloy of gallium and aluminum, with aluminum at about 10 % in weight (as mentioned in 7.1.1), was selected as the contact zone.

The first couple of experiments indicated the importance of the quality of the electrical contact (uniform wetting) at the back of the seed in achieving thick single crystal growth. Figure 8.2(a) shows a picture of the backside of the seed at the end of run LPEE1-04. The darker regions indicate areas in which none or very little current passed during the growth. This resulted in excessive current density at other areas of the seed, which then lead to rapid loss of surface integrity. Figure 8.2(b) shows a back view of the seed of the end of run LPEE1-07. A good wetting was achieved. This resulted in the passage of uniform electric current through the seed.

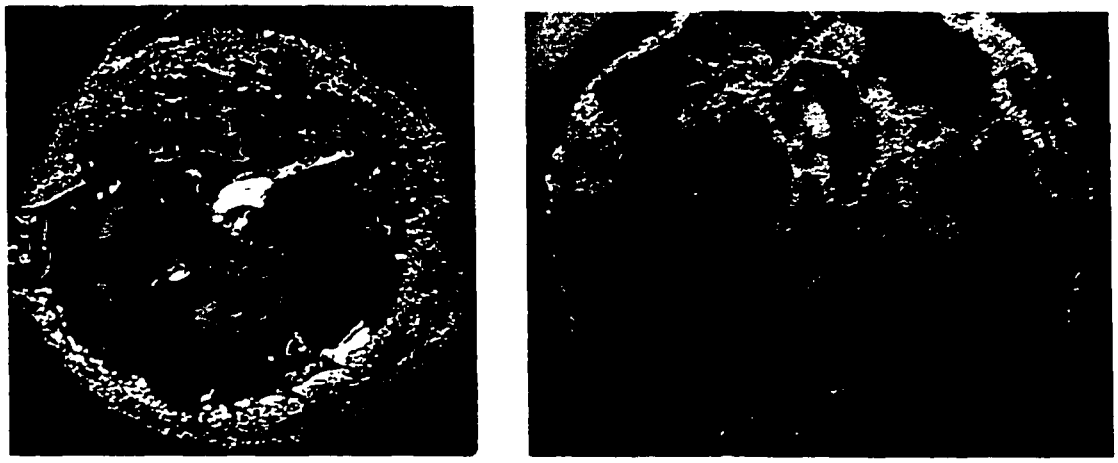

Figure 8.2. *Back contact of substrate.*

A good wetting of the backside of the seed was not easily achieved. Many crucible

geometries were studied, and the best results (at later runs LPEE-01 and onwards) were obtained using a contact zone with a thickness of 250 microns, kept under minimal positive gauge pressure during growth. This pressure is helpful in preventing non-wetting of some areas on the back of the seed. The pressure must be chosen with care, as excessive pressure can result in bending, or even breaking, of the seed, as occurred in some of the experiments.

8.2.1 Magnetic Field Distribution

While the magnet was operating at 20KGauss, the axial and radial magnetic field profiling was performed to determine the strength and the distributions of the field along the column where the growth crucible is positioned. This was done using a probe and a traverse system in the axial and radial directions. The field profile was taken without the presence of the crucible and the furnace. The presence of the crucible and the furnace should normally not effect the field distribution because the materials used in the system were supposed to be nonmagnetic materials. However, experience show that the field distribution may be affected.

Plots showing magnetic field versus distance along the magnet in both axial and radial directions are shown in figures 8.3. As can be seen, the variation of the field is less than 0.01 % in the region where the growth cell is located. These profiles help determining the location of the crucible where the field is uniform.

8.3 Preparation of Growth Materials

The materials used for a typical $InGaAs$ LPEE crystal growth experiment are the following:

- A $GaAs$ single crystal, 6-nines purity, 425 - 1200 μm in thickness, polished on a 100 plane, to act as the substrate for the growth.
- A $InGaAs$ source, 6-nines purity, around 3000-4000μm in thickness.
- Gallium pellets, In pellets, and $GaAs$ chips, 6-nines purity, to form the solution.
- Gallium and aluminum pellets, 4-nines purity, to form the contact zone alloy.

Both the substrate and the source are obtained from large diameter wafers. To fit into the crucible, as seen in Chapter 7, they must be reduced to a square shape, a natural config-

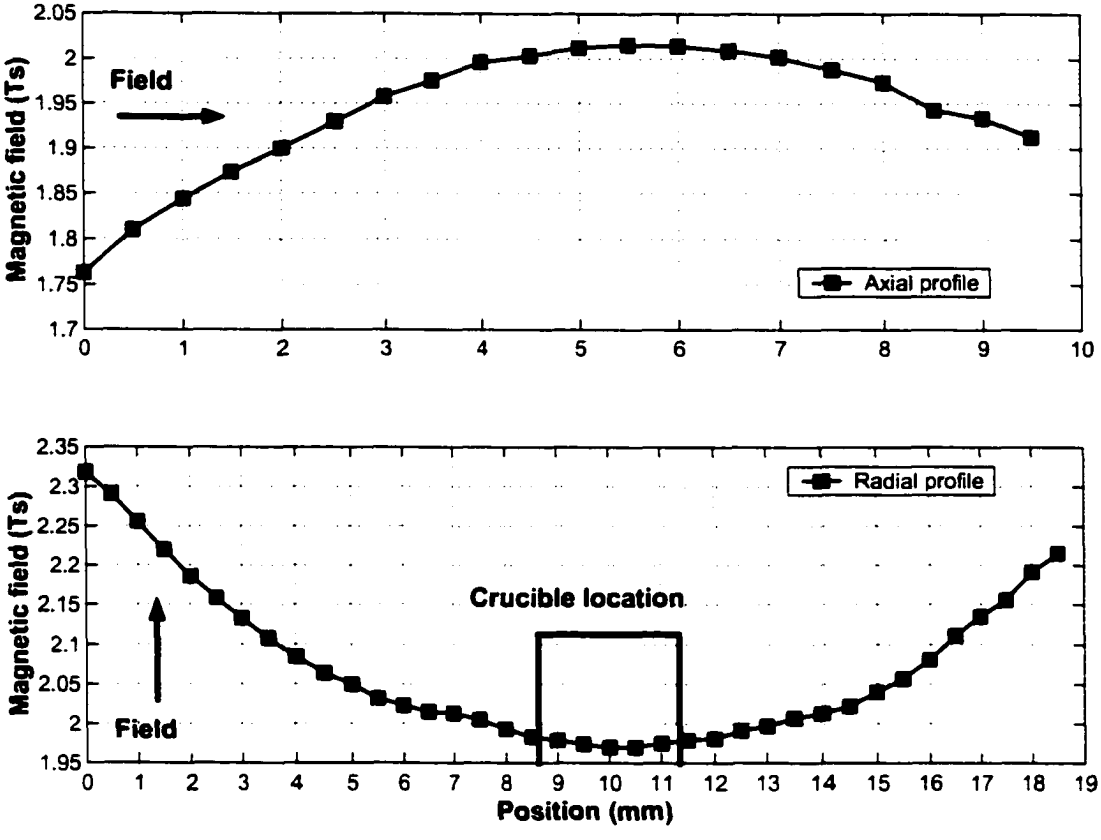

Figure 8.3. *Magnetic field profiles*

uration for 100 $GaAs$ crystals. For the substrate, this can be done by scratching one edge of the substrate at the location where the cut is required, using a sharp, hard tool (the tip of a knife or of a tungsten marker, for example). The part of the wafer which is of interest (the future substrate) is then placed on a uniform surface, with the cleaving line along the edge of this surface. By applying pressure on the unsupported side of the wafer, it will cleave along the principal direction of the crystal, resulting in a straight $< 110 >$ edge.

For the source material, if it is a single crystal, the first step should be to scratch deeply one surface of the wafer along the principal direction. Then, the wafer is placed along a sharp edge, such as the corner of a table, and snapped in two by tapping lightly on the unsupported side. If the source material is polycrystalline, the wafer should be cut using diamond-based tools.

When working at this stage of the material preparation, both on the substrate and the source, one should use polyethylene gloves and clean tools to avoid contamination of the materials.

Once the growth materials have been given their required dimensions, it is now time to proceed with the surface treatments. For this part of the material preparation process, one must wear the following protective gear:

- Heavy rubber gloves.
- Safety apron.
- Safety goggles.
- Laboratory coat.
- Cleanroom cap and mask.
- Protective shoe covers.

All these are first and foremost used to provide the wearer protection against the strong acids that are required for the etching operations. At the same time though, their use also minimizes the amount of impurities to reach the materials, thus offering higher chances of thereafter growing high quality crystals.

8.3.1 Surface Treatment of Materials

Here, we describe the steps used for the surface treatment of the substrate ($InGaAs$) and the source ($GaAs$). Please note that this is only one of the many possible processes available to clean and etch the surface of $InGaAs$ and $GaAs$ materials. Other methods, often of similar quality, can be found in the literature [93, 94, 95, 96, 97]. Which method should be used is left at Researcher's discretion

Since this surface treatment operation is mainly important in the case of the substrate, the substrate should be treated on its own, while the source material can be treated with the $GaAs$ chips that are to be dissolved in the solution. Also, note that the materials should not be allowed to dry between each of these steps, as this would lead to unwanted oxidation of the surfaces. The process is as follows:

1. Clean the materials in acetone for about three minutes in an ultrasonic cleaner. This removes humidity from the materials surface.

2. Clean in methanol for about three minutes in an ultrasonic cleaner. This step is used to wash off the acetone from the surfaces of the materials.
3. Rinse thoroughly in de-ionized water.
4. Etch for 60 seconds, while mixing constantly, in a $H_2SO_4 : H_2O_2 : H_2O = 4 : 1 : 1$ in volume solution. The solution should be at a temperature close to 60°C during etching, to insure an adequate etching rate. In this solution, the H_2SO_4, (sulfuric acid) is the complexing agent, the H_2O_2 (peroxide) is the oxidizing agent, and the de-ionized water is the diluting agent. This step is used to remove a few atomic layers from the materials. Note that for the substrate, the surface in free contact with the solution during etching should be the one on which the crystal growth will later be performed.
5. Rinse thoroughly in de-ionized water.
6. Etch for 5 minutes using concentrated HF (HydroFluoro-acid). The HF being a complexing agent, this step is used to remove residual oxides that might be left over from step 5.
7. Rinse thoroughly in de-ionized water.
8. Rinse thoroughly in methanol. Keep the materials in methanol until they are placed in the crucible for the start of the experiment. This storage period should be limited to a few hours.

8.3.2 Surface Treatment of Metals

For the treatment of gallium, indium, and aluminum, the first three steps are identical as those described in 8.3.1. For gallium, the forth step consists of etching for at least 10 minutes in a concentrated solution of HCl (HydroChloric acid), with no need of mixing. For indium, same as Ga except using less concentrated HCl . As for aluminum, the forth step is replaced by an etching of 2 minutes in a H_3PO_4 (phosphoric acid) solution, 50 % vol, while mixing periodically. The etching is completed with the steps 7 and 8 of the surface treatment process given in 8.3.1.

Table 8.1 lists a summary of a host of chemical solutions which were used in the course of this work.

Table 8.1. *List of chemical solution used in etching*

Material	Etching Solution	Action/Time
$GaAs$	$H_2SO_4 : H_2O_2 : H_2O = 4 : 1 : 1$ HF	Mix/60s
Ga	$HCl : H_2O = 1 : 9$	No Mix/10-15min
$InGaAs$	$H_2SO_4 : H_2O_2 : H_2O = 4 : 1 : 1$ HF	Mix/60s
In	$HCl : H_2O = 1 : 9$	No Mix/
Al	$H_3PO_4 : H_2O = 1 : 1$	Mix/120s

8.4 Typical LPEE Crystal Growth Experiment

In this section, we enumerate the successive operations which are required in a crystal growth experiment, when using the facility presented in this thesis. Please refer to figure 7.8 for the designation of the various components.

Before the start of Step I, we assume that the reactor tube was etched and crucible parts were cleaned and baked-out. See appendix A for more detail.

1. Material preparation. See section 8.3.1.
2. Remove the crucible from the reactor tube, and insert the growth materials within their respective parts (see Chapter 7). At this point, the growth materials are taken directly from the methanol in which they were kept after the etching process, and should be handled with clean tweezers only. The operator should wear a cleanroom cap, a mask, gloves and a coat, to avoid contamination of the materials and/or the crucible. Try to perform this operation as quickly as possible, to minimize the time during which the materials and crucible are exposed to air.
3. Replace the crucible back inside the reactor tube.
4. Connect the TMP to the flange vacuum outlet.
5. Depressurize the reactor tube. Start the backing pump. When the pressure drops under 10^{-2} mbar on the Pirani gauge, turn on the TMP. Keep both pumps running until the pressure drops under 10^{-4} mbar on the hot ion gauge.

6. Isolate the reactor tube. Close valve. Turn off the TMP, and open the vent valve on the TMP to accelerate its return to atmospheric pressure. Once the TMP has stopped, turn off the backing pump and close valve and the TMP's vent valve. Disconnect the TMP from flange.
7. Fill-up the reactor tube with hydrogen. Shut off the outlet of hydrogen, and open the inlet. Very slightly open the valve. The pressure reading on metering should drop to a high vacuum level. Allow the reactor tube to fill-up slowly; a sudden rush of gas in the tube might cause it to shatter. When the pressure reading on the pressure gauge is higher than the atmospheric pressure, open the valve completely.
8. Establish a steady flow of hydrogen through the reactor tube. Open outlet valve in the flange and the valve to the bubbler. The flow of hydrogen should then be visible in the bubbler. Adjust metering to reach a flow close to 100 ml/min.
9. Turn on the furnace, and warm up the system to growth temperature. Once the growth temperature is obtained, allow at least two hours for the solution materials to equilibrate with the source material.
10. If a meltback of the substrate is desired, increase the temperature of the system by a few degrees, and wait for some time to allow the substrate, source and solution to reach thermal equilibrium.
11. Apply a DC current for the whole duration of the crystal growth. Stop DC current to terminate growth.
12. Stop the furnace, and let the system return to RT.
13. Stop the hydrogen flow.
14. Open the reactor tube, and remove the crucible. Take the growth materials and the grown crystal out of the crucible.
15. Replace the crucible in the reactor tube.

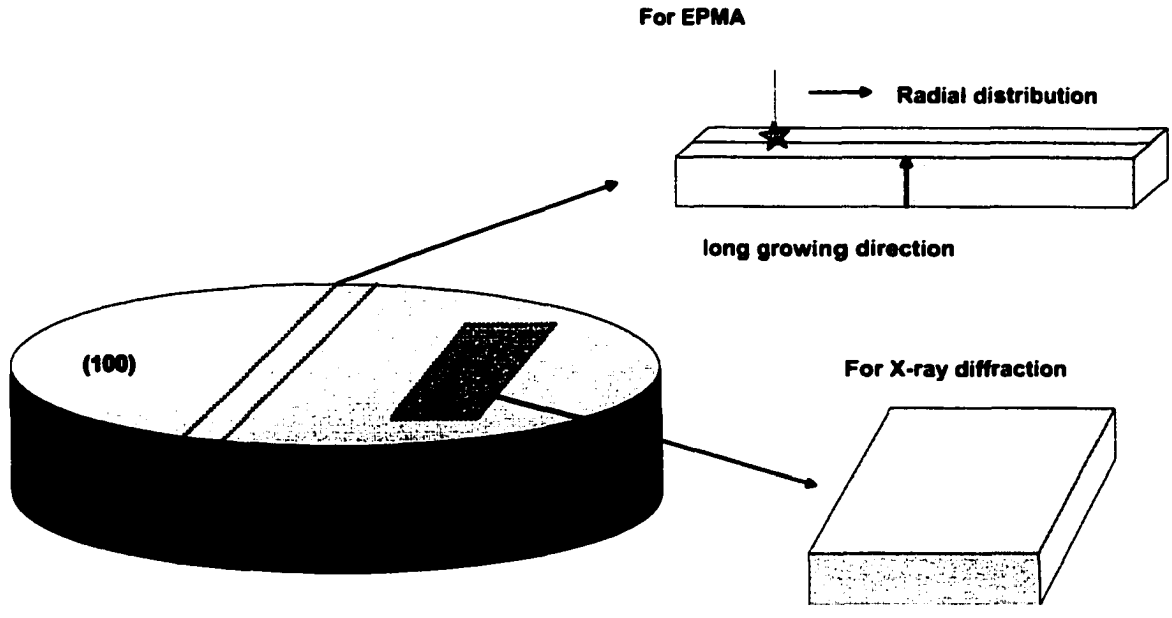

Figure 9.1. *A representation of samples used in EPMA.*

9.1 Electron Probe Micro Analysis (EPMA)

All the EPMA measurements were done in the Research Institute of Electronics Laboratory at Shizuoka University in Japan by Dr. Akira Tanaka. The scanning was done along the radial and growth (axial) directions.

The EPMA (point EPMA) was performed at three radial and three axial locations (growth direction) on the cross-section. On the same samples, EPMA (scanning EPMA) was performed across the grown crystal at three radial locations, refer to figure 9.2.

EPMA basically works by bombarding a micro-volume of a sample with a focused electron beam (typical energy = 5-30 Kev) and collecting the X-ray photons thereby induced and emitted by the various elemental species. Because the wavelengths of these X-rays are characteristic of the emitting species, the sample composition can be easily identified by recording WDS spectra (Wavelength Dispersive Spectroscopy). WDS spectrometers are based on the Bragg law and use various moveable, shaped monocrystals as monochromators.

An electron microprobe uses a beam of focused electrons to excite X-rays from a small area of a polished sample. Low-energy thermionic electrons are produced from a tungsten

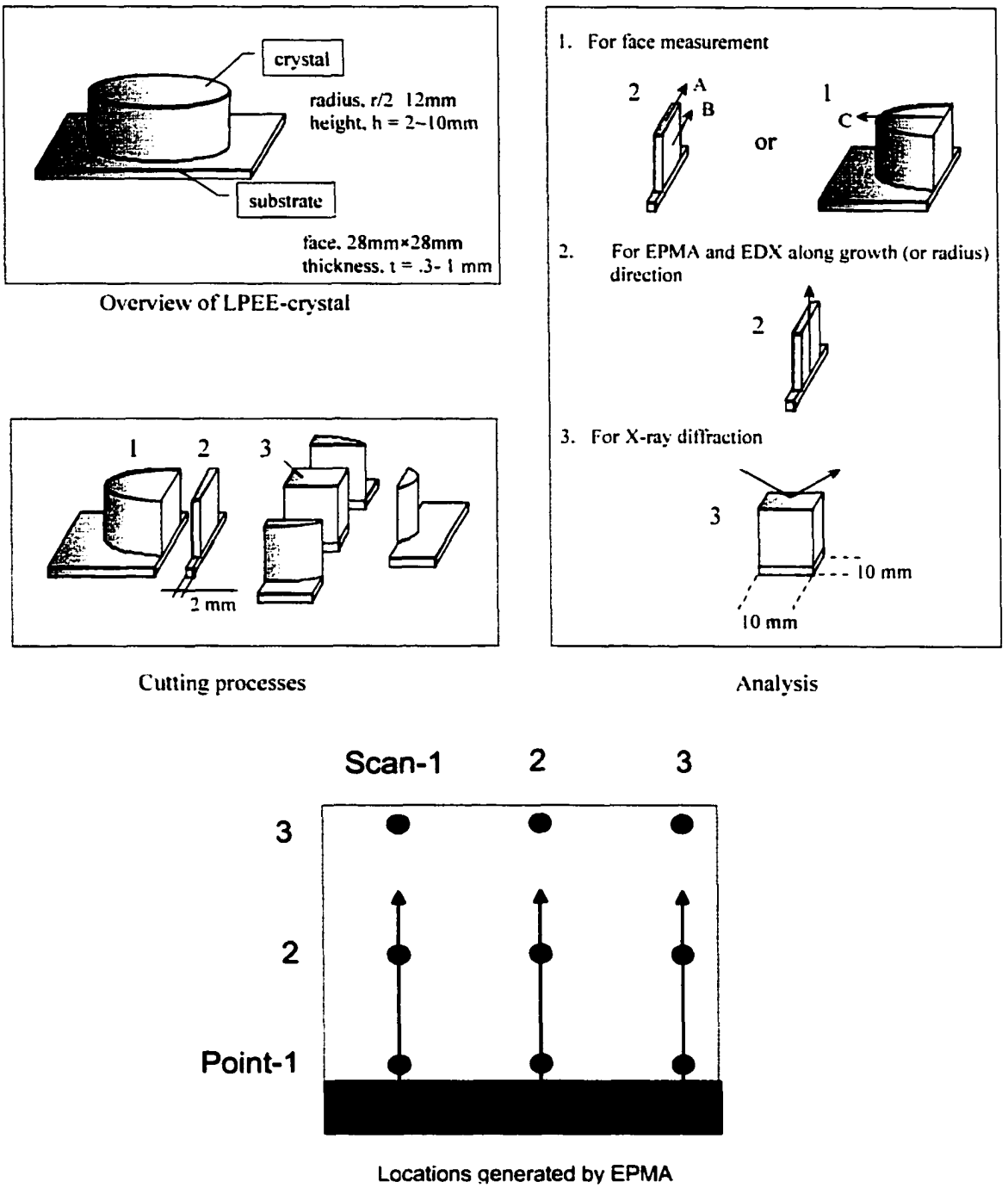

Figure 9.2. *Cutting procedure to prepare samples for analysis.*

filament and accelerated by a positively biased anode plate to 10-30 thousand electron volts (KeV). The anode plate has a hole in its center and the electrons pass through it and are

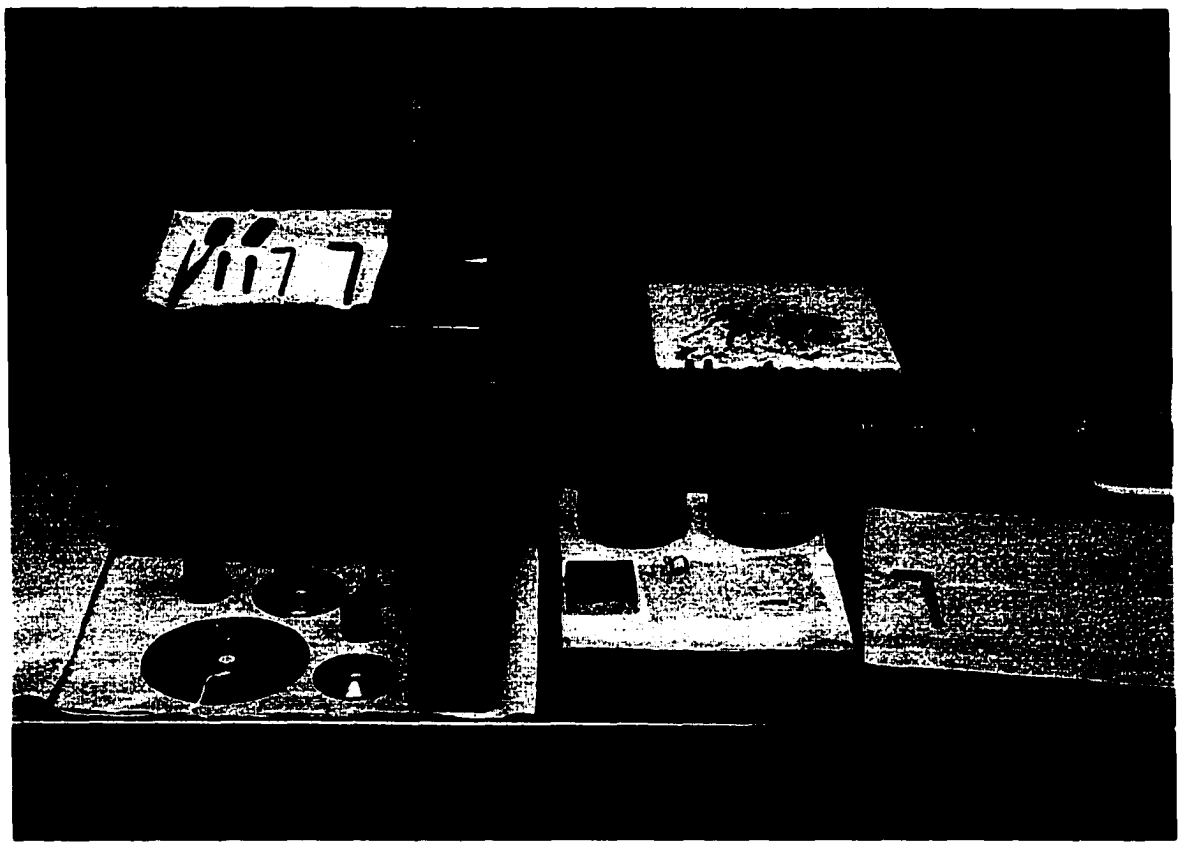

Figure 9.3. *Photograph of the samples preparation.*

collimated and focused by a series of magnetic lenses and apertures. The electron beam is used to bombard the sample and produces analytical X-rays from it. The resulting X-rays are diffracted by crystals, detected, and their intensities measured. In contrast to X-ray fluorescence (XRF) analysis, in electron microprobe analysis X-rays are excited from a very small volume (about 4 to 9 μm^3) and the analysis is made in a textural context. The unknown composition is determined by comparison with X-ray intensities from materials with known compositions (standards). In our case the standards were $GaAs$ and $InAs$.

9.2 X-ray Microanalysis

The x-rays consist of two components - the background and the characteristic peak - that are produced by different mechanisms. The background continuum is a collection of x-

rays generated by the beam electrons when they are decelerated by atomic nuclei. This phenomenon is known as bremsstrahlung and is illustrated in figure 9.4 (a). The transition of a core electron to a lower energy state results in the emission of an x-ray, whose energy is characteristic of the particular atom and this is illustrated in figure 9.4 (b). A collection of such x-rays forms discrete peaks that can be used to reveal the composition of the specimen. $GaAs$ and $InAs$, as well as some pieces of $In_xGa_{1-x}As$ where x is known, were chosen as standards for the grown crystal.

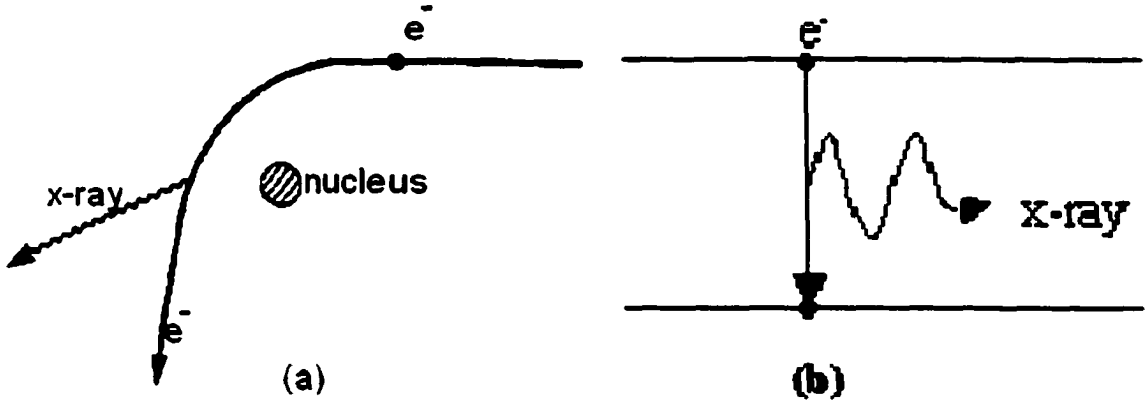

Figure 9.4. *(a) Deceleration of an electron in the presence of a nucleus. (b) Transition of an electron from one energy state to a lower allowed energy state.*

Measurements were done for the cross-section of some of the same samples which were sent to Japan for the EPMA. X-rays generated at seven locations on the cross-section by a 10 Kev electron beam were collected for a real time of 1200 s with the stage tilted to 50^o.

Chapter 10

Results and Discussion

This chapter presents the experimental results of the LPEE growth process of $GaAs$ and $InGaAs$ that were obtained by using the setup and technique presented in earlier chapters. The layer thickness was studied in conjunction with various growth parameters and conditions such as electric current density, growth time, source material, solution composition, and applied external magnetic field.

Most of the growth parameters necessary for the successful operation of the growth setup were worked out by growing $GaAs$ first, before attempting the growth of the ternary alloy $InGaAs$ (with 4% In-content, i.e.,$In_{0.04}Ga_{0.96}As$). The main reason for such an approach was due to the fact that we wanted first to improve the growth technique and its procedures using a known-, well tested- material. Then the efforts were to focus on the growth of the ternary alloy $InGaAs$. With the improvements to be made in the growth procedures of $GaAs$, $InGaAs$ crystals would be grown with the properties of the LPEE growth and with the thickness of a melt growth.

The influence of the applied magnetic field (the effect of the magnetic field on the natural convection in the solution and the Joule heating in the source) on the growth rate and also on the quality of the grown crystal are presented in Section 10.1.2.

It is demonstrated that the control of growth conditions, through the use of an external magnetic field, improves the quality and thickness of the grown crystals through the suppression of the natural convection in the solution, and in turn prolonging the growth process, and leading to uniform and stable growth interfaces.

Several crystal growers have attempted to use LPEE to grow bulk ternary crystals. However, most have reported only modest levels of success (4 mm thick) because of the difficulties in controlling the effect of convection and Joule heating in the system. The biggest challenges in growing crystals by LPEE are the reduction of the convection in the solution

and the minimization of the effect of the Joule heating in the source material.

10.1 Growth Rate and Growth Characteristics

The growth rate of the grown crystals was subsequently determined as a function of electric current density and growth time. For this purpose, over sixty growth experiments were performed during this study. A significant number of these experiments were unsuccessful for various reasons such as nucleation, the use of high electric current density and strong applied magnetic field, or equipment malfunction. The data obtained from successful runs are presented in tables 10.1 and 10.2. These tables will be used as reference to all figures. Constant growth rates observed in earlier experiments indicated that the LPEE growth process is almost a steady state process. First, a small number of crystals were grown in the absence of magnetic field for different growth times and at different electric current density levels. Later, using the same growth conditions, crystals were grown under external magnetic field. Single crystals were obtained, refer to figure 10.1. Details are presented below.

10.1.1 Results Without External Magnetic Field

Experiments were performed first with no applied magnetic field. The main purpose was to determine the average growth rate as a function of the applied electric current density and the growth time. Most of the crystals where grown under low current density levels (3, 5, and 7 A/cm^2). Attempts to increase the electric current density to higher levels failed, and resulted in loss of the surface integrity probably due to the strong convection in both the liquid solution and the liquid contact zone. Experiments were conducted for various growth periods (from 1 to 8 days) at the temperature of $800°C$. The results are presented in figure 10.2 and figure 10.3. The average thickness of the grown crystals varies with the growth time and the applied electric current density levels.

Good crystal morphologies were generally obtained, as observed visually and microscopically. Morphology improved whenever good care was taken in cleaning the materials.

The relation between the growth time and the crystal thickness is shown in figure 10.3. As expected, the thickness (also implies indirectly the growth rate) increases with time. It was concluded previously [5, 72] that the growth rate in LPEE is a linear function of

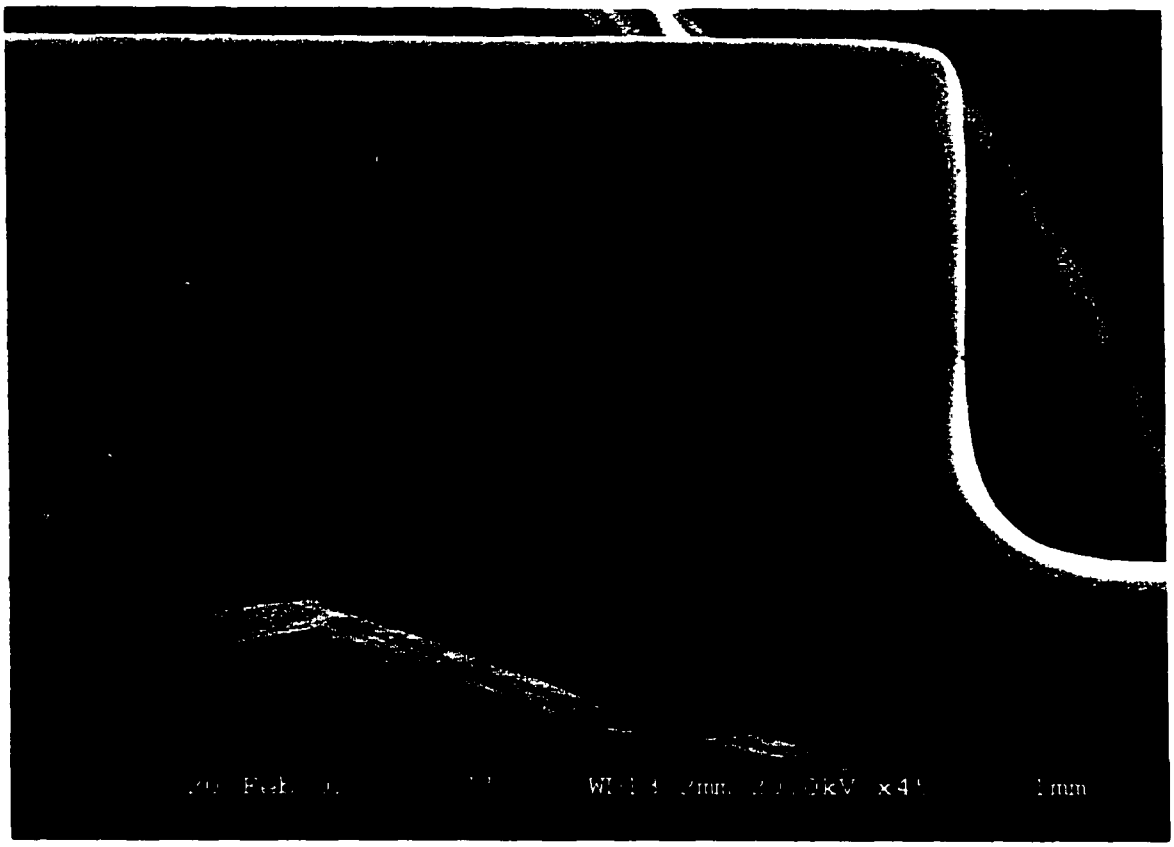

Figure 10.1. *Compositional variation in In ($In_{0.04}Ga_{0.96}As$) with growth thickness*

the applied electric current density. The results shown in figure 10.3 indicate that this is approximately the case at lower electric current density levels, but that there is a deviation (with a higher rate) from linearity at higher electric current densities. The same conclusions can be seen clearly from figures 10.3. The increase in growth rate at higher electric current densities can be attributed to the enhanced contribution of the natural convection in the solution.

This itself is a significant contribution made through the novel growth system and the growth technique developed during the present research work.

The thicknesses of grown crystals at 3 A/cm^2, with no magnetic field, are between 1.5 mm to 4.5 mm, which correspond to an average growth rate of 0.57 mm/day, as shown in figure 10.2 and figure 10.3.

The maximum thickness of 4.5 mm was achieved in 8 days under 3 A/cm^2. By increas-

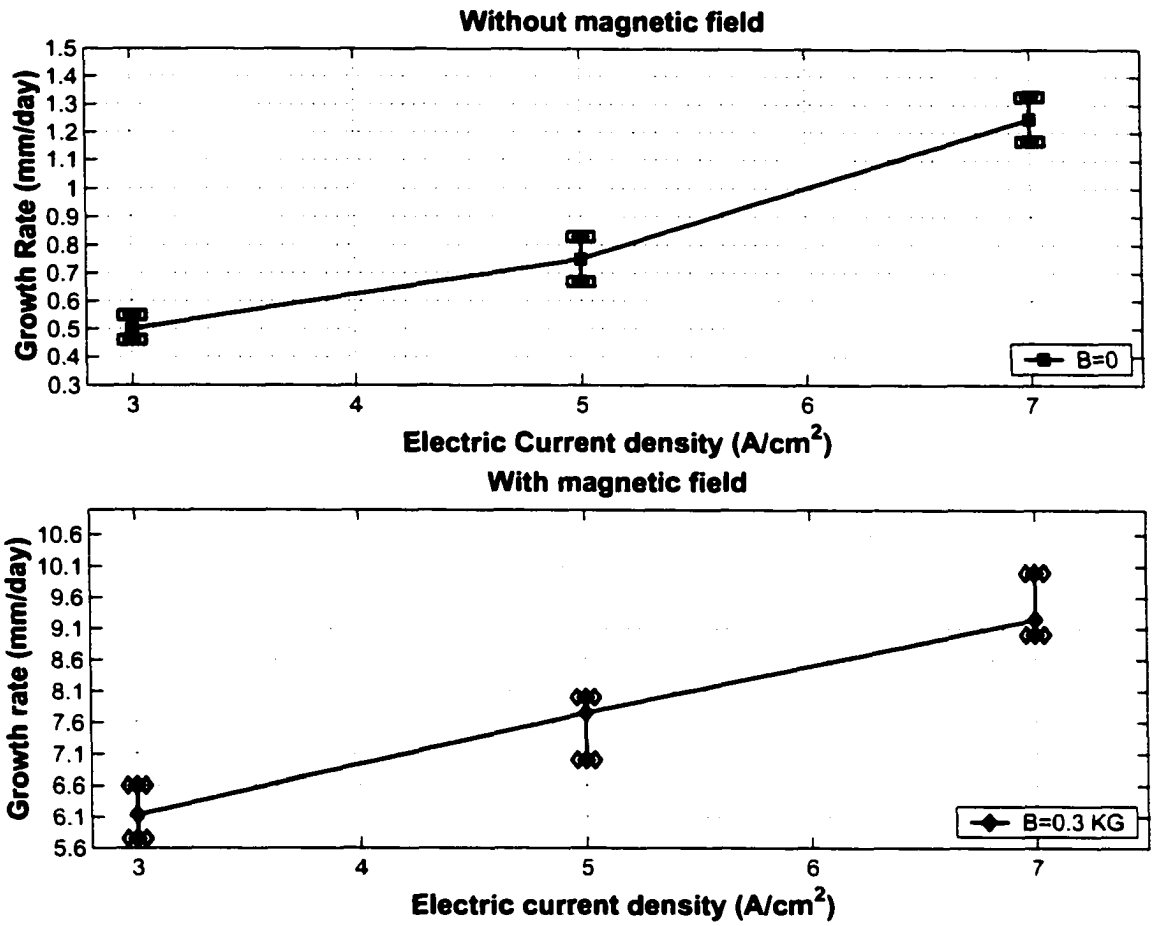

Figure 10.2. *Dependence of growth rate on current density for B=0.0 and B= 4.5 KGauss*

ing the electric current density to 5 A/cm^2 and 7 A/cm^2, the maximum average thicknesses were increased to 2.25 mm and 3.75 mm (in 3 days), respectively, refer to figure 10.6. It must be noted that some maximum crystal thicknesses were limited to the availability of the source material in the system. Some specific experiments were therefore performed to verify the observed growth rates.

The results obtained on growth rate are consistent with those of the literature [5, 72] where crystals of 4 mm thickness grown by LPEE were reported. The photographs of some of the grown crystals of LPEE shown in figure 10.4 indicate the presence of polycrystalline growth at the top crystal. For a stable growth, the surface morphology seen at the top of the crystals resembles an LPE growth, but in this case, this is a secondary growth that occurred during the cooling period of the cycle leading to polycrystalline growth since the cooling

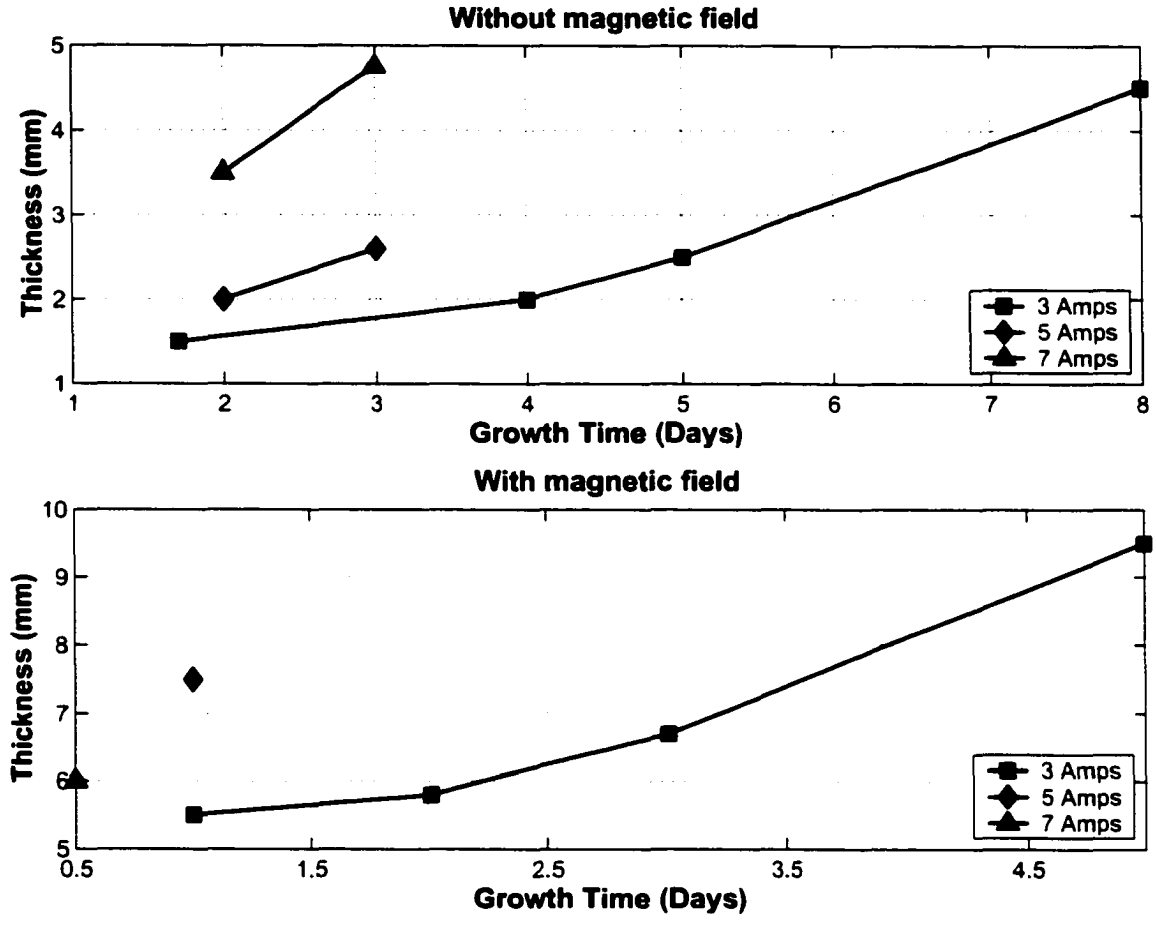

Figure 10.3. *Dependence of layer thickness on time for B=0.0 and B= 4.5 KGauss*

rate was much faster than a typical LPE growth. For example, by turning off the furnace power the cooling rate is close to 2 C^o/min. This corresponds to a very fast LPE growth, and flat crystalline layers separated by inclusion, and valleys formed, refer to figure 10.5.

10.1.2 Results with Applied External Magnetic Field

As mentioned earlier, in order to suppress the natural convection in the liquid solution for the purpose of prolonging and stabilizing the LPEE growth process for growing bulk single crystals (thicker crystals), an applied static magnetic field was used. The static applied magnetic field induces a magnetic body force that acting on the moving particles of the liquid solution and counter balances the buoyancy force. The combined effect of these two

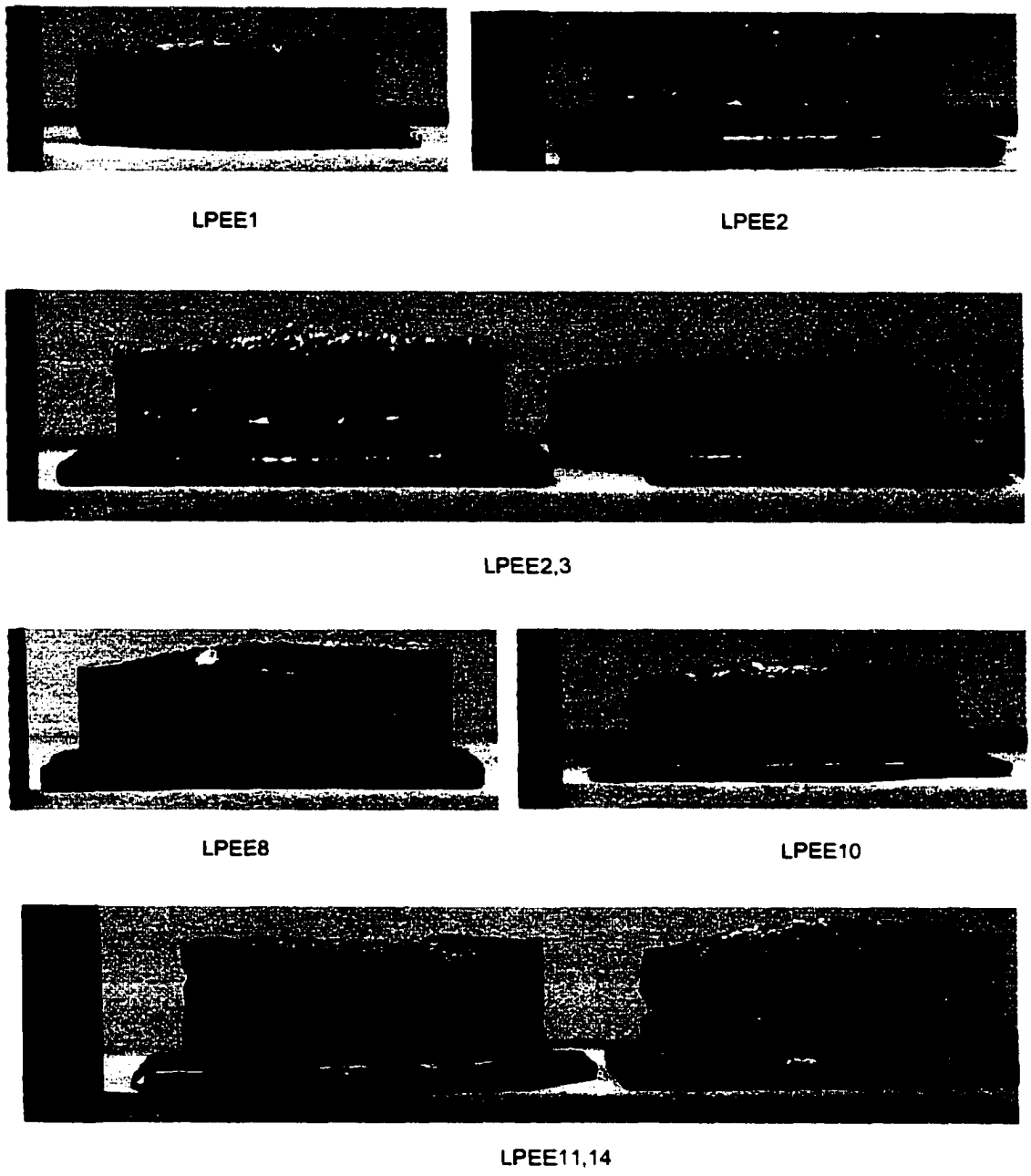

Figure 10.4. *Photographs of some of the grown crystal by LPEE at University of Victoria, at B=0.0 (no magnetic field).*

body forces suppresses the convection and prolongs the growth. This beneficial effect of an applied magnetic field was the initial intention of the present research program. However, the unexpected effect (a very positive effect) of the applied magnetic (at lower field intensity

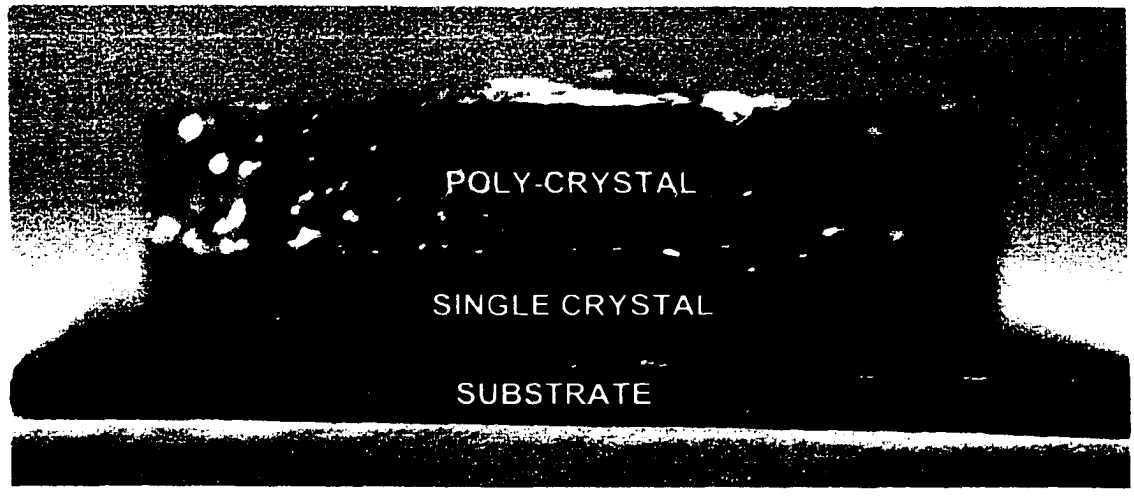

Figure 10.5. *Photograph of a grown crystal that illustrate the secondary growth during the cooling period(LPE).*

levels) was the significant increase in the growth rate (about 7 - 16 fold). As explained below, such a drastic increase in the growth rate elevates the LPEE growth process to the category of a bulk growth.

Thus far, the only disadvantage of LPEE was its low growth rate (about 0.6 mm/day for a 3 A/cm^2 electric current). However, novel design features of the state-of-the-art LPEE growth system at UVic, and the application of an external magnetic field allowed the growth of crystals with a growth rate of about 4.5 mm/day (at the 4.5 KGauss magnetic field and 3 A/cm^2 electric current density), and an average growth rate of about 11 mm/day (at 4.5 KGauss and 7 A/cm^2). This is simply a breakthrough in LPEE, making it absolutely a bulk growth technique and putting it in competition with other bulk growth techniques.

The average thickness was increased to 6.0 mm using 3 A/cm^2 in 2 days, comparing with the value of 1.5 mm that was achieved in three days using the same electric current density without applying the external magnetic field. The maximum thickness of about 9mm was achieved in one day using the current density of 5 A/cm^2. The reason of not growing a crystal thicker than 9 mm is simply due to the unavailability of the source material. The crucible used could not hold more materials. Otherwise, we think that the growth of larger crystals is possible. In the last run, the source material was completely depleted. To justify that the new design is capable of growing crystals thicker than $9mm$, the current density was increased to 7 A/cm^2. A crystal of about 9 mm thick was achieved in just $1/2$

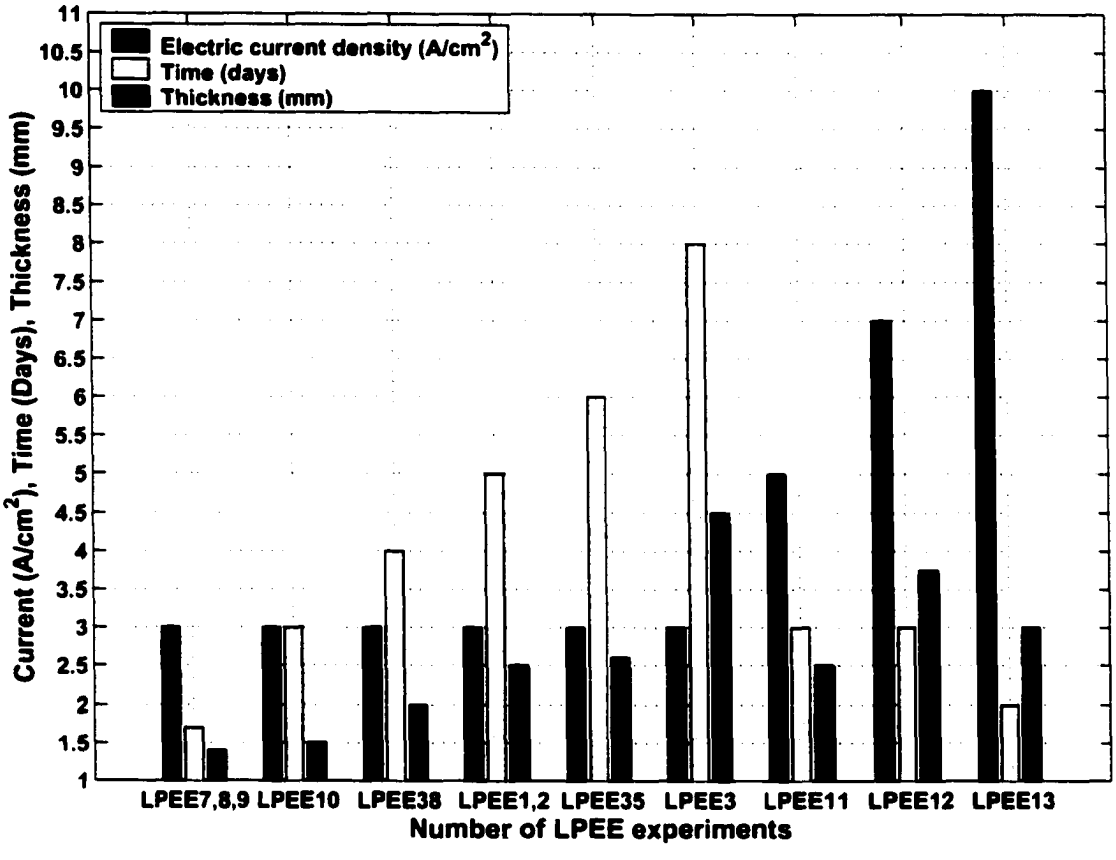

Figure 10.6. *The thickness of LPEE crystal as a function of current density and growth time, at B=0.0 KGauss (no magnetic field).*

day.

Typical LPEE single crystals are shown in figure 10.8. The humped (dome) shape in the middle is a typical characteristic of the LPEE growth setup used, as has been observed in all experiments in which the magnetic field was used. This is consistent with the inner shape of the new crucible and the path of the electric current.

Figures 10.6 and 10.7 show the thicknesses of crystals grown at 3 A/cm^2 with and without an applied magnetic field. As can be seen from figure 10.7, excellent results were obtained. The increase in crystal thickness was significant, about 4 times in some cases.

The thickest single crystal was obtained in the final run. Over 8 mm of single crystal was recorded before the depletion of all the source material. Note that, as shown in table 10.2, this result was achieved in all runs at both the lower and higher current densities.

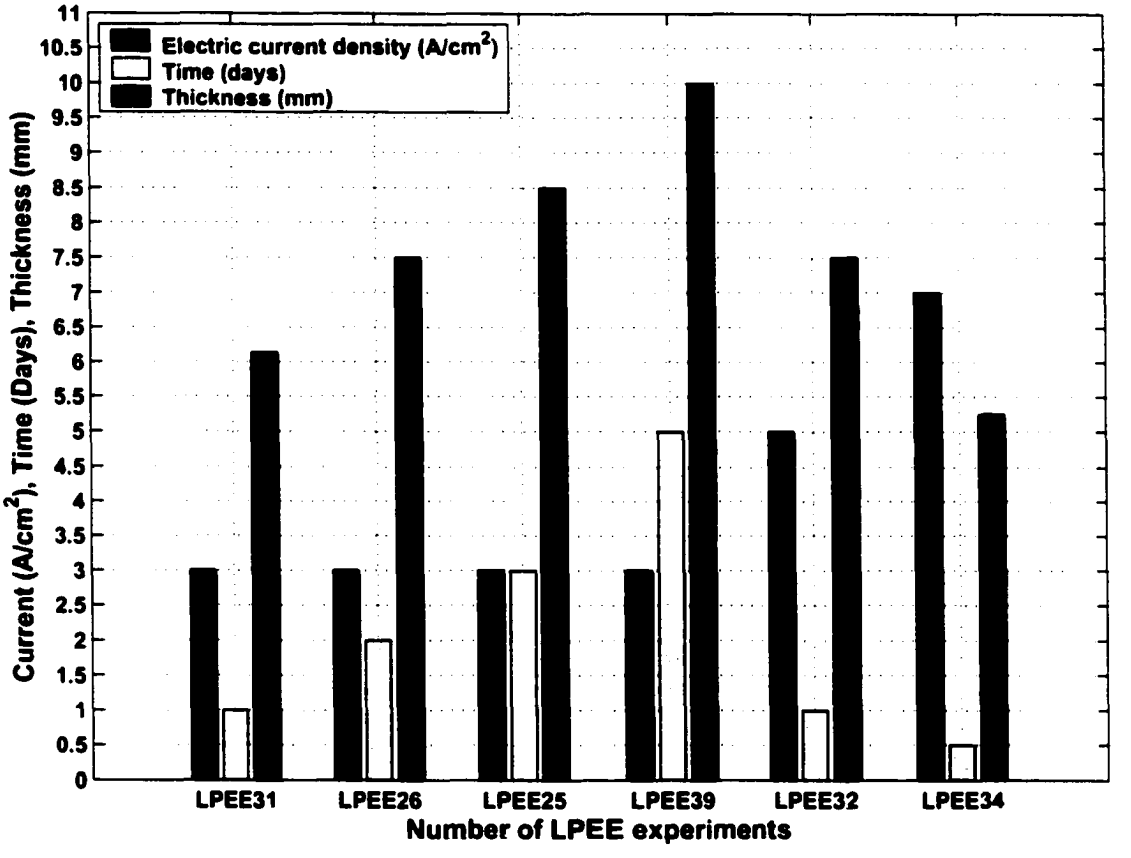

Figure 10.7. *The thickness of LPEE crystal as a function of current density and growth time, at B=4.5 KGauss*

As shown in tables 10.1 and 10.2, several growth experiments were conducted under the same growth conditions (as possible as can be) including the growth time, electric current density and other growth parameters. Results show a fair reproducibility. Considering the very complex nature of the growth process, the conducted experiments can be considered satisfactory. However, several possible improvements can be made to increase the stability of equipment by increasing the air quality in the Crystal Growth laboratory. This issue will be discussed in the future work section.

After run LPEE42, the crucible was redesigned to allow the growth of a crystal of up to 24 mm in diameter and 20 mm in thickness. This new crucible will be used to grow $CdZnTe$ crystals through the current research programs of the Crystal Growth Laboratory at the University of Victoria. Some other binary and ternary alloys such $SiGe$ can also be

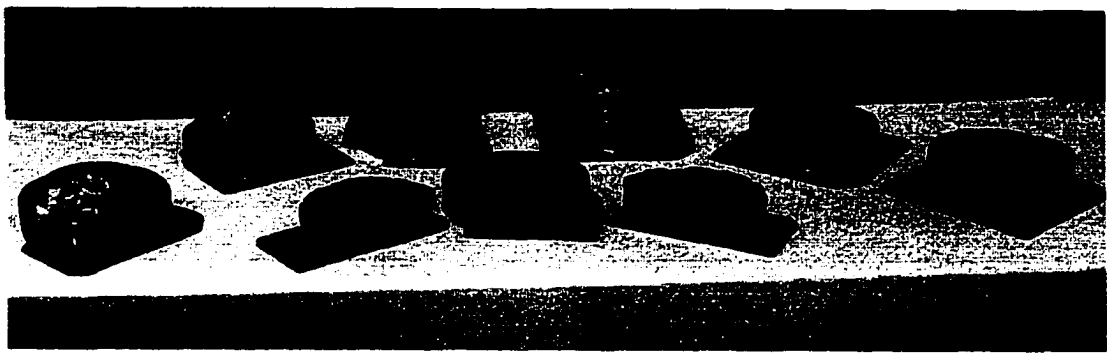

LPEE2,3,10,11,13,25,26,31,32

LPEE25

LPEE32

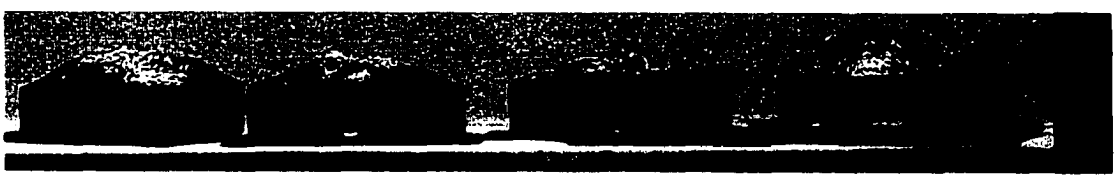

LPEE25.26.31.32

Figure 10.8. *Photographs of some of the grown crystals by LPEE at the University of Victoria, at B= 4.5 KGauss magnetic field level.*

grown.

10.2 Composition Distribution

A number of characterization techniques were used to determine the concentration and distribution of indium in the grown $InGaAs$ crystals. Results are presented in the following

sub-sections.

10.2.1 Electron Probe Micro-Analysis (EPMA)

Cleaned samples of various wafers, refer to Chapter 9, were analyzed for Indium content in the Research Institute of Electronics, Shizuoka University, Japan, by the Electron Probe Micro-Analysis (EPMA).

The compositional uniformity of an $In_{0.04}Ga_{0.96}As$ bulk single crystal was investigated by the method of Electron Microprobe Analysis. As mentioned in Chapter 9, all the EPMA measurements were obtained by Professor A. Tanaka at the Research Institute of Electronics of Shizuoka University, Japan. Data were acquired in the projected area corresponding to the thickness of the grown crystal and the diameter, refer to figure 9.2. The axial and radial composition distributions, x, were measured at different locations in the grown crystal. Results are presented in the form of line graphs (scanned distributions).

Figure 10.9 shows the composition distribution measured along the growth direction for LPEE38. The results indicate the uniformity of the In distribution along the grown crystal. No major fluctuation can be seen in the In composition. Rather, the distribution looks almost the same in all locations and all crystals. A slight decrease in the In composition towards the surface of the crystal can be seen. The same results were obtained for the Ga and As values. The uniformity patterns obtained in grown crystals show the potential of the LPEE technique in growing ternary single crystals of superior compositional uniformity as desired by the device industry.

The In composition distributions for LPEE39-LPEE42 are shown in figures 10.10 - 10.13. Again, they show the same pattern as LPEE38.

The main advantage of LPEE is its capability of producing crystals of uniform composition. This is clearly shown in figure 10.13. The solid line represents the experimental results of the In composition variation along the crystal thickness, for the crystal grown by the new LPEE procedure. It is uniform throughout the thickness of crystal. For the comparison purpose, the In composition of both the $GaAs$ and $In_{0.04}Ga_{0.96}As$ crystals, are shown in figure 10.16. It can be seen in figure 10.16 how flat the In composition is in the case of $GaAs$, and shows a sudden jump to 4% after the substrate section in the case of $In_{0.04}Ga_{0.96}As$.

The Axial (growth direction) and radial variations in indium concentration, as measured

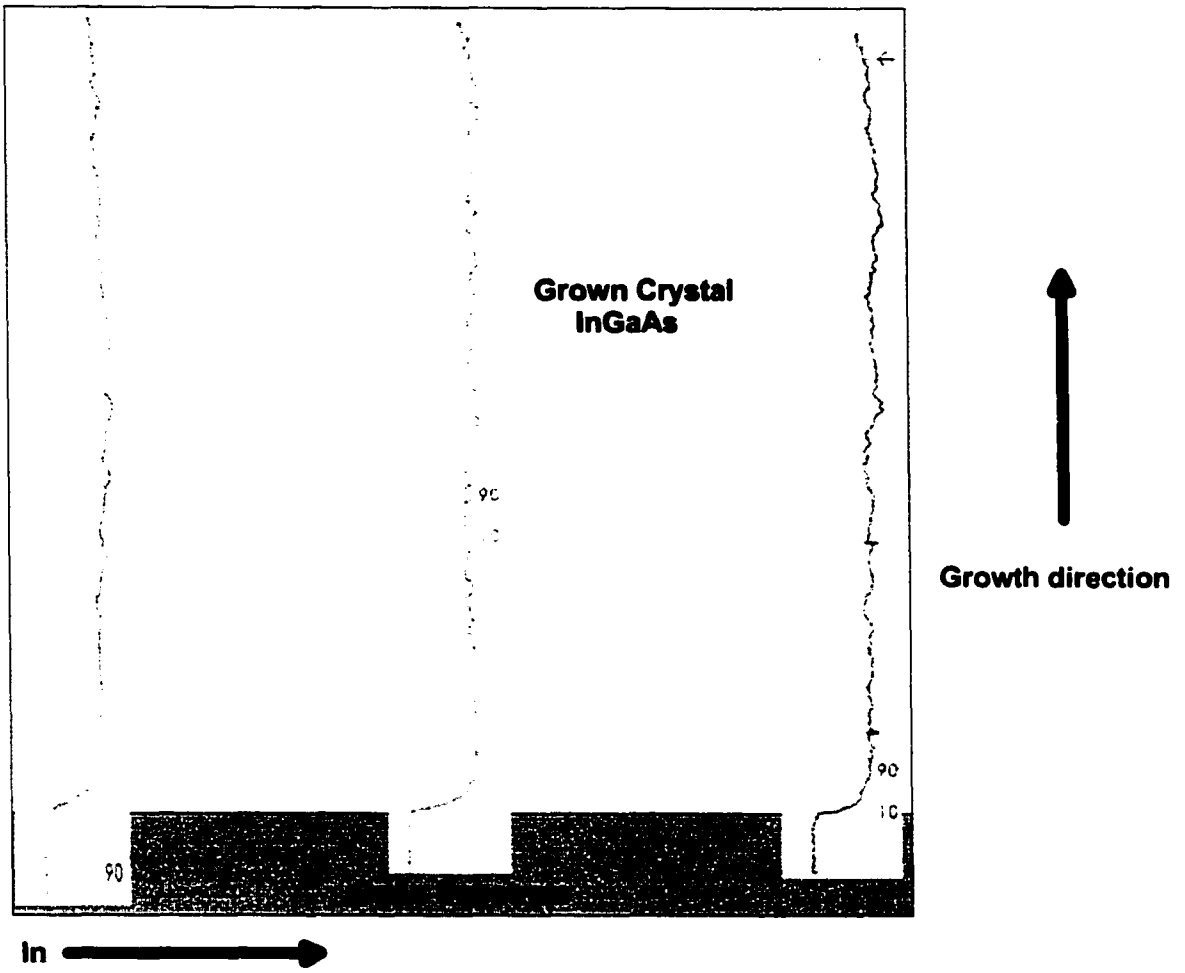

Figure 10.9. *Compositional variation in In ($In_{.04}Ga_{.96}As$) along the axial and radial directions, LPEE38*

by EPMA, are illustrated in figures 10.14 and 10.15. These data were obtained at specific points instead of scanning along a line. The error in x is within 5% of its value.

It was concluded previously, theoretically, [5, 72] that the increasing electric current density has an adverse effect on the compositional uniformity of the grown crystals. However, by using the new growth system developed during this thesis work, it was shown that the increase of electric current density will not affect the uniformity of the In composition in the crystal, refer to figures 10.9-10.13. But as mentioned in sections 10.1.1 and 10.1.2, instead it will increase the growth rate while keeping the In concentration uniform.

The source material is also very important for compositional uniformity. After a couple

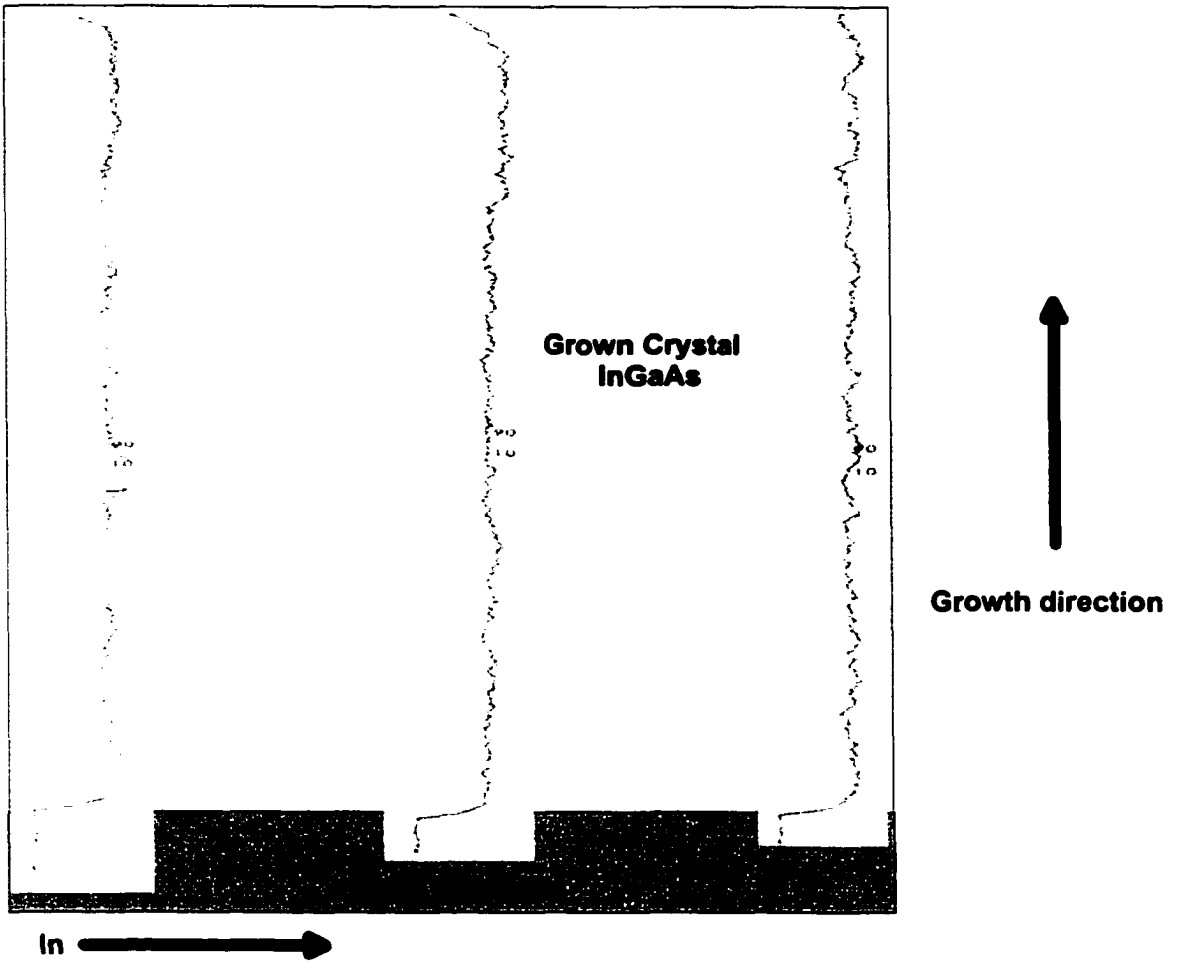

Figure 10.10. *Compositional variation in In ($In_{.04}Ga_{.96}As$) along the axial and radial directions, LPEE39*

of preliminary experiments, it was concluded that the use of a source with the same composition of the grown crystal is a requirement. In some earlier experiments, a $GaAs$ source was used. The In % in the grown crystals was almost zero, as expected. Experiments were conducted under the same condition with using a source material that has the same solid composition. The composition variation was uniform and has the same In percentages as the source material used, refer to figure 10.16.

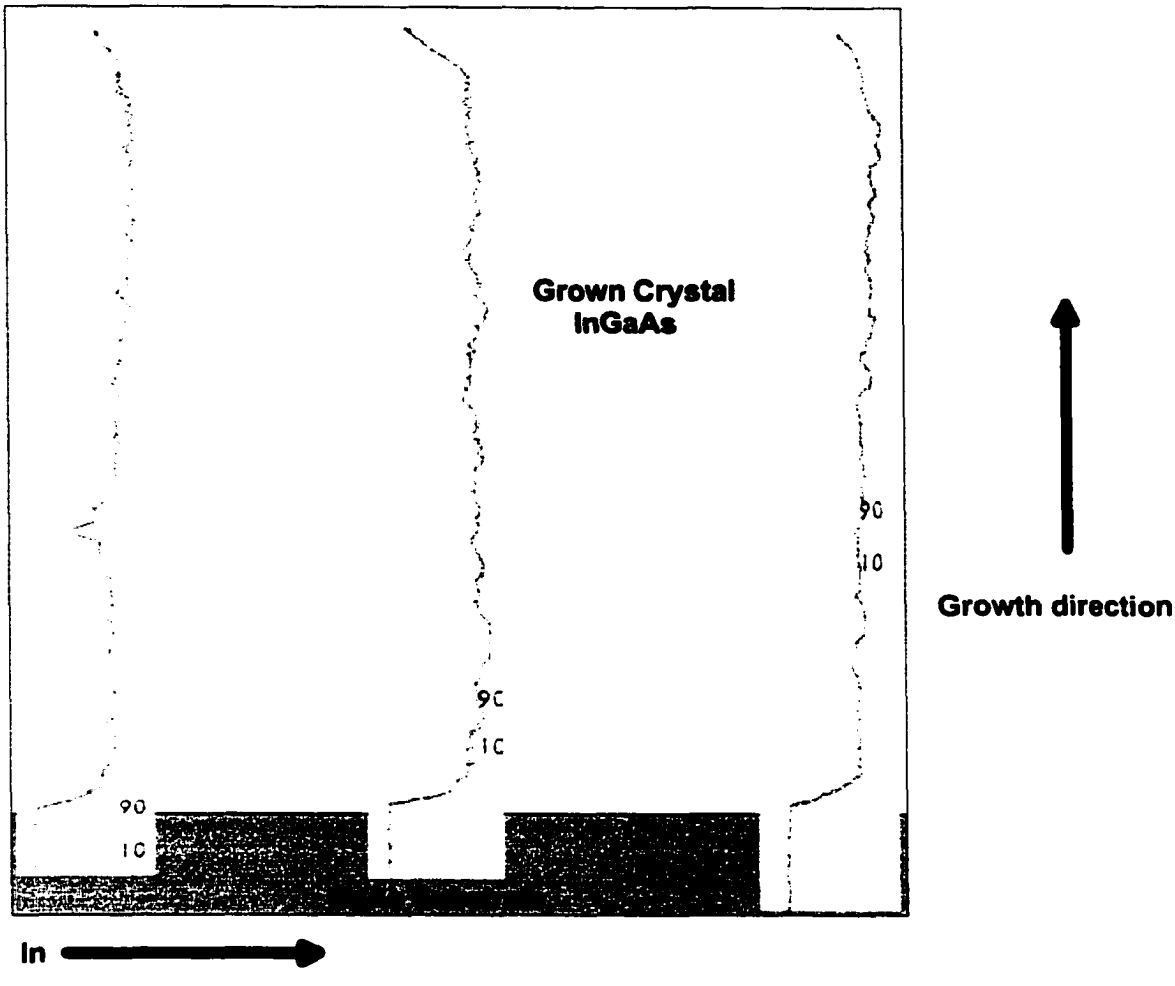

Figure 10.11. *Compositional variation in In ($In_{.04}Ga_{.96}As$) along the axial and radial directions, LPEE40*

10.2.2 X-ray Micro-analysis

Several samples of $In_{0.04}Ga_{0.96}As$ were sent to the Department of Physics, Simon Fraser University, Canada, to evaluate the uniformity of the In composition in crystals. The characterization technique used was Scanning electron microscopy.

Figure 10.17 shows a summary of the characterization results for the compositional variation in In. The ratios, K_{In} and K_{Ga} from the cross-sectioned $In_{0.04}Ga_{0.96}As$ are tabulated in table 10.3.

Once the intensity of the characteristic peaks, GaL_{α}, AsL_{α}, and $InL_{\alpha 1}$, were obtained

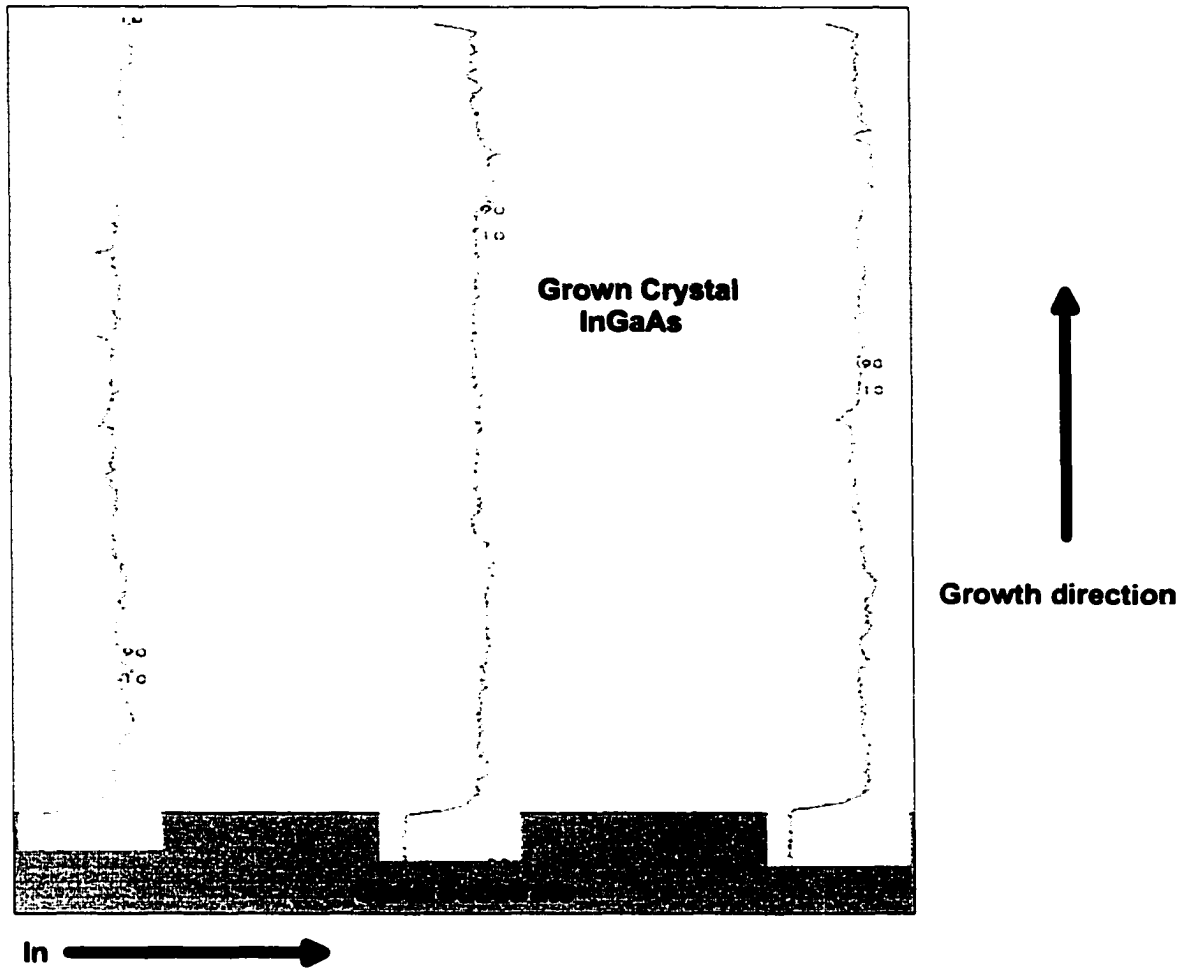

Figure 10.12. *Compositional variation in In ($In_{.04}Ga_{.96}As$) along the axial and radial directions, LPEE41*

from each spectrum, the ratio, K_{Ga}, of the GaL_α peak intensity from each $InGaAs$ standard and the measured locations on the cross-section of the $InGaAs$ crystal to that from the $GaAs$ film were calculated. Similarly, the ratio, K_{In}, of the $InL_{\alpha 1}$ peak intensity from the standards and the measured locations of the cross-sectioned crystal to that from the $InAs$ film were calculated.

In using the x-ray detector in the Energy Dispersive X-ray Spectroscopy (EDX) available at SFU, based on the In x-ray emission peak referenced to an $InAs$ crystal, a relatively flat composition of $x = 0.040 \pm 0.005$ was observed. In is decreasing towards the surface of the crystal as can be seen. The other data taken, comparing a Ga peak with respect to a

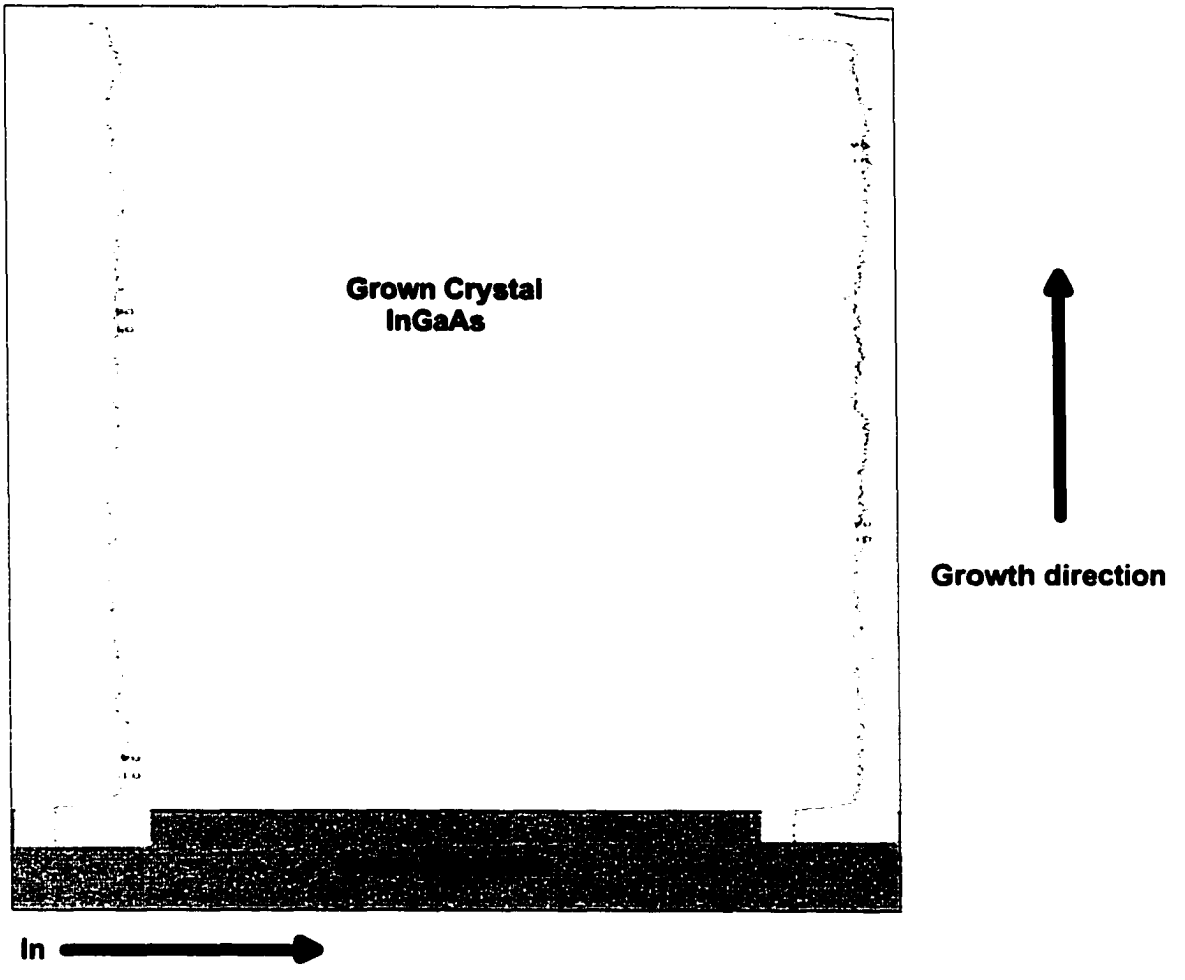

Figure 10.13. *Compositional variation in In ($In_{.04}Ga_{.96}As$) along the axial and radial directions. LPEE42*

$GaAs$ reference, gives results that do not agree with the In data (at least for 2 points). If these 2 points are not taken into account, one can say that the data agrees with the In. The accuracy here is not better than $x = 0.005$ In.

These results are in complete agreement with the results obtained at Shizuoka University, Japan using EPMA.

In summary, the new LPEE crucible designed and developed for this study produced thick $In_{0.04}Ga_{0.96}As$ crystals with uniform In composition in both the radial and axial (growth direction) directions. Results show that the LPEE technology developed at UVic is capable of growing bulk binary or ternary alloy crystals with uniform composition. The

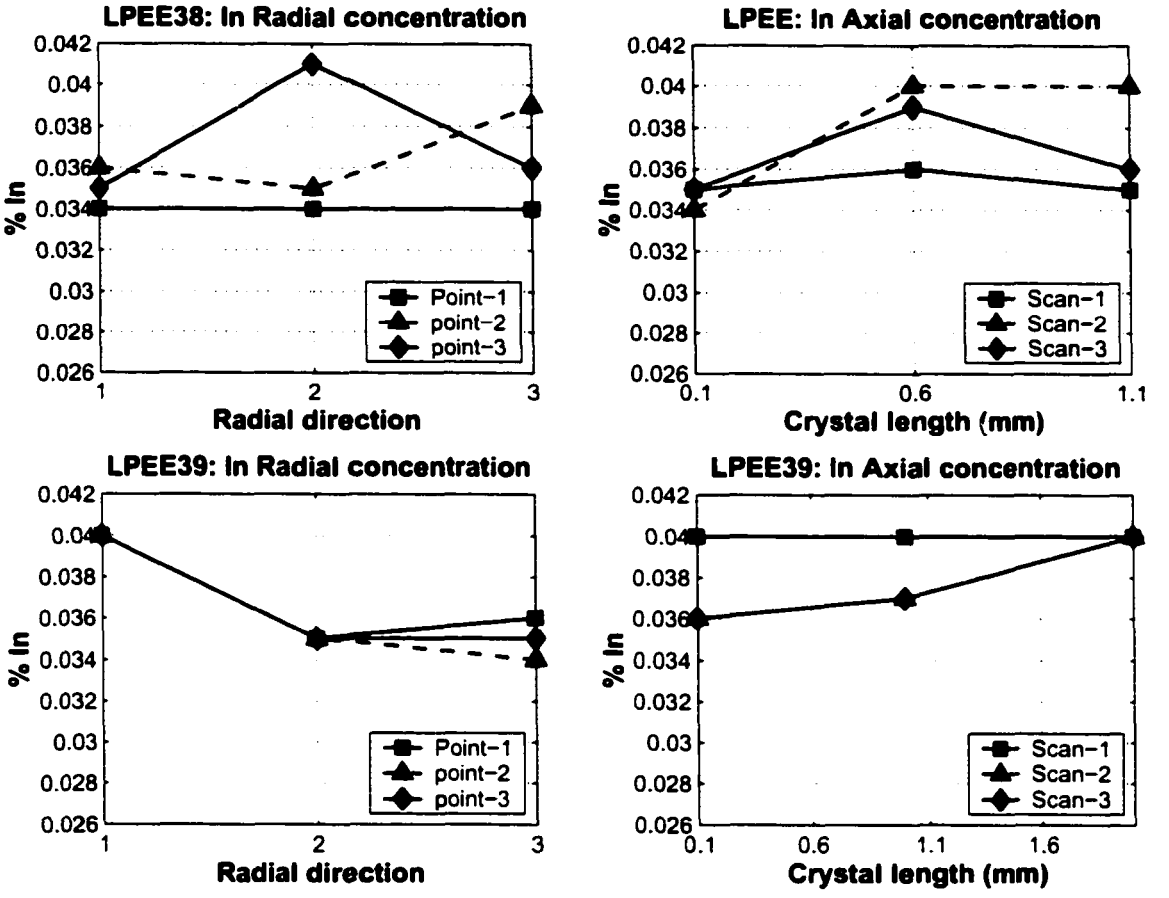

Figure 10.14. *Axial and radial compositional variation in In ($In_{.04}Ga_{.96}As$) using point EPMA, LPEE38,39.*

growth process can be extended to other materials.

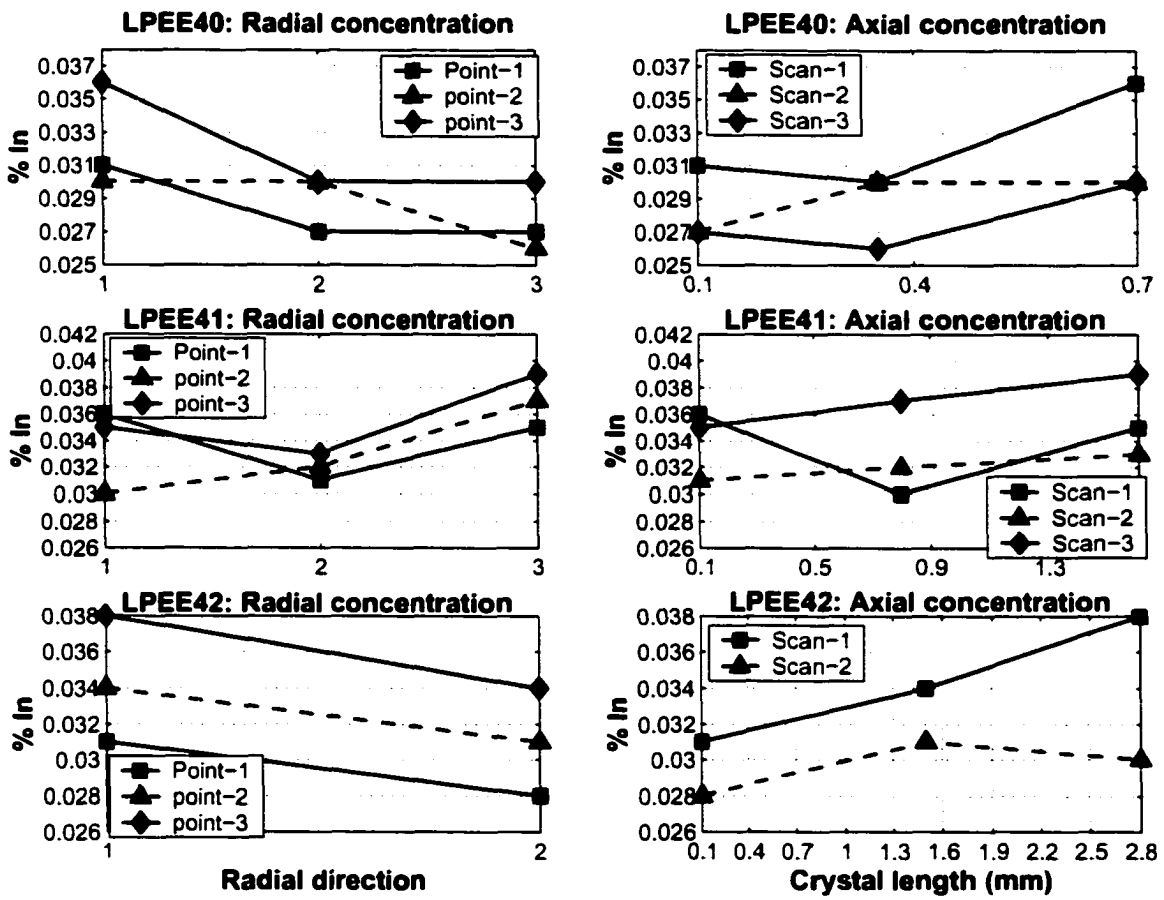

Figure 10.15. *Axial and radial compositional variation in In ($In_{.04}Ga_{.96}As$) using point EPMA, LPEE40,41,42.*

Table 10.1. *Summary of LPEE experiments without applied magnetic field.*

Experimental Identification	Current Density (A/cm^2)	Growth Duration (days)	Magnetic field (KGauss)	Results
LPEE1	3	5	0	Single crystal for the first 2.5 *mm* of growth, then LPE poly growth, total thickness 4.5, flat surface.
LPEE2	3	5	0	Exactly same as LPEE1
LPEE3	3	8	0	Single crystal, 4.5 *mm* thick, uniform surface, no LPE-poly growth, the whole solution was used.
LPEE7	3	1.7	0	Single crystal for the first 1.3 *mm* of growth, then LPE poly growth, total thickness 4.5, good LPEE-LPE interface, LPE surface is not flat.
LPEE8	3	1.7	0	Same as LPEE7, but flat LPEE-LPE surface
LPEE9	3	1.7	0	Exactly same as LPEE7
LPEE10	3	3	0	Single crystal for the first 1.5 *mm* of growth, then LPE-poly growth, total thickness 4.5 *mm*, flat uniform surface.
LPEE11	5	3	0	Single crystal for the first 2.5 *mm* of growth, then LPE-poly growth, total thickness 4.5 *mm*, non-uniform surface.
LPEE12	7	3	0	Single crystal for the first 2.5 *mm* of growth, then LPE-poly growth, total thickness 5.0 *mm*, not uniform and wavy surface.
LPEE13	7	3	0	Single crystal for the first 3.0 *mm* of growth, then LPE-poly growth, total thickness 5.0 *mm*, flat uniform surface and LPEE-LPE face.
LPEE14	7	3	0	Same as LPEE13
LPEE15	10	2	0	Single crystal for the first 2.0 *mm* of growth, then LPE-poly growth, total thickness 5.0 *mm*, thicker form one side than the other.
LPEE16	10	2	0	Single crystal for the first 2.0 *mm* of growth, then LPE-poly growth, total thickness 5.0 *mm*, hole in the substrate, surface uniform.

Table 10.2. *Summary of LPEE experiments under magnetic field.*

Experimental Identification	Current Density (A/cm^2)	Growth Duration (days)	Magnetic field (KGauss)	Results
LPEE4	3	5	2	Big hole through the crystal, very strong magnetic field (2.0 KGauss).
LPEE5	3	5	2	Same as LPEE4.
LPEE6	3	5	2	Same as LPEE4.
LPEE25	3	3	0.45	Single crystal, 5.0 to 9.0 mm thick, single-hump shape, swirl back contact.
LPEE26	3	1	0.45	Single crystal, 5.0 to 9.0 mm thick, single-hump shape.
LPEE27	3	1	0.6	Not good.
LPEE31	3	1	0.45	Single crystal, 5.0 to 9.0 mm thick, single-hump shape, not flat surface.
LPEE32	5	1	0.45	Single crystal, 5.0 to 10.0 mm thick, single-hump shape, very good surface.
LPEE34	7	0.5	0.45	Single crystal for the first 3.5 to 4.0 mm thick, then LPE poly growth, single-hump shape.

Table 10.3. *Compositional variation and the ratios, K_{In} and K_{Ga} in In ($In_{.04}Ga_{.96}As$) with growth thickness .*

Beam Position	Growth Thickness (mm)	K_{Ga}	x	K_{In}	x
1	0.310	0.957	0.0216	0.045	0.0432
2	0.600	0.958	0.0214	0.048	0.0468
3	0.890	0.932	0.0348	0.039	0.0373
4	1.110	0.911	0.0464	0.052	0.0501
5	1.400	0.909	0.0473	0.032	0.0310
6	1.548	0.932	0.0349	0.049	0.0472
7	1.858	0.931	0.0356	0.050	0.0480

- For K_{Ga} the error is ± 0.001
- For K_{In} the error is ± 0.004

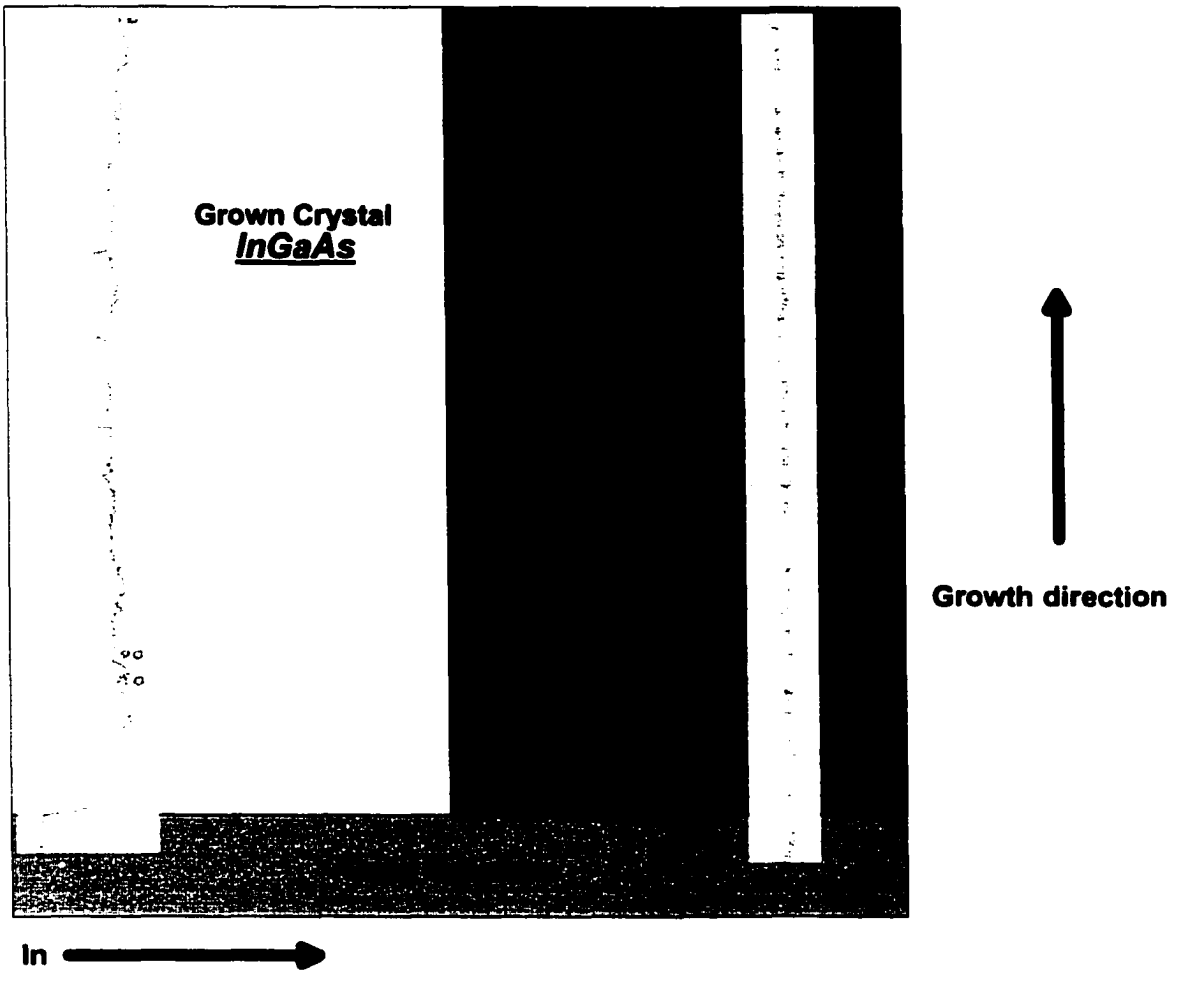

Figure 10.16. *Comparison of compositional variation in* In *between* $In_{.04}Ga_{.96}As$ *and* $GaAs$ *crystals*

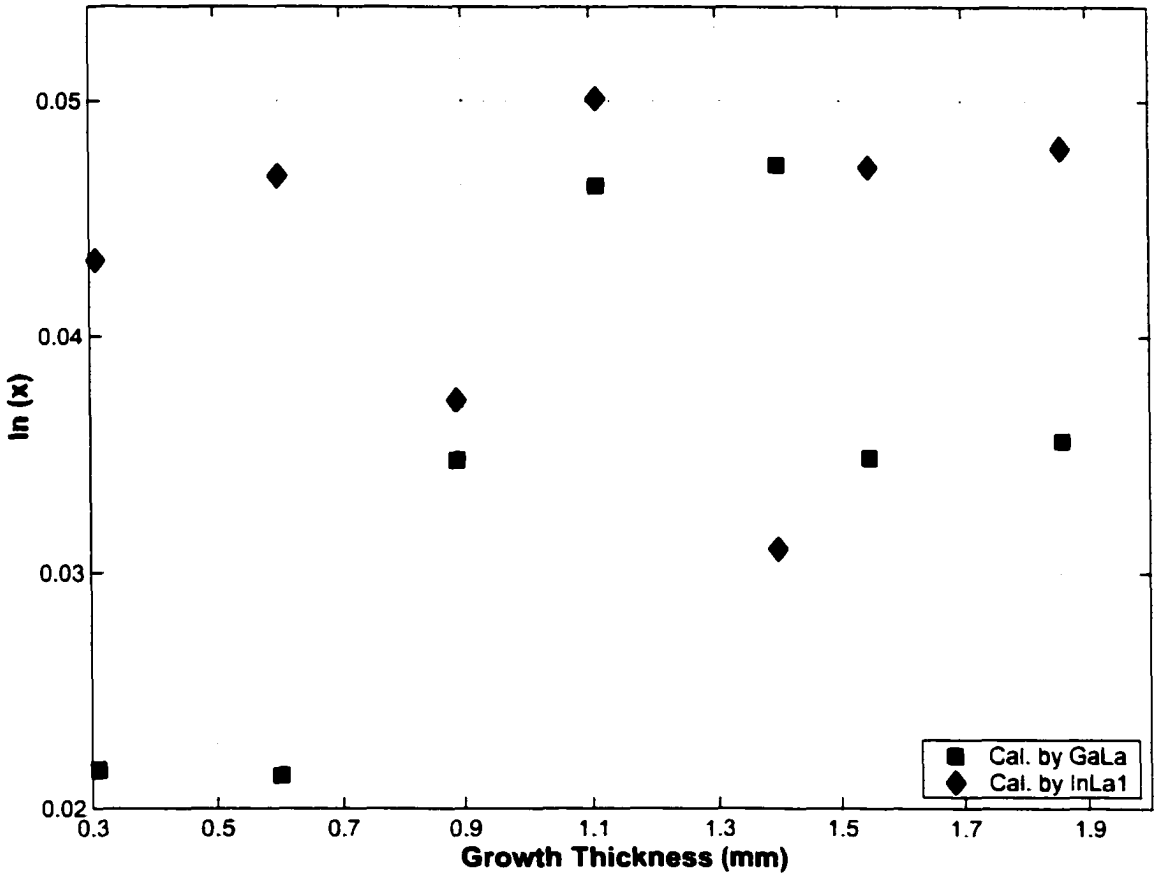

Figure 10.17. *Compositional variation in In ($In_{.04}Ga_{.96}As$) with growth thickness*

Chapter 11

Summary and Conclusions

The growth process of Liquid Phase Electroepitaxy (LPEE) has been successfully upgraded to the category of a bulk growth technique by growing a large of number of $GaAs$ and $InGaAs$ single crystals (more than 5 mm in thickness). This has been achieved through the optimization of various growth parameters, the successful application of external magnetic field, and the development of a novel growth crucible in which the adverse effects of Joule heating was minimized for a prolonged and stable growth. The growth rate has been increased 7 to 16 fold. These scientific and technological achievements that allowed the growth of bulk crystals of binary and ternary systems are significant research achievements in the field of crystal growth.

In addition, the LPEE grown bulk crystals displayed compositional uniformity comparable to those of thin epitaxial layers. This is also a very important feature of the LPEE growth system developed through this thesis work.

The literature has a significant body of information on epitaxially (thin layers) grown $InGaAs$ layers by LPEE. Most of our understanding of the LPEE growth technique is based on the evaluation (characterization) of such epitaxially grown layers. No information has been reported on the LPEE grown bulk $InGaAs$ crystals. The reason for this is simply due to the scientific and technological difficulties involved in growing bulk crystals of $InGaAs$; only few samples are available, $\geq$4 mm in the literature.

The present research has expanded the existing knowledge of growing bulk $InGaAs$ by reexamining the functions of the crucible components, minimizing the adverse effects of Joule heating in the crucible and the natural convection in the solution, and using effectively the benefit of applied magnetic field. Electrical connections in the growth systems were improved, and an innovative contact zone system was developed to provide the required uniform electric conductivity. A large number of crystals were grown under various

magnetic field and electric current density levels; at least 40 samples were grown. The relationships between the growth rate and the applied magnetic field and electric current have been established. It was shown experimentally that a uniform electrical contact at the back of the seed is the key in growing thick single crystals. Such a design allowed the use of higher electric current densities (3, 5, and 7 A/cm^2). Higher growth rates and larger crystal thicknesses can be achieved using higher electric current and magnetic field levels. However, further increases in the levels of applied electric current and magnetic field present formidable scientific and technological challenges, leading to uncontrollable growth due to strong convection in the liquid zones including the contact zone, and also to low quality crystals. In addition, magnetic field non-uniformities at higher levels lead to unstable growths.

The state-of-the-art LPEE system developed at UVic, because of its novel design features, has achieved a growth rate of about 4.5 mm/day (with the application of an external fixed magnetic field of 4.5 KGauss and 3A/cm^2 electric current density), and a growth rate of about 11 mm/day (with 4.5 KGauss magnetic field and 7 A/cm^2 electric current density). This is simply a breakthrough in LPEE growth, making it absolutely a bulk growth technique and putting it in competition with other bulk growth techniques.

Characterization of the grown crystals by EPMA has shown that the grown crystals have remarkable compositional uniformity in both the radial and growth directions.

There are a number of technological and scientific achievements as a result of this thesis work. It is hoped that the results obtained here will take the current research efforts in LPEE at the University of Victoria to the next level; a commercial-scale crystal growth system with a capability that will allow the growth of other bulk crystals of III-V and II-IV materials such as $CdZnTe$ and $SiGe$.

11.1 Future Work

Future experimental work in this field may include the growth of other important ternary semiconductors such as $CdZnTe$ and $SiGe$. Further research may be carried out to optimize the application of the electric current density for maximum crystal thickness. This can be achieved through a step-by-step approach; lowering the applied electric current density level while the growth is progressing. Such an approach may prolong the growth process

further for a stable growth.

There is no theoretical limit on the diameter of the crystals that can be grown by LPEE. The convection in the liquid zones, being one of the major adverse factors during growth, may introduce limitations on the size of the grown crystals. The growth of crystals of diameters larger than 25 mm may present challenges. It may require further optimization of the growth parameters of LPEE.

Up to now, only $GaAs$ and $InGaAs$ were grown using the LPEE facility. However, the facility, with some modifications, can be used to growth other materials such as $CdZnTe$ and $GeSi$.

The possible improvements to the growth platform are:

- Design and machine different crucible configurations to study and optimize the growth parameters.
- Improve of the air quality within the laboratory (cleaner environment).
- Use glove boxes, in which all the preparation of the material and manipulations on the crucible would be preformed.
- Use better quality source materials.

Some final thoughts: the present melt methods used to grow bulk $GaAs$ and $InGaAs$ crystals, by their very nature, are very limited in quality, both in crystal perfection and in electronic characteristics, that can be achieved. LPEE offers a means to improve some of those characteristics. Even though further theoretical and experimental work is needed to bring LPEE into the field of commercially produced $GaAs$ and $InGaAS$ substrates, one should not shy away from the challenge. The possibilities are there, and it is certainly worth to spend the time and efforts to accomplish the objective.

Bibliography

[1] M. Zambbuto, *"Semiconductor Devices"*, McGraw-Hill, 1989.

[2] C. D. Brandle, *Crystal Growth*, chapter "Crystal Pulling ", p. 275, Pergamon Press, 2nd edition, 1980.

[3] Wurzinger, P. Oppolzer, H., P. Pongratz,, and P.Skalicky, "TEM characterization of LEC-Grown $GaAs$ substrates," *J. Crystal Growth*, vol. 110, pp. 769, 1991.

[4] H. Ono, "Dislocation reactions and lineage formation in LEC grown $GaAs$ crystals," *J. Crystal Growth*, vol. 89, pp. 209, 1988.

[5] T. Bryskiewicz, C. F. Boucher, J. Lagowski, and H. C. Gatos, "Bulk $GaAs$ crystal growth by Liquid Phase Elecroepitaxi," *J. Crystal Growth*, vol. 82, pp. 279–288, 1987.

[6] T. Bryskiewicz and A. Laferriere, "Growth of alloy substrates by Liquid Phase Elecroepitaxi; theoretical considerations," *J. Crystal Growth*, vol. 129, pp. 429–442, 1993.

[7] S. Dost and H. A. Erbay, "A continuum model for Electroepitaxy," *Int. J. Engng. Sci.*, vol. 10, no. 33, pp. 1385–1402, 1995.

[8] H. A. Erbay, T. Bryskiewicz, and S. Dost, "Temperature distribution in electroepitaxial growth of GaAs," Ottawa, Canada, May 27-28 1992, Spacebound, pp. 53–58.

[9] F. A. Witt, "Crystal growth and segregation under zero gravity," *J. Electrochem. Soc.*, vol. 125, pp. 1832–1840, 1978.

[10] S. Motakef, "Magnetic field elimination of convective interference with segregation during vertical bridgman growth of doped semiconductors," *J. Crystal Growth*, vol. 104, pp. 833–850, 1990.

[11] A. Chen, *Semiconductor Alloys*, Plenum Press, 1995.

[12] L. Smart and E. Moore, *Solid State Chemistry*, Chapman & Hall, 1992.

[13] S. McGuigan, R. N. Thomas, H. M. Hobgood, G. W. Eldridge and B. W. Swanson, "Semi-insulating III-V materials," in *Hakone*, Ohmsha Ltd, 1986.

[14] G. B. Stringfellow, "Lattice parameters and crystal structure of $InGaAs$," in *Indium Gallium Arsenide*, EMIS, 1986.

[15] J. L. Werber and J. Van De Ven, "Residual strain measurements in thick $In_xGa_{1-x}As$

layers grown on $GaAs$ (100) by Molecular Beam Epitaxy," *J. Crystal Growth*, vol. 88, pp. 221, 1988.

[16] M. G. Astles, *Liquid Phase Epitaxial Growth of II-V Compound Semiconductor Material and their Device Apllications*, Adam Hilger, 1990.

[17] T. Sukegawa, M. Kimura, and A. Tanaka, "phase equilibria in ternary III-V systems," *J. Crystal Growth*, vol. 92, pp. 46, 1988.

[18] T. Sukegawa, K. Yamashita, H. Katsuno, M. Kimura, and A. Tanaka, "Growth of a $GeSi$ thick alloy layer on a Si substrate by Liquid Phase Epitaxy," *J. Crystal Growth*, vol. 109, pp. 186, 1991.

[19] T. Ozawa, Y. Hayakawa, and M. Kumagawa, "Growth of III-V ternary and quaternary mixed crystal by the rotationary Bridgman method," *J. Crystal Growth*, vol. 109, pp. 212, 1991.

[20] T. Ozawa, Y. Hayakawa, and M. Kumagawa, "Interface instability in the growth of $Ga_{1-x}In_xAs_ySb_{1-y}$ and thermodynamic considerations," *J. Crystal Growth*, vol. 115, pp. 728, 1991.

[21] B. R. Pamplin, "Deep levels in bulk LCE single crystal $In_xGa_{1-x}As$," *J. Crystal Growth*, vol. 129, pp. 429, 1980.

[22] J. Czochralski, "Czochralski growth of $SiGe$ single crydtals," *J. Phys. Chem.*, vol. 92, pp. 219, 1918.

[23] P. Schlossmacher, M. Otte, K. Urban, and H.Rufer, "Identification of Zn-As phase in Zn-doped LCE-$GaAs$," *J. Crystal Growth*, vol. 121, pp. 671, 1992.

[24] S. Motakef, K. W. Kelly, and K. Koai, "Comparison of calculated and measured dislocation density in LEC-grown $GaAs$ crystals," *J. Crystal Growth*, vol. 113, pp. 279, 1991.

[25] D.R. Wight, "GaAs: Materials, devices, and circuit," John Wiley & Sons, 1985.

[26] E. M. Swiggard, "Liquid Encapsulated Vertical Zone Melt growth of $GaAs$ crystals," *J. Crystal Growth*, vol. 94, pp. 556, 1989.

[27] S. Mizuniwa, M. Kashiwa, T. Kurihara, K. Nakamura, S. Okubo, and K. Ikegami, "phase equilibria in ternary III-V systems," *J. Crystal Growth*, vol. 99, pp. 676, 199.

[28] K. Hoshikawa, H. Nakanishi, H. Kohda, and M. Sasaura, "phase equilibria in ternary III-V systems," *J. Crystal Growth*, vol. 94, pp. 643, 1989.

[29] E. D. Bourret and E. C. Merk, "phase equilibria in ternary III-V systems," *J. Crystal Growth*, vol. 110, pp. 395, 1991.

[30] G. A. Wolff and A. I. Mlavsky, "Traveling Solvent Technique," in *Crystal Growth, Theory and Techniques*, C. H. L. Goodman, Ed., vol. 1, chapter 3. Kluwer Academic Publishers, 1974.

[31] R. Triboulet and Y. Marfaing, "$CdTe$ growth by multipass THM and sublimation," *J. Crystal Growth*, vol. 51, pp. 89, 1981.

[32] V. M. Glazov, S. N. Cizevskaja, and N. N. Glagoljeva, *Liquid Semiconductour*, Plenum Press, 1996.

[33] C. T. Foxon and B. A. Joyce, "Growth of thin films and heterostructures of III-V compounds by Molecular Beam Epitaxy," in *Growth and Characterisation of Semiconductors*, R. A. Stradling and P. C. Klipstein, Eds., pp. 35–64. Adam Hilger, 1990.

[34] J. O. Williams, "Metal Organic Chemical Vapour Deposition MOCVD for the preparation of semicondutor materials and devices," in *Growth and Characterisation of Semiconductors*, R. A. Stradling and P. C. Klipstein, Eds., pp. 17–33. Adam Hilger, 1990.

[35] T. Bryskiewicz, M. Bujaski, B. Bryskiewicz, J. Lagowski, and H.C. Gatos, ""LPEE growth and characterization of $In_{1-x}Ga_xAs$ bulk crystals," .

[36] T. Bryskiewicz, P. Edelman, Z. Wasilewski, D. Coulas, and J. Noad, "Properties of very uniform $In_xGa_{1-x}As$ single crystals grown by LPEE," *J. appl. Phys*, vol. 68, pp. 3016, 1990.

[37] T. Bryskiewicz and A. Laferriere, "Growth of alloy substrate by LPEE; throretical conssiderations," *J. Crystal Growth*, vol. 129, pp. 429, 1993.

[38] K. Nakajima and T. Kusunoki, "Constant temperature growth of uniform-composition $In_xGa_{1-x}As$ bulk crystals by supplying $GaAs$," *18th Int. Symp. on GaAs and Related Compounds, in Inst. Phys. Conf. Series*, vol. 2, pp. 67, 1992.

[39] M. Kumagawa, A. F. Witt, M. Lichtensteiger, and H. C. Gatos, "Current-controlled growth and dopant modulation in LPE," *J. of the Electrochemical Society*, vol. 120, pp. 583, 1973.

[40] D. J. Lawrence and L. F. Eastman, "Electric current controlled growth and doping modulation in $GaAs$ LPE," *J. of Crystal Growth*, vol. 30, pp. 267, 1975.

[41] J. J. Daniele and C. Michel, "Peltier-induced growth of $GaAlAs$," in *Proceedings of the 5th International Symposium on GaAs and Related Compounds*,, 1975.

[42] L. Jastrzebski, Y. Imamura, and H. C. Gatos, "Thickness uniformity of $GaAs$ layers-grown by LPEE," *J. of the Electrochemical Society*,, vol. 1140, pp. 1140, 1978.

[43] T. Bryskiewicz and K. Mazuruk, "LPEE from a limited solution volume," *Institute of Physics Conference Series*, vol. 56, pp. 147, 1981.

[44] J. J. Daniele, D. A. Cammack, and P. M. Asbeck, "$GaAs/GaAlAs$ DH lasers grown by peltier-induced LPE," *J. of Applied Physics*, vol. 48, pp. 914, 1977.

[45] D. J. Lawrence and L. F. Eastman, "Electric current controled lpe on N^+ and semi-insulating substrates," *J. of Electronic Materials*, vol. 6, pp. 1, 1977.

[46] Y. Imamura, L. Jastrzebski, and H. G. Gatos, "Defect structures and electronic characteristics of $GaAs$ layers grown by LPEE and thermal LPE," *J. of Electrochemical Society*, vol. 126, pp. 1381, 1979.

[47] L. Jastrzebski and H. C. Gatos, "Current-controlled growth, segregation and amphoteric behavior of Si in $GaAs$ from Si-doped solutions," *J. of Crystal Growth*, vol. 42, pp. 309, 1977.

[48] L. Jastrzebski, J. Lagowski, and H. C. Gatos, "Outdiffusion of recombination centers from substrate into LPE layers; $GaAs$," *J. of the Electrochemical Society*, vol. 126, pp. 2231, 1979.

[49] T. Bryskiewicz, "Peltier-induced growth kinetics of LPE $GaAs$," *J. of Crystal Growth*, vol. 43, pp. 567, 1978.

[50] T. Bryskiewicz, "LPEE of semiconductor compounds," *Progress in Crystal Growth and Characterization*, vol. 12, pp. 29, 1986.

[51] T. Bryskiewicz, C. F. Boucher, J. Lagowski, and H.C. Gatos, "Bulk $GaAs$ crystals grown by LPEE," *J. of Crystal Growth*, vol. 82, pp. 279, 1987.

[52] C. F. Boucher, O. Ueda, T. Bryskiewicz, J. Lagowski, and H. C. Gatos, "Elimination of dislocations in bulk $GaAs$ crystals grown by LPEE," *J. of Applied Physics*, vol. 61, pp. 359, 1987.

[53] T. Bryskiewicz, M. Bugajski, J. Lagowski, and H. C. Gatos, "Growth and characterization of high quality LPEE $GaAs$ bulk crystals," *Journal of Crystal Growth*, vol. 85, pp. 136, 1987.

[54] T. Bryskiewicz, P. Edelman, Z. Wasilewski, D.Coules, and J. Noad, "Properties of very uniform $In_xGa_{1-x}As$ single crystals grown by LPEE," *J. of Applied Physics*, vol. 68, pp. 3018, 1990.

[55] L. Jastrzebski, J. Lagowski, H. C. Gatos, and A. F. Witt, "Liquid-Phase Electroepitaxy: Growth kinetics," *J. Appl. Phys.*, vol. 49, pp. 5909, 1978.

[56] W.R. Wilcox, "Influence of convection on the growth of crystals from solution," *J. Crystal Growth*, vol. 65, pp. 133–142, 1983.

[57] L. Jastrzebski, J. Lagowski, H. C. Gatos, and A. F. Witt, "Liquid-Phase Electroepitaxy: Growth kinetics," *J. Appl. Phys*, vol. 49, pp. 5909, 1978.

[58] S. Dost, N. Djilali, and Z. Qin, "A two-dimensional diffusion model for Liquid Phase Electroepitaxial growth of $GaAs$," *J. Crystal Growth*, vol. 143(3/4), pp. 141–154, 1994.

[59] N. Djilali, Z. Qin, and S. Dost, "Role of thermosolutal convection in Liquid Phase Electroepitaxial growth of $GaAs$," *J. Crystal Growth*, vol. 149, pp. 153–166, 1995.

[60] R. O. Bell, "An analysis of the temperature distribution during crystal growth by THM," *J.l of Electrochemistry Society*, vol. 121, pp. 1366, 1974.

[61] L. Jastrzebski, J. Lagowski, H. C. Gatos, and A. F. Witt, "Outdiffusion of recombination centers from substrate into LPEE layers; $GaAs$," *J. Appl. Phys*, vol. 49, pp. 5909, 1978.

[62] A. G. Elliot, A. Flat, and D.A. Vanderwater, "phase equilibria in ternary III-V systems," *J. Crystal Growth*, vol. 121, pp. 349, 1992.

[63] T. Bryskiewicz, "Peltier–induced growth kinetics of Liquid Phase Epitaxial $GaAs$," *J. Crystal Growth*, vol. 43, pp. 567–571, 1978.

[64] L. Jastrzebski, Y. Imamura, and H. C. Gatos, "Thickness uniformity of $GaAs$ layers growth by Electroepitaxy," *J. Electrochem. Soc*, vol. 125, pp. 1140–1146, 1978.

[65] T. Bryskiewicz, C. F. Boucher, J. Lagowski, and H. C. Gatos, "Bulk $GaAs$ crystal growth by Liquid Phase Electroepitaxy," *J. Crystal Growth*, vol. 82, pp. 279–288, 1987.

[66] S. Dost, "Numerical simulation of Liquid Phase Elecroepitaxi growth of $ingaas$ under magnetic field," *ARI-the Bullettin of ITU*, vol. 51, pp. 235, 1999.

[67] B. A. Nerad and P. J. Schlichta, "Ground-based experiments of convection during the growth of crystals from solutions," *J. Crystal Growth*, vol. 75, pp. 1832–1840, 1986.

[68] Y. Imamura, L. Jastrzebski, and H. C. Gatos, "Surface morphology of $GaAs$ layers grown by LPEE and thermal LPE," *J.l of the Electrochemical Society*, vol. 125, pp. 1560, 1978.

[69] Z. Qin and S. Dost, "A model for Liquid Phase Elecroepitaxi growth of ternary alloy semiconductors. PART III-Application," *Int. J. Appl. Electromagnetics and Mechanics*, vol. 2, no. 7, pp. 129–142, 1996.

[70] S. Dost and Z. Qin, "A numerical simulation of liquid phase electroepitaxial growth of GaInAs," *J. Crystal Growth*, vol. 187, pp. 51–64, 1998.

[71] D. J. Carlson and A. F. Witt, "phase equilibria in ternary III-V systems," *J. Crystal Growth*, vol. 108, pp. 508, 1991.

[72] T. Bryskiewicz, E. Jiran, and B. Bryskiewicz, "Properties of $In_xGa_{1-x}AS$ crystals grown by LPEE on pattered gaas substrates," San Francisco, USA, April 4-8 1994, MRS Spring Meeting.

[73] B. Bryskiewicz, T. Bryskiewicz, and E. Jiran, "Internal strain and dislocations in $In_xGa_{1-x}As$ crystals growth by LPEE," *J. Electronics Material*, in press.

[74] T. Bryskiewicz, M. Bugajski, B. Bryskiewicz, J. Lagowski, and H. C. Gatos, "LPEE growth and characterization of $In_{1-x}Ga_xAs$ crystals," Inst. Phys. Ser., 1988, vol. 91, p. 259.

[75] G. Bischopink and K. W. Benz, "Growth of $Al_xGa_{1-x}Sb$ and GaSb bulk crystal with liquid phase electroepitaxy (LPEE)," *J. Crystal Growth*, vol. 128, pp. 466, 1993.

[76] J. J. Daniele and A. J. Hebling, "Peltier-Induces Liquid Phase Epitaxy and compositional control of mm-thick layers of (Al, Ga As)," *J. Appl. Phys*, vol. 52, pp. 4325, 1981.

[77] Z. R. Zytkiewicz, "Influence of convection on composition profile of thick GaAlAs layers growth by LPEE," *J. Crystal Growth*, vol. 131, pp. 426, 1993.

[78] Z. R. Zytkiewicz, "Compositional control of thick GaAlAs layers (x $\leq$0.72) growth by LPEE," *J. Crystal Growth*, vol. 121, pp. 457, 1992.

[79] T. Bryskiewicz, P. Edelman, Z. Wasilewski, D. Coules, and J. Noad, "Properties of very uniform $In_xGa_{1-x}As$ single crystals grown by LPEE," *J. Eletrochem. Soc.*, vol. 68, pp. 3018, 1990.

[80] S. Dost and Z. Qin, "A model for Liquid Phase Elecroepitaxi under an external magnetic field PART I-Theortical," *J. Crystal Growth*, vol. 153, pp. 123–130, 1995.

[81] Z. Qin and S. Dost, "A model for Liquid Phase Elecroepitaxi growth of ternary alloy semiconductors. PART II-Numarical," *Int. J. Appl. Electromagnetics and Mechanics*, vol. 7, no. 2, pp. 109–128, 1996.

[82] MB. Panish and M. Ilegems, "phase equilibria in ternary III-V systems," *Progress in solid state chemistry*, vol. 7, pp. 29–84, 1972.

[83] H. Sheibani, Y.C. Liu, S. Sakai, B. Lent, and S. Dost, "The effect of applied magnetic field on the transport mechanisms of liquid phase electroepitaxy," *Int. J. Engng. Sci.*, vol. 5, pp. 129, 2002.

[84] S. Dost and H. Sheibani, "Liquid Phase Electroepitaxial growth of $GaInAs$ crystals under magnetic field," *Mechanics of Electromagnetics materials And Structures*, vol. 19, pp. 1383–7281, 2000.

[85] I. Harter, P. Dusserre, T. Duffar, J .-Ph. Nabot, and N. Eustathopoulos, "Wetting of III-V melts on crucible materials," *J. of Crystal Growth*, vol. 125, pp. 129, 1992.

[86] U. Konig and W. Keck, "Contact angles between III-V melts and several substrates," *J. of the Electrochemical Society*, vol. 130, pp. 685, 1983.

[87] *Product and Vacuum Technolog Reference Book*, Leybold Vacuum Products Inc., 1992.

[88] H. A. Erbay, T. Bryskiewicz, and S. Dost, "Temperature distribution in electroepitaxial growth of $GaAs$," *Proceedings of Spacebound '92*, vol. 92, pp. 53, 1992.

[89] J. J. Daniele, D. A. Cammack, and P. M. Asbeck, "$GaAs/GaAlAs$ DH lasers grown by peltier-induced LPE," *J. of Applied Physics*, vol. 48, pp. 914, 1977.

[90] T. Bryskiewicz and K. Mazuruk, "LPEE from a limited solution volume," *Institute of Physics Conference Series*, vol. 56, pp. 147, 1981.

[91] J. J. Daniele and C. Michel, "Peltier-induced growth of $GaAlAs$," *Proceedings of the 5th International Symposium on $GaAs$ and Related Compounds*, 1975.

[92] M. B. Panish, S. Sumski, and I. Hayashi, "Preparation of multilayer LPE heterostructures with crystalline solid solutions," *Transactions of the American Institute of Mining, Metallurgical and Petroleum Engineering (AIME)*, vol. 2, pp. 795, 1971.

[93] C. J. Smithells and E. A. Brandes, *Metals Reference Book.*

[94] M. S. Abrahams and C. J. Buiocchi, "Etching of dislocations on the low-index faces of $GaAs$," *J. of Applied Physics*, vol. 36, pp. 2855, 1965.

[95] G. H. Olsen and M. Ettenberg, "Universal strain/etchant for interfaces in III-V compounds," *J. of Applied Physics*, vol. 45, pp. 5112, 1974.

[96] M. V. Sullivan and G. A. Kolb, "Chemical polishing of $GaAs$ in Bromine-Methanol," *J. of the Electrochemical Society*, vol. 110, pp. 585, 1963.

[97] J. M. Woodall, H. Rupprecht, and W. Reuter, "LPE growth of $Ga_{1-x}Al_xAs$," *J. of the Electrochemical Society*, vol. 116, pp. 899, 1969.

Appendix A

Reactor Tube Etching and Crucible Bake-out

In this appendix, we present the procedures used to etch the reactor tube and bake-out the crucible. Before the start of a crystal growth experiment, it is important to clean the reactor tube and crucible components in order to minimize possible contamination of the growth materials. Any impurity within the reactor tube will represent a possible source of contamination when subjected to high temperatures, as is the case during LPEE.

These following procedures should also be used whenever the operator has a reason to believe that the crucible or the inside of the reactor tube has been contaminated (as in the case of prolonged exposure to air or humidity, for instance).

A.1 Reactor Tube Etching

Protective gear must be worn in order to prevent injury from the acid used during the etching of the quartz tube. Here are the steps required to clean the reactor tube:

1. Remove the reactor tube from the growth platform.
2. Clean the exterior ends of the tube, using acetone.
3. Etch the interior of the tube using 100 ml of 5-10 % vol $.HF$ (fluoro-acid) solution. The solution should be prepared with distilled water. Always keep the solution in motion inside the tube to provide uniform etching.
4. Remove the HF solution, and rinse thoroughly using distilled water. The HF solution should be conserved, at it will be needed again in the next step.

5. Pour the HF solution on exterior of tube, and let it drip along the tube into a container. Repeat this process as often as needed, until the solution spreads evenly on all of the tube's surface when poured, indicating that the totality of the tube's exterior surface has been etched.
6. Rinse the tube thoroughly using distilled water.
7. Rinse thoroughly the interior and exterior of the tube using methanol.
8. Leave the tube to dry for a few hours. During this period, the tube should be resting horizontally on a clean surface, in an area of restricted access.
9. Put the tube back on the crystal growth platform. Keep a steady stream of nitrogen flowing through it whenever it is not in use thereafter.

A.2 Crucible Cleaning and Bake-out

The crucible bake-out can be done before or after the reactor tube etching. If it is done before, the bake-out, should be performed in a vacuum conditions, as the subsequent etching operation will remove the material that will have sputtered on the inside of the tube. If the bake-out is done after the reactor tube etching, it should be performed in a high purity hydrogen atmosphere, thus minimizing the deposition of impurities on the tube's interior.

Here is the description of the bake-out process:

1. Remove the crucible components from inside of the reactor tube.
2. Clean the boron nitride and graphite components using distilled water and an ultrasonic cleaner. Each component should be placed for a few minutes within the ultrasonic bath, then rinsed. Repeat this process, always using clean distilled water, as many times as required for each component. The components will be considered clean when no particle is seen in suspension in the water after the ultrasonic cleaning.
3. Bake these components in an oven at 200°C for roughly 30 minutes, in order to remove the bulk of their humidity.
4. Install the crucible back in the reactor tube.
5. Depressurize to 10^{-4} mbar or lower, using the TMP system.
6. In the case of a hydrogen atmosphere bake-out, fill the reactor tube with high purity hydrogen, and keep a steady flow (around 100 ml of hydrogen per minute) through

the tube during the whole duration of the bake-out.

7. Heat system at least 50°C above the highest temperature that will be used during the crystal growth experiments. Keep this bake-out temperature for two hours.
8. Cool down to room temperature.
9. Keep the crucible within reactor tube thereafter.

Appendix B

Equipment and Materials Specifications

BORON NITRIDE

Carborundum HP grade boron nitride.

Calcium borate binder, maximum use temperature in inert atmosphere 1850^{o}C.

Density 1.90 g/cm^3, open porosity 15.26 %.

Thermal expansion coef. to 1500^{o}C: 2.95x10^{-6} $mm/mm/^o$C parallel to pressing direction, and $0.87x10^{-6}$ $mm/mm/^o$C perpendicular to pressing direction.

DIGITAL PANEL METER

Omega, DP41-TC-A-S2.

6-digit temperature indicator for thermocouples type J,K,T,E,R,S,B,N,J.

Min/Max storage, 12 readings per second, 0.2^o C accuracy.

110 Vac input, analog output 4-20 mA, isolated RS-232 communication port.

DC POWER SUPPLY

Xantrex, XKW 10-100.

110 or 220 Vac input, 10 Vdc and 100 A maximum output.

Fixed voltage or fixed current mode.

GRAPIDTE

Poco SFG-2 grade graphite.

Density 1.1 g/cm^3, average pore size 0.2 μm, typical particle size $<$ 1 μm.

Total ash impurity $<$ 5 PPM.

Thermal expansion coef. to 1000^{o}C: 7.7x10^{-6} $mm/mm/^o$C.

PYROLYTIC BORON NITRIDE

Advanced Ceramic Corporation pyrolytic boron nitride.
Calcium borate binder, maximum use temperature in reducing atmosphere 1850°C.
Density 12.15 g/cm^3, no open porosity.
Thermal expansion coef. to 1200°C: 2.5x10^{-6} $mm/mm/°C$ parallel to deposition direction, and 30x10^{-6} $mm/mm/°C$ perpendicular to deposition direction.

QUARTZ TUBE

Sandfire Scientific Ltd, 55 mm ID, 59 mm OD and 540 mm in length.
Thickened to 3.5 mm on the inside for 30 mm.
Spinning to make a flange, at one end. Close at the other end.
Thermal expansion coef. to 1000°C: 0.55x10^{-6} $mm/mm/°C$.

TUBULAR FURNACE

Mellen, TT12-2.5X12M-3Z.
1100°C, 1200°C, and 1300°C (for Z1, Z2, and Z3 respectively) solid tubular furnace, 495, 990, 495 Watts, 63 mm ID, 3 zones with length 152 mm, 304mm, 152 mm.
Mellen , three zone phase angle fired SCR controllers and power supplies, with UDC3000 digital controllers and type-K thermocouples.
Independent over-temperature alarms, RS-422 communication port and programmability of one of the controllers with 12 segment setpoints.

TURBOMOLECULARPUMP

Leybold Turbovac TMP 50.
Grease lubricated, with ceramic ball bearings.
Ultimate pressure 8x10^{-9} mbar, pumping speed 29 l/sec.
Leybold NT10 TMP 50 frequency converter, 110 Vac input.
Trivac D4A dual stage rotary vane pump as backing pump.

VACUUM GAUGE

Leybold Inficon IG3-11 0000.
Hot cathode ion gauge controller with pirani measurement module, 110 V AC input.

G6 hot cathode filament ion sensor with dual tungsten filament, 10^{-9} to 10^{-2} mbar range. TR901 pirani gauge sensor, 10^{-3} to 10^{3} mbar range.